To the Graduate Council:

I am submitting herewith a thesis written by Jeffrey Allen Jansen entitled "Microstructural Analysis of Three Iron Meteorites: Arispe, Inland Forts and Ocotillo." I have examined the final copy of this thesis for form and content and recommend that it be accepted in partial fulfillment of the requirements for the degree of Masters of Science, with a major in Metallurgical Engineering.

Charlie R. Brooks

Charlie R. Brooks, major professor

We have read this thesis
and recommend its acceptance:

R. A. Buchanan

Associate Vice Chancellor
and Dean of the Graduate School

Microstructural Analysis of Three Iron Meteorites: Arispe, Inland Forts and Ocotillo

A Thesis
Presented for the
Master of Science
Degree
The University of Tennessee, Knoxville

Jeffery Allen Jansen
December 1992

Acknowledgements

The author wishes to acknowledge Bob McGill for assistance in the scanning electron microscopy and EDS analysis, major professor Charlie R. Brooks for his guidance throughout the research, and committee members Raymond A. Buchanan and Anthony J. Pedraza for their helpful suggestions. Thanks are also extended to Dr. Michael B. McNeil for providing the Inland Forts sample.

Abstract

The microstructure of three iron meteorites, Arispe and Ocotillo (coarse octahedrites), and Inland Forts (an ataxite), were examined using optical and scanning electron microscopy. Emphasis was placed on the plessitic structures in the two octahedrites; pearlitic, spheroidal, acicular, martensitic and comb plessite structures were common.

The pearlitic and spheroidal plessite structures in Arispe were typically found in the vicinity of cohenite ($(Fe,Ni)_3C$) 'nests'. The pearlitic plessite often coarsened in these regions as well. The acicular and comb plessite usually were present in the bulk of the meteorite.

Ocotillo contained numerous retained taenite stringers, and these stringers had decomposed to a variety of plessite morphologies. Regions of coarsening and spheroidization of the pearlitic structure were commonly observed. A large troilite-graphite inclusion also was present.

The structures observed in the ataxite Inland Forts were different from those present in the two octahedrites. The microstructure consisted of small particles of ferrite with associated schreibersite, in a banded matrix structure. The matrix appeared banded due to an

orientation effect of the structure. The matrix consisted of three regions, a coarse, oriented two-phase region, a fine, oriented two-phase region, and a clear region.

Possible formation mechanisms of the plessitic structures are discussed, however all aspects of these plessitic structures are not fully explained.

Table of Contents

List of Figures

Chapter I

INTRODUCTION

Iron meteorites are often studied to gain information not available in man-made iron-nickel alloys due to the low diffusion rates of iron and nickel at low temperatures. Since meteorites cool extremely slowly (estimated cooling rates of 10-100°C/10^6 years), analysis of the structures can be used to try to experimentally corroborate the iron-nickel and iron-nickel-phosphorous phase diagrams. This comparison between theoretically calculated phase diagrams and experimental evidence is possible since meteorites are considered to be at near equilibrium during their entire cooling process. Therefore structures present in iron meteorites must be accounted for by the phase diagram.

The structures and minerals present in meteorites can also be used to determine the preterrestrial history of these bodies, such as heat treatments and mechanical shock events. Understanding the structure of meteorites and their preterrestrial history and origin therefore can provide us with clues to the origins of the universe.

There is also interest in the structure of meteorites since the composition of some meteorites is near that of the Invar alloys, 30 - 35% nickel, which, along with the low thermal expansion coefficient, also exhibit resistance to swelling under neutron and heavy ion irradiation, which

has direct applications in the nuclear industry [1].

In this study, five iron meteorites have been examined with optical and scanning electron microscopy to characterize the microstructural features. The use of transmission electron microscopy was also attempted to resolve some of the finer structures present in a sample of Arispe. Four of the meteorites were classified as octahedrites, and one (Inland Forts) was classified as an ataxite.

Chapter II

DEFINITIONS AND TERMINOLOGY

Since much of the early work on meteorites was carried out by geologists, some of the the terminology commonly used in their study of meteorites may be confusing to metallurgists. Therefore I will begin by briefly defining the more important terms.

I. Asteroids, Meteoroids, Meteors, and Meteorites

Meteorites are believed to have originated in the asteroid belt, a region of cosmic debris between the orbits of Mars and Jupiter. Masses in the belt can range from the microscopic to several kilometers in diameter, and are known as asteroids. When an asteroid leaves the asteroid belt and travels through outer space, it is termed a meteoroid.

Occasionally meteoroids are captured by the earth's gravitational field, and are pulled through the earth's atmosphere. Upon passing through the earth's atmosphere, these masses are termed meteors. During entry through the atmosphere, friction due to air resistance causes meteors to burn. (These are commonly known as shooting or falling stars.)

Meteors, since they originate as asteroids, have a wide range in size. The microscopic particles pass through the atmosphere slowly due to low mass and air resistance, and have very little heating due to air friction. Due to their low heating, these dust-sized particles reach the earths surface. The small meteors have enough mass to cause sufficient friction to completely burn up during entry, and so never reach the earth's surface. The very large meteors acquire enough kinetic energy to totally vaporize on impact, leaving nothing but a crater (Meteor Crater, Arizona). Since microscopic meteor material is very hard to recover due to its small size, meteors that reach the earth's surface and can be recovered are limited to between fist-sized and several tons.

Any meteor material that survives passage through the earth's atmosphere and reaches the surface is termed a meteorite. Due to the short time it takes to pass through the earths' atmosphere, meteorites only burn on a thin outer layer, so the preterrestrial structure is preserved on the inside of the meteorite.

II. Classification

Meteorites are divided into three groups: stones, stony irons, and irons. The stone meteorites consist primarily of silicates. The stony irons consist of

approximately half silicates, half iron-nickel metal. The iron meteorites consist primarily of iron-nickel metal, but also contain many nonmetallic inclusions. The majority of meteorites are of the 'stony' variety, with only 7% of the meteorites being iron meteorites. In this thesis the discussion is limited to the iron meteorites.

The iron meteorites are divided into six subgroups: nickel-rich ataxites, octahedrites, hexahedrites, nickel-poor ataxites, metabolites, and brecciated octahedrites [2].

The majority of iron meteorites fall into the octahedrite category. Generally, octahedrites contain between 7 and 11% nickel. Octahedrites have oriented plates of α precipitated along the {1 1 1} planes of the prior γ as the meteorite cooled, resulting in what is known as the Widmanstatten pattern [3].

Hexahedrites contain less than 7% nickel. Upon cooling, initially the hexahedrites form the oriented α plates as in the octahedrites. Due to their low nickel content, upon cooling the α field of the phase diagram is entered and the α plates grow until the meteorite appears as large single crystals of α [4].

The nickel-poor ataxites are very similar to hexahedrites, and due to their similarity in nature, nickel-poor ataxites are often grouped with hexahedrites. Many current researchers have eliminated this group [4],

and meteorites previously classified as nickel-poor ataxites have been reassigned. So the nickel-rich ataxites are often just referred to as ataxites.

The nickel-rich ataxites generally consist of more than 12% nickel [2]. Ataxites do not display the Widmanstatten pattern that is common in most iron meteorites. Ataxites structure often is not discernable macroscopically [4].

Metabolites are low-nickel, 7 to 11% nickel, that also don't exhibit the oriented plates of the Widmanstatten pattern. It is not known whether the pattern was never initially formed or if it was removed during a possible reheating event.

Brecciated octahedrites exhibit the Widmanstatten pattern, but it's orientation changes every few inches, rather than maintaining the same orientation through out the sample [2].

There are two classification systems currently being used for meteorites. One system is based on the chemical composition, usually percent nickel, gallium, germanium, and iridium, and the second is based on macrostructure visible with a hand lens. Fortunately, the composition affects the macrostructure present, so meteorite classification by the two different criteria often agree.

Many of the iron-nickel meteorites form the distinctive Widmanstatten pattern during cooling, and the

kamacite (α-phase) band width of this pattern is used as a guide for classification.

III. Phases Present in Iron Meteorites

A. Metallic Phases

There are four major metallic structural components present in the iron meteorites: kamacite, the low-nickel α-phase; taenite, the high-nickel γ-phase; plessite, which is a general term for the two-phase mixture of kamacite and taenite, and metakamacite, α_2, a martensitic structure.

1. Kamacite

The low-nickel structure is known as kamacite, or α, and is also commonly called ferrite. Kamacite is body-centered cubic (bcc) ferritic iron with up to 7.5% nickel in solid solution, with the nickel substituting into the iron sites of the bcc lattice [4]. It is a homogeneous structure, with the exception of a nickel depletion near the α/γ boundary and at interfaces with other inclusions [5]. Kamacite generally nucleates from taenite in preferred orientations as the meteorites slowly cools from high temperatures.

2. Taenite

The γ-phase, or austenite, has the face-centered cubic (fcc) structure and is significantly harder than kamacite, and is known as taenite. Taenite that is present at room temperature consists of at least 25% nickel in solid solution. Taenite is stable at higher temperatures, but as the meteorite cools, the low-nickel kamacite nucleates and grows in it, until the only taenite remaining at room temperature is in the form of retained stringers between the kamacite plates [4].

3. Plessite

Plessite is a general term for the two-phase mixture of kamacite and taenite that forms in the retained taenite stringers during cooling. Plessite is believed to be the product of different formation mechanisms, and the formation mechanism determines the morphology of the plessite.

Some of the more common plessite structures include lamellar (or pearlitic), spheroidized, and acicular (which exhibits a microwidmanstatten pattern with martensite in between the oriented kamacite bands). It is also not uncommon to see coarsening or spheroidization of these plessitic structures.

4. Metakamacite

Metakamacite, α_2, is formed by a martensite transformation at low temperatures, and is often referred to as martensite due to it's similarity in appearance to the structure found in steels. Metakamacite has the body-centered tetragonal crystal structure (distorted bcc), and is usually either lath or lenticular in nature. The morphology has been found to depend on the nickel content, with lenticular martensite forming when the nickel content is greater than 20% [6].

B. Non-metallic Phases

There are also many nonmetallic phases found in iron-nickel meteorites. Minerals such as phosphides, carbides, and sulfides are quite common in some meteorites, and these often have a direct effect on the resulting microstructure.

1. Cohenite

Cohenite, $(Fe,Ni)_3C$, is a common carbide that has an orthorhombic structure and is hard (Vickers hardness of 1100) but also ductile [4]. Cohenite contains up to 3% nickel. It has only been observed in meteorites containing

less than 7% nickel, and cohenite typically grows within the kamacite [7].

2. Schreibersite and Rhabdite

Schreibersite and rhabdite are a common phosphide, $(Fe,Ni)_3P$, that have the same chemical composition and crystal structure, but differ in morphology. This phosphide is tetragonal in structure, magnetic, and softer and more ductile than cohenite [4]. Schreibersite is usually large globular particles, while rhabdite is small and prismatic in cross-section and needle-like in three dimensions. Rhabdite is usually found in meteorites with lower nickel contents, within the kamacite bands [8]. Schreibersite tends to nucleate at the kamacite/taenite grain boundaries [8].

3. Troilite

Troilite, FeS, is also a fairly common mineral in meteorites, and usually occurs as large inclusions. Troilite is nonmagnetic when pure, and is strongly anisotropic. It is often present with graphite, chromite, and numerous silicates in Group I meteorites [4]. Troilite is also commonly surrounded by successive layers of schreibersite, cohenite, and kamacite [9]. It is believed

that troilite nucleates and then serves as a heterogeneous nuclei for the above mentioned and additional non-metallic and metallic phases [9].

4. Chromite

Chromite, $FeCr_2O_4$, is quite frequently found in iron meteorites. It has the cubic spinel structure, and it is quite hard (Vickers hardness of 1100, similar to cohenite). Chromite can occur in many different morphologies, from a very cubic crystal to a massive, irregular shaped particle [4]. Chromite is often seen in the presence of troilite nodules, and along with troilite is present in the high temperature single-phase taenite region [9]. Therefore upon cooling, it often acts as a heterogeneous nuclei for other minerals.

Chapter III

LITERATURE REVIEW

The study of meteorites dates back nearly 200 years, to 1808, when Alois von Widmanstatten first revealed the octahedral structure of an iron meteorite by etching. Since then much research has been done on meteorites, with many advances on theories of origin and formation of structures of meteorites in the past 50 years.

I. Iron-Nickel Phase Diagram

The iron-nickel equilibrium phase diagram is complex (Figure 1), with the low temperature portion of the diagram still in the process of being determined. A thermodynamically calculated diagram by Chuang et al.[10] takes into account the magnetic contributions to the Gibbs free energy, and some experimental work by Reuter et al. [11] corroborates portions of the calculated diagram with physical evidence from the structures present in meteorites.

Due to the low diffusion rates of nickel in iron, time constraints make it impossible to prepare low temperature equilibrium structures in the laboratory, unless the diffusion rates are increased with electron irradiation techniques [12]. So in the study of the equilibrium phase

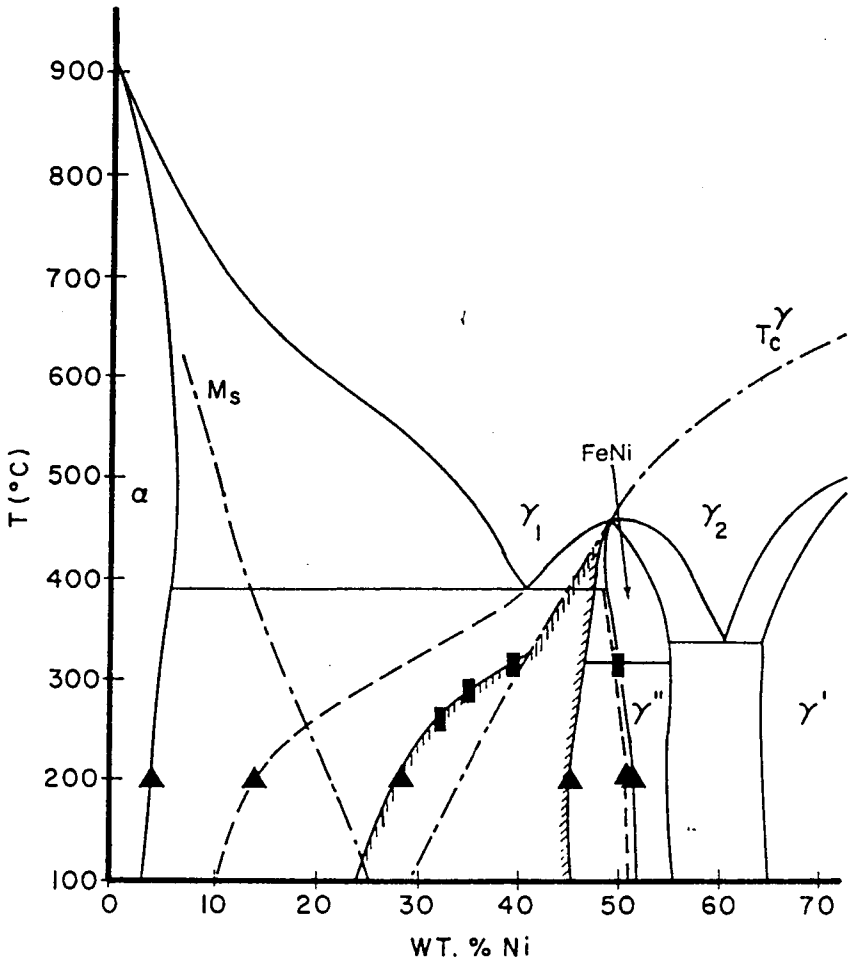

Figure 1. Iron-nickel phase diagram [11]. α is kamacite, γ_1 is paramagnetic taenite, γ_2 is ferromagnetic taenite, γ' is ordered Ni_3Fe, γ'' is ordered FeNi, and FeNi is the disordered form of γ''. Dotted/dashed lines show the M_s temperature and the Curie temperature for γ. Dashed lines show the miscibility gap, and hatched lines show the spinodal decomposition area.

diagram, the extremely slowly cooled meteorites are of great help since they are considered near equilibrium during their entire cooling process.

The iron-nickel phase diagram contains both equilibrium and metastable phase regions, since at temperatures below about 400°C thermodynamic equilibrium is never truly achieved. Therefore, since both equilibrium and metastable phases are present in meteorites that have cooled at the extremely slow rate of 700°C to 200°C over 10^8 years, the only practical diagram to consider is the metastable phase diagram [11].

The composition of meteorites fall on the iron-rich side of the iron-nickel phase diagram. They also contain small amounts of many other elements, such as phosphorous, sulfur, carbon, gallium, germanium, and iridium. Many of these elements often occur in inclusions and other precipitates in the matrix, particularly carbides, phosphides, and sulfides. However, small amounts of carbon, phosphorous, gallium, germanium, and other elements are distributed throughout the structure and may have an effect on the low temperature diffusion rate in the high-nickel phase [13], therefore affecting the final structure.

II. Common Structures in Iron Meteorites

A. Kamacite

Kamacite, or α, is the low-nickel bcc structure that is equivalent to ferrite in steels. Kamacite contains up to 7.5% nickel in solid solution, with the nickel substituting into the iron sites of the bcc lattice. It is a homogeneous structure, with the exception of a nickel depletion near the α/γ boundary and at interfaces with other inclusions [5].

Kamacite nucleates from taenite in preferred orientations as the meteorites slowly cools from high temperatures. The kamacite/taenite boundary follows the Nishiyama-Wasserman orientation relationship,

$$\{1\,1\,0\}_{fcc} \parallel \{1\,1\,1\}_{bcc},\ \langle 0\,0\,1\rangle_{fcc} \parallel \langle -1\,0\,1\rangle_{bcc}$$ [14].

B. Taenite

As previously stated, the fcc γ-phase, or taenite that is present at room temperature consists of at least 25% nickel in solid solution. Taenite is stable at higher temperatures, but kamacite nucleates and grows in the taenite as the meteorite cools, until the only taenite remaining in the meteorite at room temperature is in the form of retained stringers between the kamacite plates.

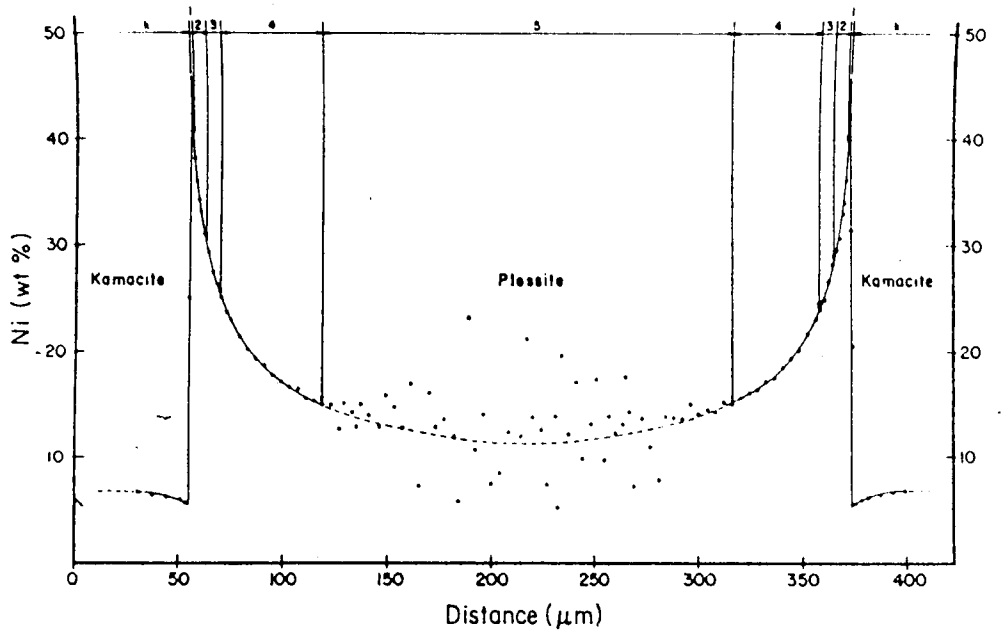

Figure 2. Typical M-type concentration profile of a retained taenite stringer [14].

These stringers exhibit an M-type nickel concentration profile due to the low nickel diffusion rate at lower temperatures, see Figure 2.

Different structures correspond to the differences in composition as a retained taenite stringer is crossed. A typical taenite stringer can be divided into five regions: 1) Clear Taenite 1, 2) Cloudy Zone, 3) Clear Taenite 2, 4) Martensite, and 5) Plessite [15], see Figure 3.

1. Clear Taenite 1

Clear taenite was named because of its appearance to early researchers under the optical microscope. Early researchers did not have the necessary equipment to detect the ordered structure of the region, so the region was termed 'clear taenite'.

Clear taenite 1, or CT1, through electron diffraction studies, has been found to be ordered FeNi, with the $L1_0$ superstructure [16]. This ordered structure is known as tetrataenite. This region is believed to have formed by an order/disorder transformation below 320°C [17].

Anti-phase boundaries have been observed in this region (see Figure 3a). Anti-phase boundaries are atomic-level planar defects that correspond to areas of local disorder. These anti-phase boundaries are sometimes preferentially attacked by etchant, leading some

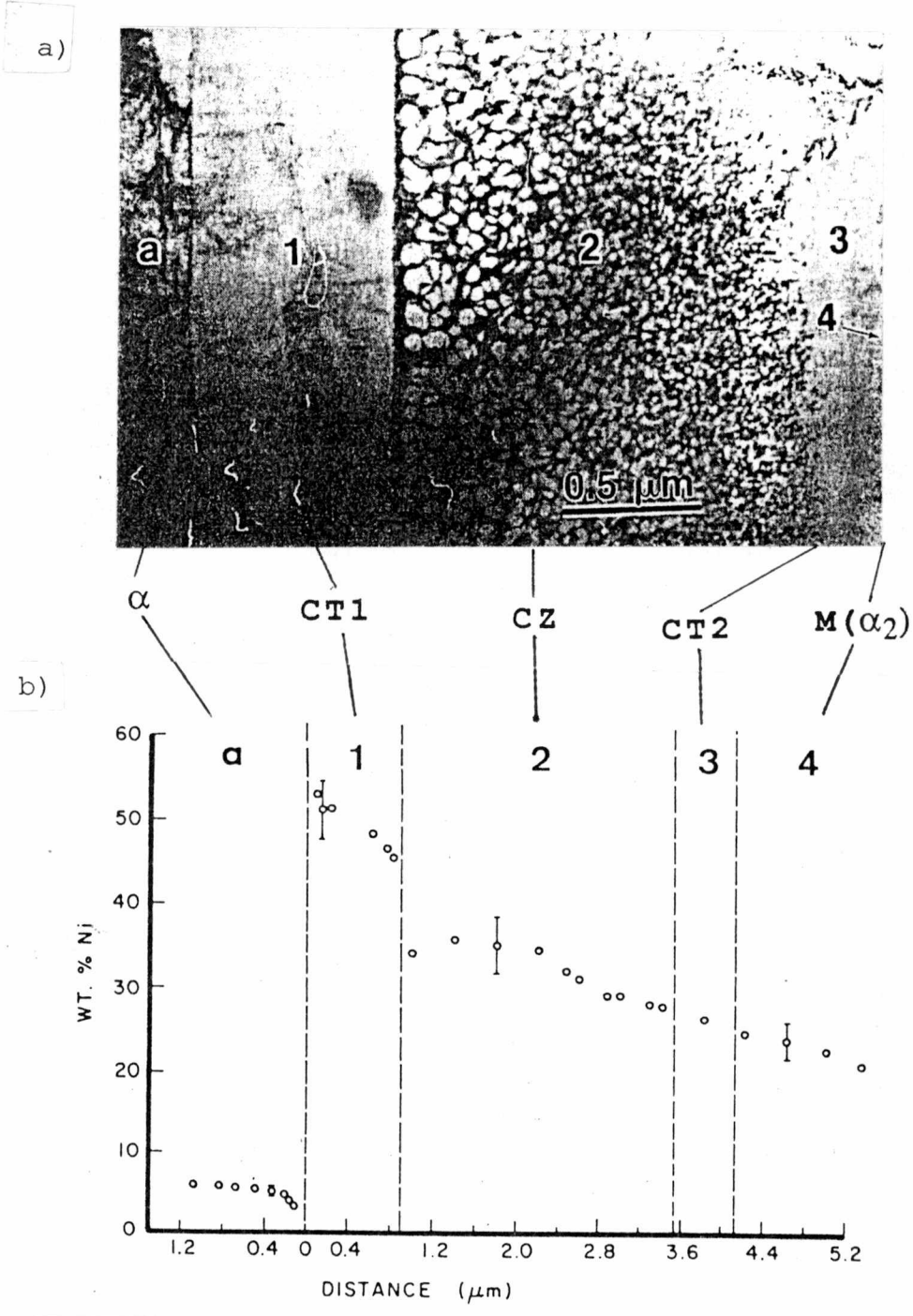

Figure 3. (a) TEM photomicrograph showing the typical structure present at an α/γ interface. (b) Typical variations in nickel content across the regions in (a) [16].

researchers to the erroneous conclusion that CT1 is a two-phase region [16].

Twins are occasionally observed in this region and are either the result of a light mechanical shock event or transformation stresses in the structure. Transformation stresses are the accepted explanation since no twins are seen in the cloudy zone [14].

The $L1_0$ superstructure breaks down into a disordered structure upon reheating, and its absence is a good indication of the whole mass being subjected to reheating after the initial cooling process [18].

2. Cloudy Zone

The cloudy zone also derived its name from the appearance of the region to early researchers. Optical microscopes do not offer enough magnification to resolve this two-phase structure, and optically it appears 'cloudy'.

The cloudy zone, CZ, is a fine two-phase region, Figure 4, that consists of a globular region, which is ordered FeNi, and a surrounding honeycomb-like region, which is described as a martensite-like phase.

The ordered globular phase has been identified as tetrataenite with the $L1_0$ superstructure. Tetrataenite is also found in the CT1 region, but the tetrataenite found in

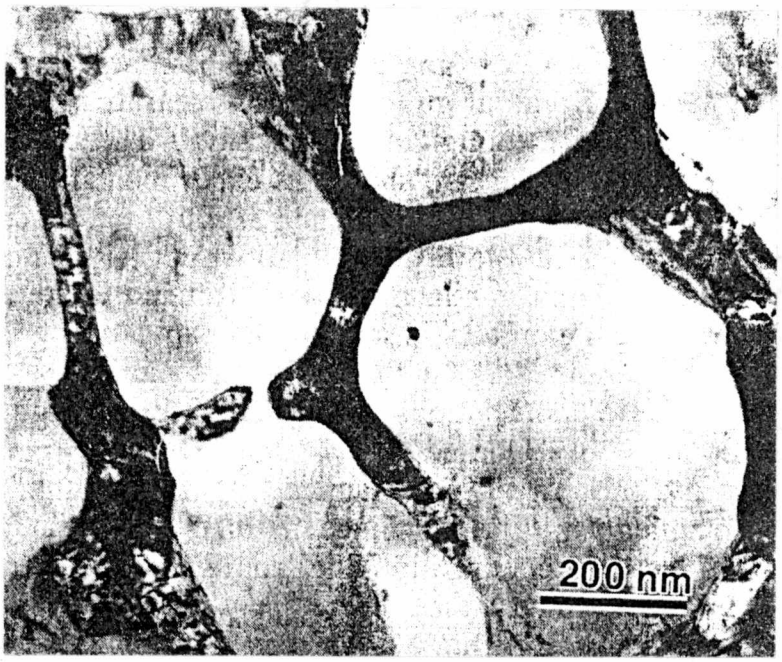

Figure 4. TEM photomicrograph of the two-phase cloudy zone, consisting of tetrataenite and martensite [16].

the cloudy zone is metastable compared to the tetrataenite found in the CT1 [11]. The tetrataenite in the CZ is considered metastable because it is believed to have formed through a spinodal decomposition reaction [17], which will be further discussed later. These regions of tetrataenite range in size from 500 to 4000Å [19].

The honeycomb region corresponds to the α-phase, which at room temperature is a martensitic structure [19]. It is not known whether the honeycomb structure is martensitic in nature before sample preparation, or if etching and thinning techniques transform another metastable structure to martensite [18,19]. Investigation has shown that this two-phase structure follows the Kurdjumov-Sachs orientation relationship;

$$\{1\,1\,0\}_{fcc} \parallel \{1\,1\,1\}_{bcc} \; ; \quad \langle 1\,-1\,1\rangle_{fcc} \parallel \langle 0\,-1\,1\rangle_{bcc} \quad [14].$$

The nickel concentration gradient of the cloudy zone varies from meteorite to meteorite, but it decreases from the CT1/CZ interface to the CZ/CT2 interface as the CZ is traversed. It has been hypothesized that this decrease in nickel concentration across the CZ has one of two explanations. First, the gradient could be explained by a decrease in the nickel composition of both phases throughout the cloudy zone as the CZ/CT2 interface is approached. The second explanation predicts a decrease in the percentage of the high-nickel globular phase with a corresponding increase in the low-nickel honeycomb phase as

the CZ/CT2 interface is approached. Careful investigation has shown that the composition of each phase seems to remain constant throughout the cloudy zone, so the second explanation is the more accepted one [16].

Through electron diffraction pattern analysis, the honeycomb structure has been determined to have the bcc lattice structure, but it is difficult to determine whether the honeycomb phase is kamacite or martensite due to the near identical value of the lattice parameters ($a_o(K)=2.864\times10^{-8}$cm, $a_o(M)=2.875\times10^{-8}$cm) [16]. At room temperature, the low-nickel content of this phase places it below the martensite start temperature, and so it is expected to be a martensitic structure. This assumption is confirmed by the appearance of many dislocations in a fine-scale lath-like structure [16].

The formation of the CZ is not due to a martensite decomposition reaction because of the high percent nickel present, which inhibits martensite from initially forming during cooling. From the latest proposed phase diagram, it is now thought that the CZ is formed through a magnetically induced spinodal decomposition reaction across an asymmetric miscibility gap, which is confirmed by the intimate mixing and high connectivity observed in meteorite samples [11]. The discontinuity in percent nickel between CT1 and the CZ can be explained by the low temperature

eutectoid transformation:

$$\gamma \rightarrow \alpha + FeNi \qquad [17].$$

Under equilibrium, when the low-nickel bcc cloudy zone is formed, a local increase in the percent nickel in CT1 near the interface is expected to occur. Investigation has revealed no such increase, so the formation of CZ, CT2, and martensite is considered a metastable transformation [16]. The duplex structure of the CZ consists of ordered FeNi and martensite, and upon reheating the FeNi becomes disordered, so the absence of the CZ is a strong indication of reheating [6].

3. Clear Taenite 2

On the other side of the cloudy zone is a region known as clear taenite 2, or CT2. This structure is also ordered, but it has been difficult to determine the exact superstructure of this region. From diffraction pattern studies, it is either ordered Fe_3Ni with the $L1_2$ superstructure, or ordered FeNi (tetrataenite) with the $L1_0$ superstructure. However it is difficult to determine which of the two structures is present since the $L1_0$ variants overlap the $L1_2$ lattice reflections. Due to the low nickel contents involved, the structure is believed to be the $L1_2$ Fe_3Ni, but it cannot be verified due to the overlapping effect of the diffraction patterns [16].

No twins are observed inside the CT2 region, unlike the tetrataenite in the CT1 region [6].

4. Martensite and Plessite

Beyond the CT2 region, the nickel content continues to decrease below the composition of the three previous regions (CT1, CZ, and CT2) present in the taenite stringers. In the center of the stringer, where the M-type concentration profile is at a minimum, martensitic or plessitic structures are often found. These structures are found in the center of the taenite stringers since they are stable at lower nickel concentrations than the other structures present in the retained stringers. In these stringers, the retained taenite becomes unstable, and either undergoes a martensitic transformation or a local decomposition into a fine mixture of kamacite and taenite, termed plessite [14]. Plessitic structures will be discussed in detail in the following section.

The presence of these inner structures are somewhat related to the stringer thickness, for when the stringer is too thin, the M-type profile does not reach a low enough nickel concentration for some or all of these structures to form.

C. Plessite

Plessite is a general term for the two-phase mixture of kamacite and taenite that is the last to develop in a retained taenite stringer during cooling. Plessite was originally thought by early researchers to be a eutectoid structure, but they were unable to reproduce it in the laboratory.

Presently, plessite is believed to be the product of different formation mechanisms: either an exsolution of kamacite and taenite from unstable taenite, or a martensite transformation possibly followed by a decomposition reaction. Which transformation mechanism occurs determines the form of the plessite present in the stringer.

These transformations have been previously categorized [20] as follows. The localized decomposition of unstable retained taenite into a mixture of kamacite and taenite, $\gamma \rightarrow \alpha + \gamma$, is termed Type I plessite. Type I plessite forms because the middle of the retained taenite stringer is so far from equilibrium that a localized decomposition is undergone in order to stabilize the structure [20].

Type II plessite describes the martensite reaction product, $\gamma \rightarrow \alpha_2$, where fcc taenite transforms to the distorted bcc martensite through a diffusionless transformation [20].

The metastable martensite may then decompose into a

mixture of kamacite and taenite, $\gamma \rightarrow \alpha_2 \rightarrow \alpha + \gamma$, which is termed Type III plessite. At around 25% nickel, which is the average composition for the middle of the taenite stringer upon cooling, the γ-phase goes through a diffusionless transformation to the metastable martensite. Upon further cooling, the martensite possibly may decompose to a more stable two-phase kamacite and taenite structure [20].

The martensite decomposition occurs by a shear mechanism, which requires no thermal activation or solute diffusion, so it is unaffected by the slow diffusion kinetics at low temperatures [11]. Evidence for this decomposition reaction is supported by the fact that the taenite regions present in the plessite do not have the same orientation as the parent taenite [14].

The cloudy zone is sometimes referred to as Type IV plessite.

All the factors that determine which of these different structures will form are not known, but some postulate that local concentrations of other elements, particularly carbon and phosphorous, may play an important role in the determination of the plessitic structure [5]. Localized increases in the percent carbon can depress the martensite start temperature so that the decomposition of martensite to kamacite and taenite is inhibited [6]. Other theories state radiative heating or impact shock events

have an effect on the final structure present [4].

D. Non-metallic Structures

Non-metallic inclusions are often found in meteorites, and sometimes have a direct effect on the resulting structure. Minerals such as phosphides, carbides, and sulfides are quite common in some meteorites. Cohenite, $(Fe,Ni)_3C$, a common carbide; schreibersite and rhabdite, $(Fe,Ni)_3P$, a common phosphide that have the same chemical composition and crystal structure, but differ in morphology; troilite, FeS; and chromite, $FeCr_2O_4$ are fairly common minerals found in meteorites [4]. These minerals often nucleate at higher temperatures, and therefore can act as heterogeneous nucleation sites for the kamacite upon cooling from the γ-region [9].

E. Neumann Bands

Neumann bands, which are mechanical twins, form within the kamacite during mild impact events. The Neumann bands often will fracture the minerals or other structures present, and sometimes appear degraded or are totally erased in meteorites that have been reheated. These bands are believed to be the result of a preterrestrial shock event, not due to impact with the earth's surface [4].

III. Formation of the Widmanstatten Pattern

Many iron meteorites exhibit the Widmanstatten pattern; in some cases the pattern is more fully developed than in others. By definition, all octahedrites exhibit this pattern and the kamacite band width is used for classification. Many other classes of meteorites also show the oriented pattern, with the exception of the ataxites, which show no macroscopic signs of the Widmanstatten pattern [5].

After solidification, the parent body cools very slowly, and the meteorite is in the complete fcc γ state. During slow cooling, kamacite nucleates such that it follows the relationship:

$$\{1\,1\,1\}_\gamma \parallel \{1\,1\,0\}_\alpha \; ; \; [1\,1\,0]_\gamma \parallel [1\,1\,1]_\alpha \qquad [21].$$

Kamacite nucleates with minimal undercooling if nucleation occurs heterogeneously, at the grain boundaries or inclusions [21]. At upper temperatures meteorites consist of large taenite crystals, and at these higher temperatures in the taenite region phosphide particles nucleate. Upon cooling, these phosphide particles then serve as nuclei for the kamacite. Homogeneous nucleation of kamacite is possible, but due to the large amounts of undercooling necessary, heterogeneous nucleation dominates as the primary mechanism of nucleation. So upon cooling,

kamacite usually will nucleate and grow on phosphide particles, which have nucleated at much higher temperatures in the taenite grains or at the taenite grain boundaries.

As the temperature continues to decrease, the movement of nickel from the α/γ boundary into the taenite is restricted due to the sluggish diffusion, and nickel concentration gradients are built up at the interface. As temperatures decrease, initially the maximum solubility of nickel in kamacite increases, and then decreases as temperature continues to drop. This causes a further nickel depletion on the kamacite side of the interface, and a corresponding nickel surplus on the taenite side. This is commonly known as the Agrell effect [23].

The composition at the middle of the stringers will remain near the composition of the γ-phase at higher temperatures. When temperatures reach approximately 350°C, the concentration gradients are 'frozen in', due to diffusion becoming too sluggish to allow for diffusion over distances greater than 1 micron [18,24].

The width of the kamacite bands increases as the percent nickel in the meteorite decreases. This occurs since in low nickel structures the kamacite nucleates at higher temperatures. When kamacite nucleates at higher temperatures, the growth process begins at higher temperatures, allowing longer times for growth to occur [24]. At lower nucleation temperatures, the kamacite has

less time to grow before the growth kinetics are diffusion limited.

These structures are impossible to duplicate in the laboratory for iron-nickel alloys because the diffusion rate requires such a low cooling rate for equilibrium to be maintained. Recently, ion irradiation has been shown to enhance the diffusion rates enough so that the beginning of the Widmanstatten pattern can be formed in the laboratory [24].

Phosphorous has also been shown to play a major role in the formation of the Widmanstatten pattern, with as little as 0.1 $^{w}/_{o}$ phosphorous added to an iron-nickel alloy allowing initiation of the formation of the pattern in laboratory alloys [24]. Increases in phosphorous content cause more phosphides to form at higher temperatures, giving the kamacite additional heterogeneous nucleation sites. Phosphorous also causes the γ/α transition temperature to be raised, and thus lowers the undercooling necessary for kamacite to nucleate, therefore giving it more time to grow at higher temperatures [24]. Increases in the amount of phosphorous also increase the diffusion rate of nickel in taenite [25].

IV. Cooling Rates

The retained taenite stringers between the kamacite plates have a sharp nickel concentration gradient (see Figure 2). This gradient is often called an M-profile, because the characteristic profile shows high nickel content at the kamacite/taenite interface, and decreasing nickel content across the taenite stringer toward the middle. Microprobe analysis experimentally yields this concentration gradient in taenite stringers, and using known diffusion rates for iron and nickel, the approximate cooling rates for the meteorites to give the experimentally determined gradient can be estimated. Undercooling, pressure, and plate impingement are a few of the factors that need to be accounted for in this approximation.

To a first approximation, it has been found that these alloys have cooled at rates between 0.5° and 400°C per 10^6 years [21].

Also from this data, estimates of the size of the parent body that would cool at such a low rate can be made, and diameters up to several hundred kilometers have been estimated [22]. Since the meteorites that impact the earth's surface are much smaller, these large parent bodies are believed to have fragmented after the formation of the original Widmanstatten pattern [22].

Recent studies have shown that the effect of

phosphorous content on the calculated cooling rate should not be neglected, due to its effect on the α/γ transition temperature and diffusion rate. While phosphorous does have an effect, its contribution is small and is often neglected for first order cooling rate approximations [24].

Chapter IV

METEORITE SPECIMENS

The octahedrites Arispe and Ocotillo, and the ataxite Inland Forts, were examined in this research.

I. Arispe

The Arispe meteorite is classified as a coarse octahedrite. It has been chemically classified by Scott and Wasson into group IC-An [26]. Group I meteorites are known for generally containing many inclusions. The results of previous elemental analysis of Arispe are shown in Table 1 [27]. Figure 5 shows the sample of Arispe available for study.

The Arispe meteorite was found near Sonora, Mexico, and was part of a fall consisting of at least 16 meteorites. In 1896, the first two masses were discovered, and a larger mass (124 kg) was discovered in 1898. Samples from this fall were recovered as late as 1953 by Nininger. The accumulated mass of all known meteorites retrieved connected with this shower is 683 kg. The age of Arispe is approximated at 300×10^6 years, with a terrestrial age of approximately 240×10^3 years [27].

Previous microstructural examination of the Arispe

Table 1: Previous Elemental Analysis of Arispe.

ARISPE – SELECTED CHEMICAL ANALYSES

References	percentage Ni	Co	P	ppm C	S	Cr	Cu	Zn	Ga	Ge	Ir	Pt
Hawley in Buddhue 1950	6.80	0.45	0.31	140	200		200				15.8*	
Goldberg et al. 1951	6.97	0.49							55.6			
Lovering et al. 1957		0.48				46	110		51	233		
Nichiporuk & Brown 1965											7.6	17.2
Smales et al. 1967						14	112	7.3	51	229		
Moore 1968, pers. comm.	6.69	0.46	0.31									
Wasson 1968, pers. comm.	6.54								50.8	260	9	

*The value is from Hawley (1939) and includes all platinum metals.

From [27]

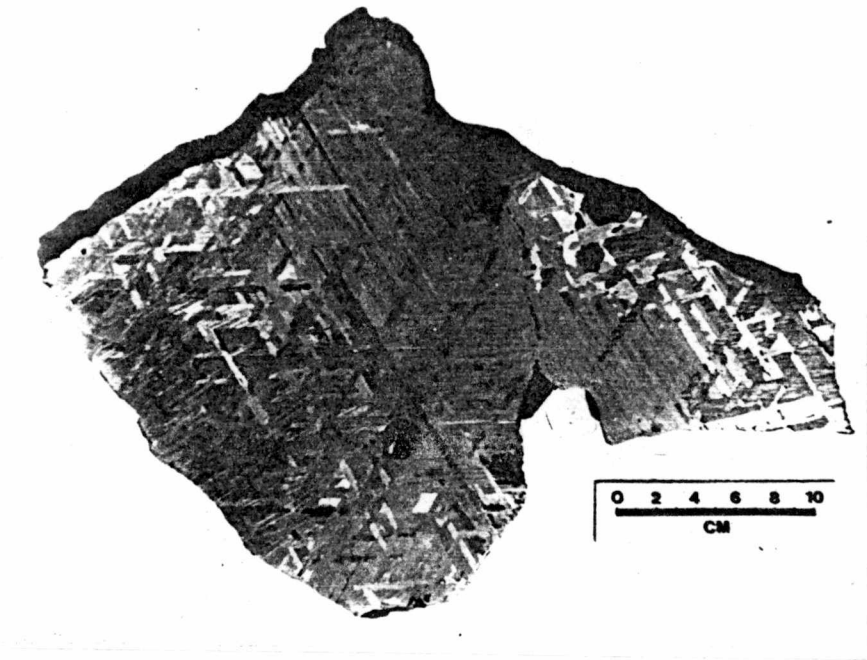

Figure 5. Section of Arispe used in this research.

meteorite has been carried out by Brooks and DeMint [28-30]. Many of the plessitic structures present in the numerous retained taenite stringers were examined, as well as identifying the general structure of Arispe and the composition of many of the inclusions present.

When Buchwald examined a section of Arispe he used the term cohenite 'nests' to describe the morphology of the cohenite. The cohenite in Arispe was comprised of these 1 - 2 cm^2 'nests', that occurred about one every 50 cm^2 [27]. This morphology of cohenite seems to be distinctive of Arispe, and has not been reported to date in other meteorites.

II. Inland Forts

The Inland Forts sample studied has been classified as a nickel-rich Type IVB ataxite [31]. It has a bulk composition of 18.9% nickel and 0.28% phosphorous, and does not exhibit a macroscopic Widmanstatten pattern [31], which is normal for ataxites.

This sample of Inland Forts has been referenced as specimen ILD83500-6. It was found in 1982, partially buried in sandy soil near Inland Forts, Antarctica [32]. The maximum length of ILD83500 is 15 cm, and the total known mass

is 2.523 kg [32]. Inland Forts has an approximate terrestrial age of 3 million years [31].

III. Ocotillo

The Ocotillo meteorite has been classified as a coarse octahedrite, Type 1A [33].

Ocotillo's structure consists of Widmanstatten kamacite plates and numerous retained taenite stringers with associated plessite present, which is typical of octahedrites. Some small non-metallic inclusions are present, with a particularly large (~1 cm^2) troilite-graphite inclusion present.

Ocotillo was discovered in 1990, in Imperial County, California. The total known mass of the fall to date is 28.57 kg [33].

Chapter V

EXPERIMENTAL PROCEDURE

I. Metallographic Sample Preparation

All meteorite samples were mounted, ground, and polished using standard metallographic techniques.

Throughout this research, on the photomicrographs OM denotes optical microscopy, SEM-SE denotes scanning electron microscopy using a secondary electron detector, and SEM-BS denotes scanning electron microscopy using a back scattered detector.

A. Arispe

The triangular section removed from the main mass termed 'A' by DeMint [34] had previously been mounted in epoxy. It was repolished using standard metallographic techniques. It was etched with 2% nital. (Heavy etching was necessary to bring out the Neumann bands.)

A rectangular section near 'B' [34] was removed with a band saw and is termed sample 'E'. This sample exhibited no particularly interesting structural features and was used as material typical of Arispe to develop a thinning technique

for preparing transmission electron microscopy (TEM) samples.

A large triangular section that contained a cohenite nest was removed from the slab using a band saw in order to prepare TEM samples through the retained taenite stringers. This section is termed sample 'F'. Figure 6 shows a schematic representation of the locations of the samples removed from the main mass.

Sample 'F' was ground and polished, and then etched with 2% nital. Optical and SEM micrographs were taken in order to document the structures present in the retained stringers prior to thinning into TEM discs.

B. Inland Forts

The Inland Forts sample was received from Dr. Michael B. McNeil in mounted and polished condition. It was repolished, and etched with 2% nital. Heavy and light etching revealed different matrix structures within this sample.

C. Ocotillo

A generally triangular sample of Ocotillo was received, having already been removed from the main mass by the geological specimen company. A fusion crust was present on

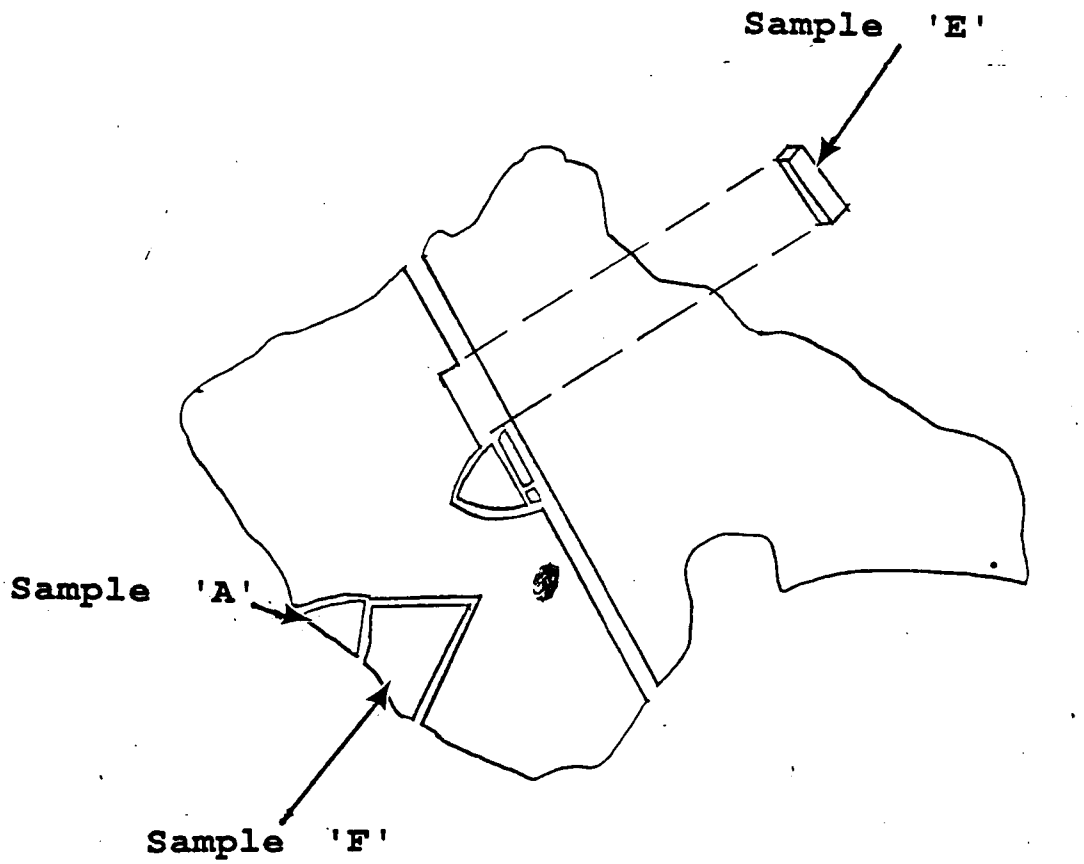

Figure 6. Schematic representation of location of samples on main slab used in this research.

one edge of the sample. It was mounted in epoxy, and ground and polished with an alumina slurry using standard metallographic techniques. A 2% nital etch was used to reveal the Widmanstatten kamacite plate structure.

II. TEM Sample Preparation of Arispe

Preparation of TEM discs involved slicing approximately 300 μm slivers of the rectangular sample 'E' with the slow speed saw, grinding the slivers down through 4/0 emery paper to approximately 100 μm, and punching 3 mm diameter discs out of the slivers. The discs were then ground to remove the burrs that occurred during punching.

At this point two approaches were taken in order to attempt to thin the discs.

In the first approach, ion milling was attempted. Prior to ion milling, the discs were dimpled, with a 40 μm dimple put in each side of the disc with a grinding dimpling machine. Then the samples were put in the Gatan Duo Ion Mill at 4V, 0.5 mA.

This approach seemed to give reasonably thin areas when examined in the TEM, but took extended times on the ion milling machine (approximately 60 hours).

The second approach involved chemical thinning, using a

jet polishing machine. The Tenupol II was used for thinning, and a 5% perchloric acid/95% acetic acid solution was the solution that was found to give the best thinning results. The Tenupol II was operated at a potential of 40 V at 25°C.

This approach seemed to yield larger thin areas, so more material could be examined in the TEM. The drawback to this thinning method was that the thinning solution would tend to dissolve some mineral inclusions at a rapid rate, not allowing the disc to be properly thinned before the jet polisher automatically shut off due to disc break through.

After samples were thinned, they were stored in small polyethylene vials in a vacuum dessicator to minimize contamination.

III. Elemental Analysis

Qualitative elemental analysis could be determined on the scanning electron microscope (SEM) using the Energy Dispersive Spectrometer (EDS) unit. This unit only gives qualitative results; it can give an idea of the major elements present, but it cannot detect trace elements. The EDS was used to attempt to identify minerals present, as well as to confirm regions of kamacite and taenite in the structure of the meteorites after optical examination.

When analyzing small particles, even at high magnifications the surrounding matrix is excited by the beam, so all observed peaks may not be purely due to the region of interest. Therefore the possibility of matrix contribution must be taken into account in EDS analysis of small particles.

The EDS also cannot detect the presence of elements below sodium (atomic number 11), so it is impossible to detect important light elements such as carbon, nitrogen, and oxygen. These elements are often present in the minerals commonly found in meteorites, and so are crucial in the positive identification of these structures. Also, local concentrations of carbon are thought to possibly have an effect on the structure present, but the carbon content cannot be determined.

All EDS data reported are given in the format of ratio of Kα peak height for a given element to the iron Kα peak height.

IV. Contamination

During the polishing process, each meteorite had an individual microcloth that was used exclusively for that particular meteorite. This was done in order to attempt to

reduce the possibility of cross contamination between the meteorites.

All samples were stored in a vacuum dessicator to attempt to reduce the formation of corrosion products on the polished surfaces. Regardless, the taenite regions would appear to oxidize after a few weeks and take on a 'fuzzy' appearance, and repolishing and etching were necessary to obtain the appearance of distinct taenite boundaries.

Chapter VI

Results

I. Arispe

A. Macrostructure

Macroscopically, the Arispe meteorite exhibited Widmanstatten oriented kamacite, the presence of non-metallic inclusions, and Neumann bands.

1. Widmanstatten Kamacite

Upon etching, the Widmanstatten pattern is obvious in Arispe (Figure 7). Arispe consists of approximately 95% Widmanstatten kamacite. These oriented plates are coarse (2.9 mm [27]), and contain many non-metallic inclusions. Some kamacite plates contain many rhabdite crystals, and there are also areas that show high concentrations of Neumann bands. On a macroscopic level, these structures appear to be pits and scratches.

The Arispe sample was originally polycrystalline, with three prior taenite grains (one large, two small) observable (Figure 7a).

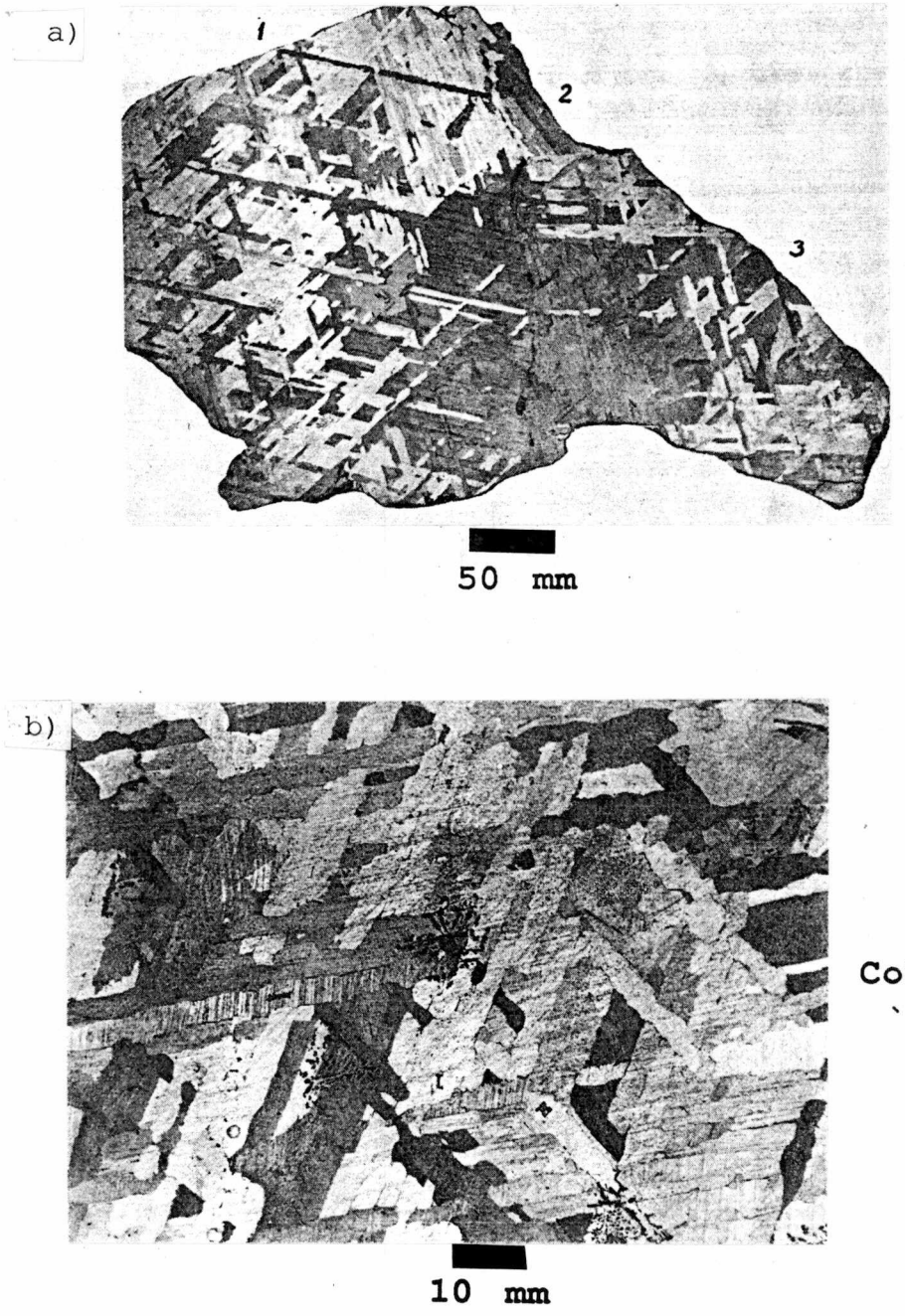

Figure 7. (a) Typical Widmanstatten pattern in Arispe. (b) Detail of Widmanstatten pattern in Arispe, with cohenite 'nests' visible [26].

2. Non-metallic Inclusions

The cohenite 'nests' and some of the larger schreibersite particles could be macroscopically seen in Arispe (Figure 7b).

a. Cohenite

The cohenite that is present in Arispe often appears as 1 - 2 cm^2 'nests', which are clearly visible on the etched surface. Retained taenite stringers can also be distinguished within these dense regions of cohenite. These structures have not been confirmed with EDS as cohenite since carbon cannot be detected, but the morphology of the structure matches Buchwald's description of cohenite nests. Sample 'A' was sent to George Vander Voort, and he used a electron microprobe to determine that these structures were carbon bearing [35].

b. Schreibersite and Rhabdite

The schreibersite was not as easily discerned as the cohenite nests, but large schreibersite grains could be seen after etching. The schreibersite appeared as shiny

inclusions, not the typical long and thin structure of the retained taenite stringers.

Rhabdite crystals were visible in some kamacite plates, and they appeared to be pits during macroscopic examination.

B. Microstructure

The primary structures of interest in Arispe are the variety of plessitic structures present within the retained taenite stringers. Also of interest are microstructural features such as non-metallic inclusions and Neumann bands.

1. Plessite

The plessite structures present in Arispe exhibited a wide variety of morphologies. One determining factor appeared to be the location of the stringer, with stringers near cohenite nests showing different structures from those stringers in the bulk of the meteorite.

a. Retained Taenite Stringers in the Bulk

The predominant morphology of plessite in the bulk of Arispe was either acicular or comb plessite.

The acicular plessite has Widmanstatten oriented kamacite plates with martensite often present in the taenite between the plates. In this morphology, the kamacite probably has nucleated along the {1 1 1} planes, just as in the macroscopic Widmanstatten pattern (Figure 8).

In Arispe, Widmanstatten kamacite plates comprise approximately 95% percent of the structure, with the remaining 5% consisting of retained taenite stringers [34]. Upon formation of the microwidmanstatten pattern in acicular plessite, there is a larger percentage of taenite present, due to the higher nickel content present in the stringer. The higher nickel content of the taenite stringer formed by the Widmanstatten pattern causes the $\gamma \rightarrow \alpha + \gamma$ reaction to occur at higher nickel contents, resulting in larger amounts of γ. These regions usually, but not exclusively, consist of martensite or martensitic products, with taenite (Figure 9, 10).

Comb plessite is also often found in the bulk of the meteorite. Structure is discernable within some parts of the stringers, while other regions initially exhibit no structure due to the thinness of the stringer (Figure 11).

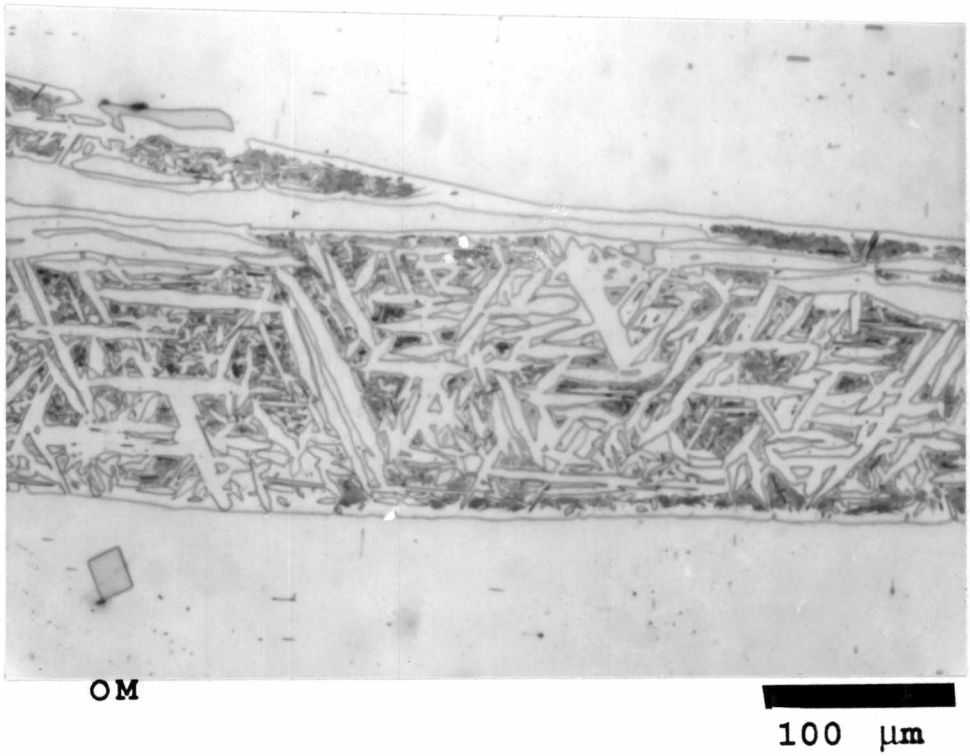

Figure 8. Typical stringer of acicular plessite located in the bulk of Arispe.

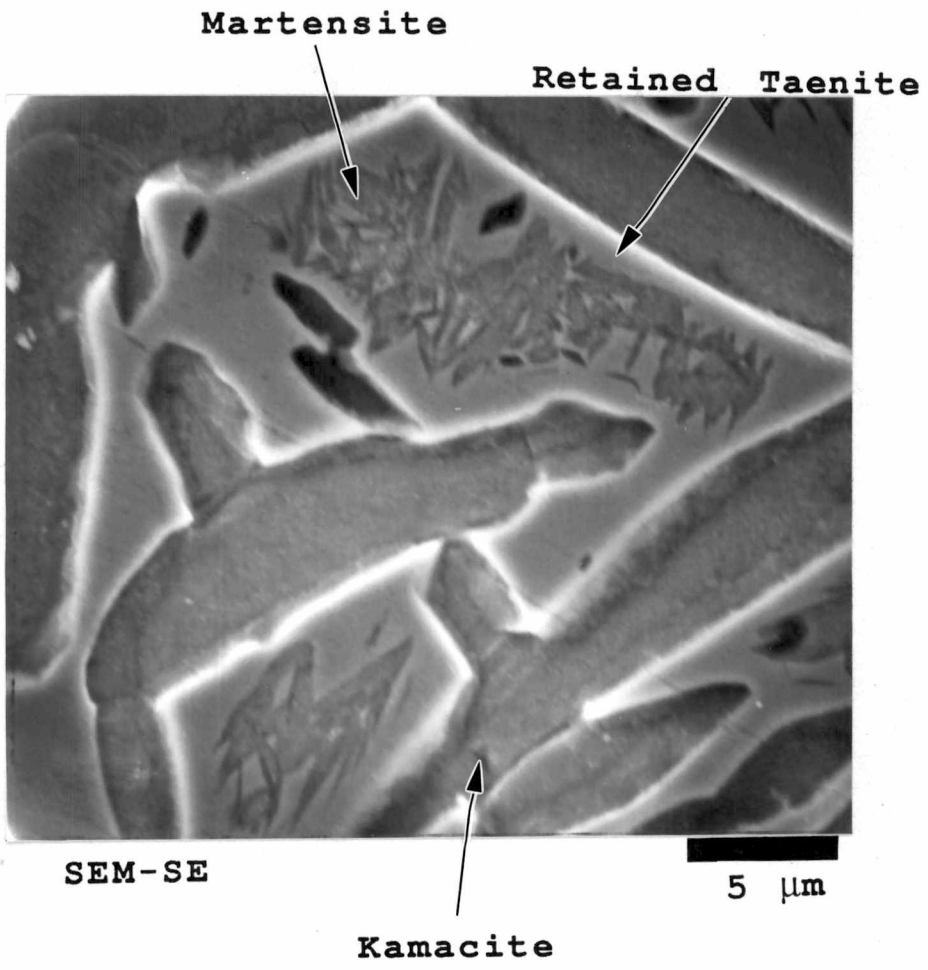

Figure 9. Acicular plessite with kamacite plates and martensite in the retained taenite.

Figure 10. Martensitic needles in the retained taenite region in acicular plessite.

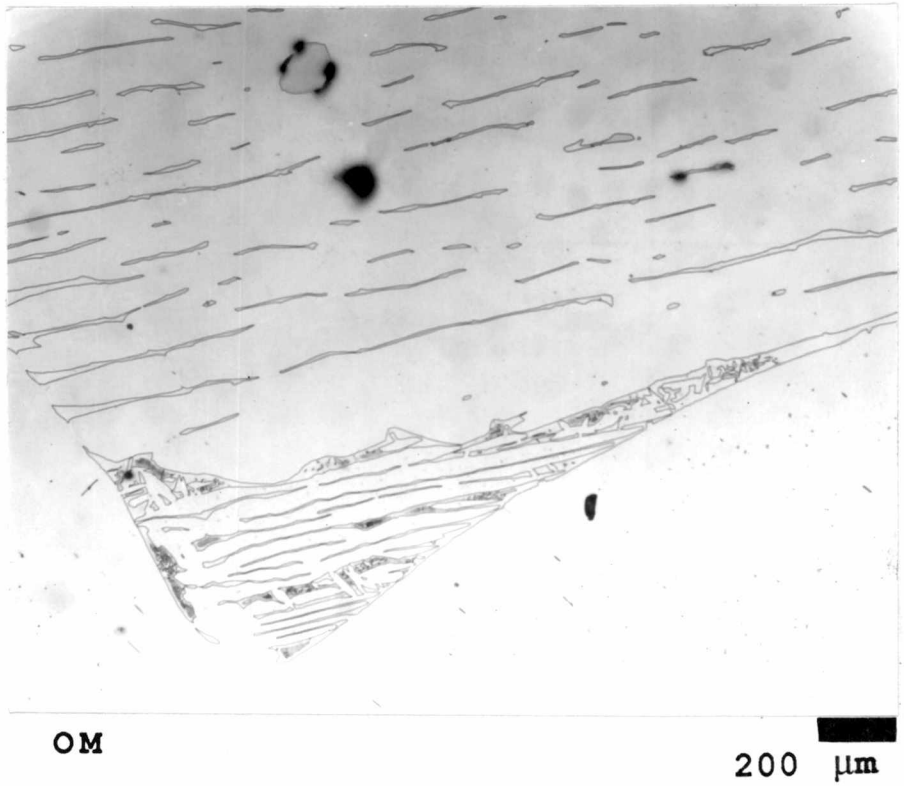

Figure 11. Typical region of comb plessite found in the bulk of the meteorite.

b. Retained Taenite Stringers Near Cohenite Nests

The plessite present in the stringers near the cohenite nests is often, but not limited to, the pearlitic morphology. Spheroidized, acicular, and martensitic plessite is not uncommon in these stringers.

Pearlitic plessite is quite common in the stringers that pass through a cohenite nest. Pearlitic plessite is composed of alternating lamallae of kamacite and taenite. The taenite lamallae are often continuous with the rim of taenite present on the edges of the stringer.

Pearlitic plessite often can be seen to spheroidize (Figure 12) and coarsen (Figure 13-16). In Figure 13a, the continuity of the taenite lamallae with the edge of the stringer is seen. Also, occasionally an interface can be seen between the regions of different coarseness at higher magnifications.

Pearlitic stringers have also been observed to have large kamacite inclusions within the plessitic structure (Figure 17). In this particular case, the coarseness of the pearlitic structure varies on either side of the inclusion. The kamacite lamallae also can be seen to be continuous with the kamacite in the inclusion.

Pearlitic plessite can compose the entire stringer, or

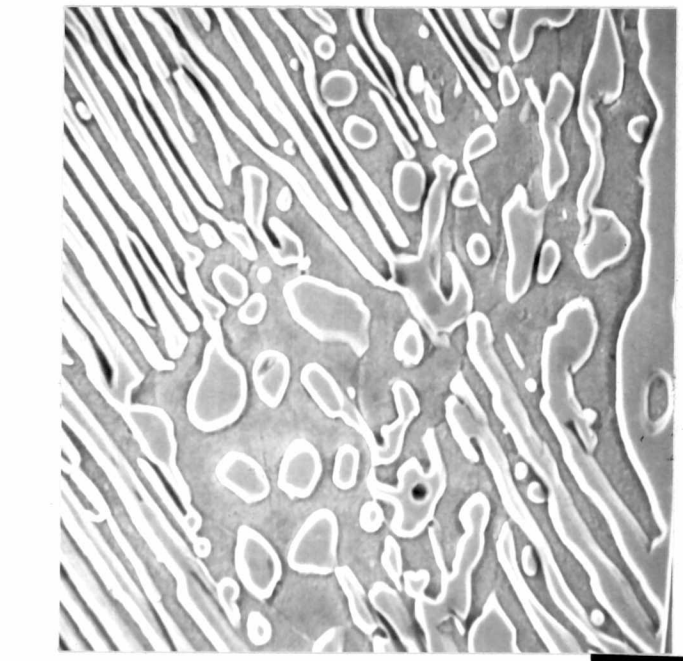

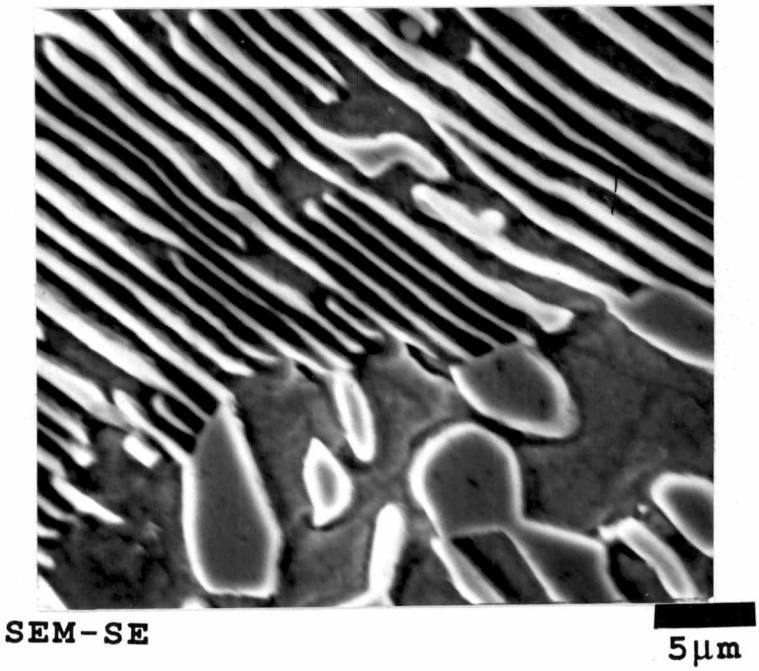

Figure 12. Typical spheroidization of pearlitic plessite.

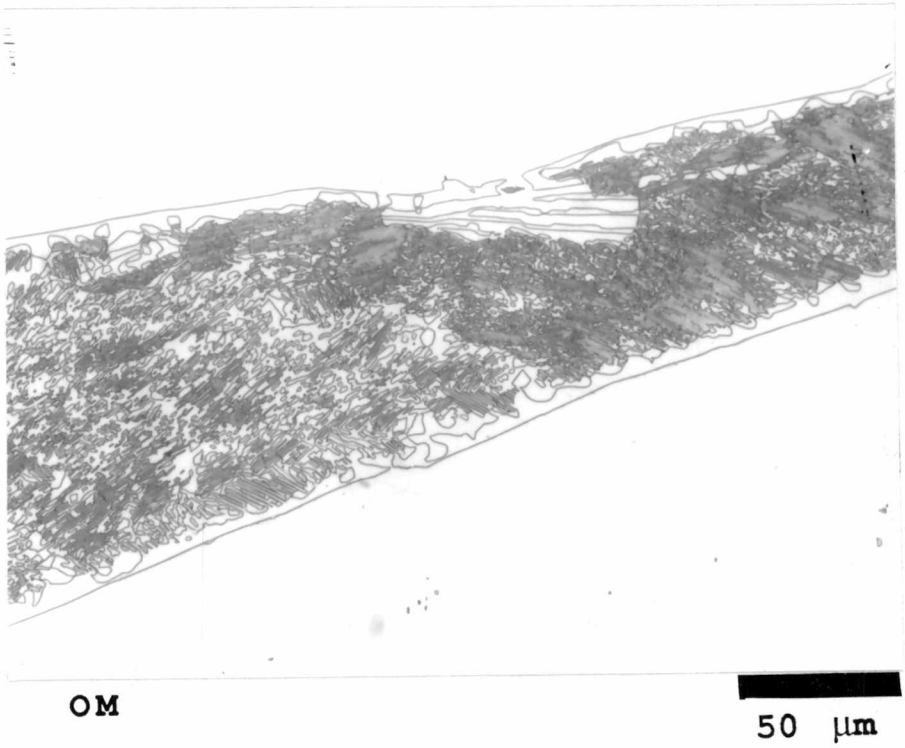

Figure 13. Typical coarsening of pearlitic plessite in Arispe.

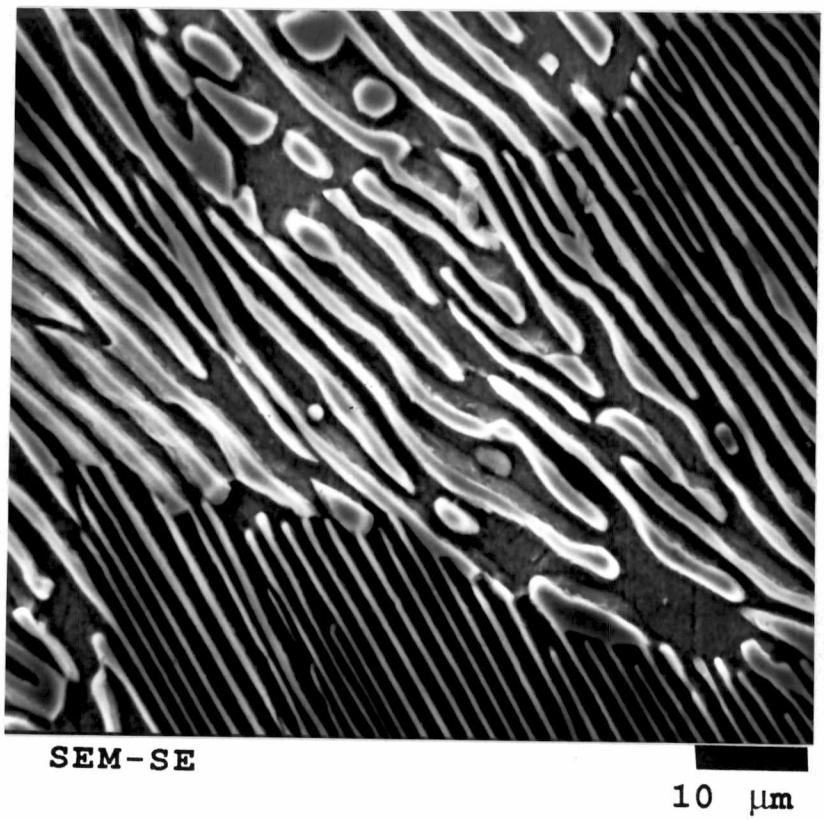

Figure 14. Coarsening reaction in pearlitic plessite.

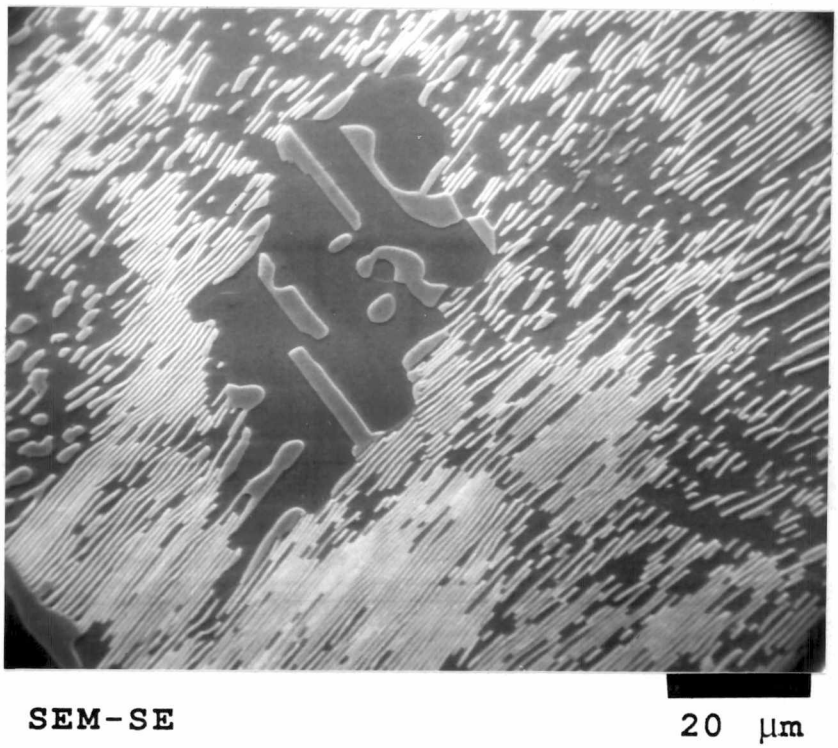

Figure 15. Region of coarsening of pearlitic plessite in Arispe.

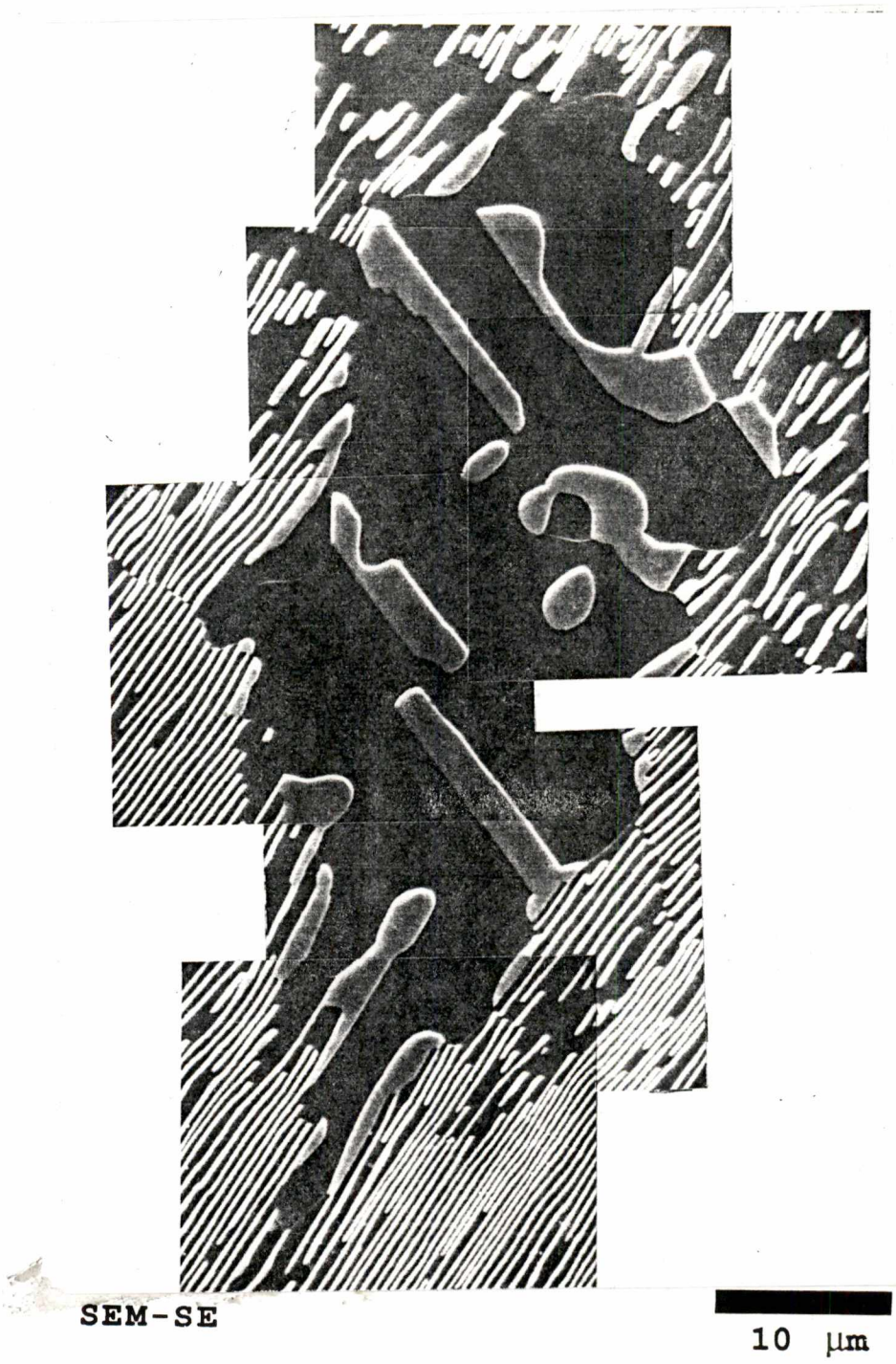

Figure 16. Complex coarsening reaction in Arispe.

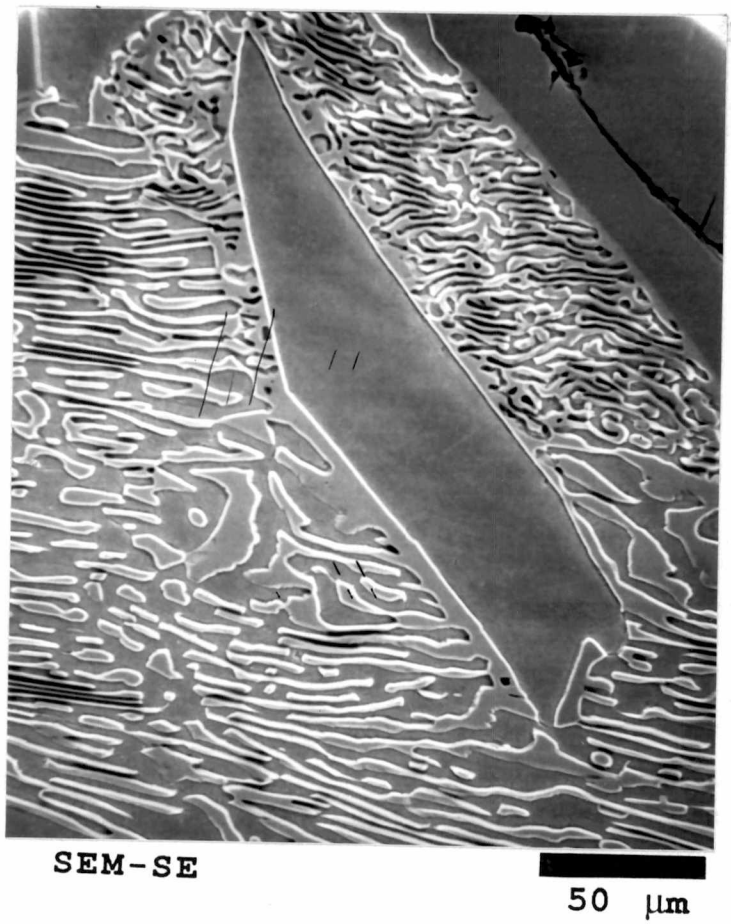

Figure 17. Large kamacite inclusion within pearlitic plessite.

be adjacent to other morphologies, such as spheroidal or acicular plessite.

Stringers have been seen to be pearlitic in nature and change to an acicular structure within a small distance (Figure 18). This structural change was usually observed only in thinner stringers. It has not been determined whether one morphology is transforming the other by the movement of an interface, or if local concentration changes are responsible for this shift in morphology.

In other areas, stringers running next to each other exhibit pearlitic, spheroidal, and acicular plessite all in close proximity to each other (Figure 19).

Stringers are also present where the plessitic structure varies across the stringer, not just along its length. One stringer (Figure 20) exhibits pearlitic structure on one side of the stringer, which spheroidizes as the middle of the stringer is approached, with acicular-type structure at the other side of the stringer. A different stringer exhibiting similar structure with a more developed acicular region (Figure 21) exhibits the presence of martensite in the taenite between the oriented plates of kamacite.

Another stringer has the appearance of typical acicular plessite. In this section of the stringer (Figure 22, 23), the taenite rim is not present. The kamacite plates are

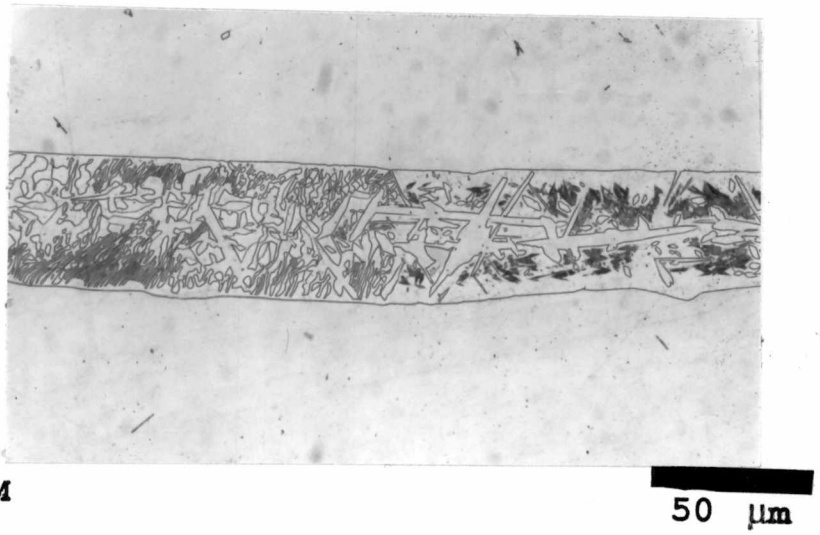

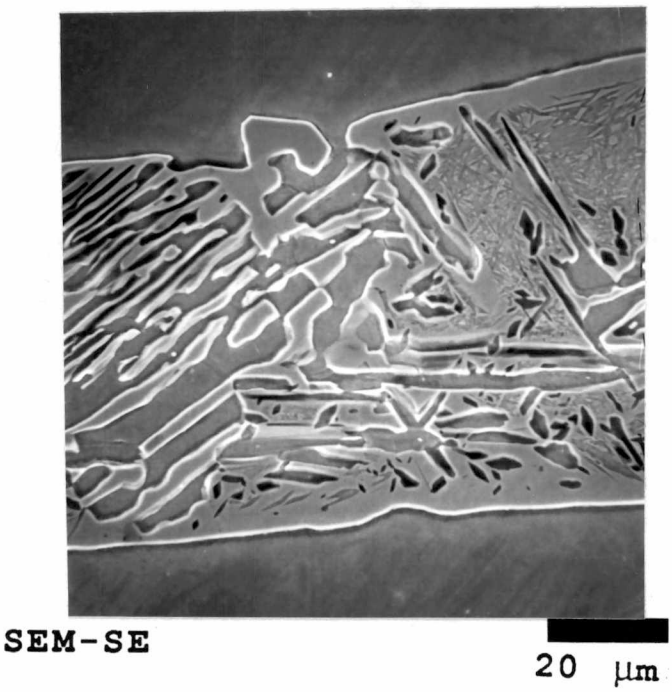

Figure 18. Stringer showing region of transition from pearlitic to acicular plessite.

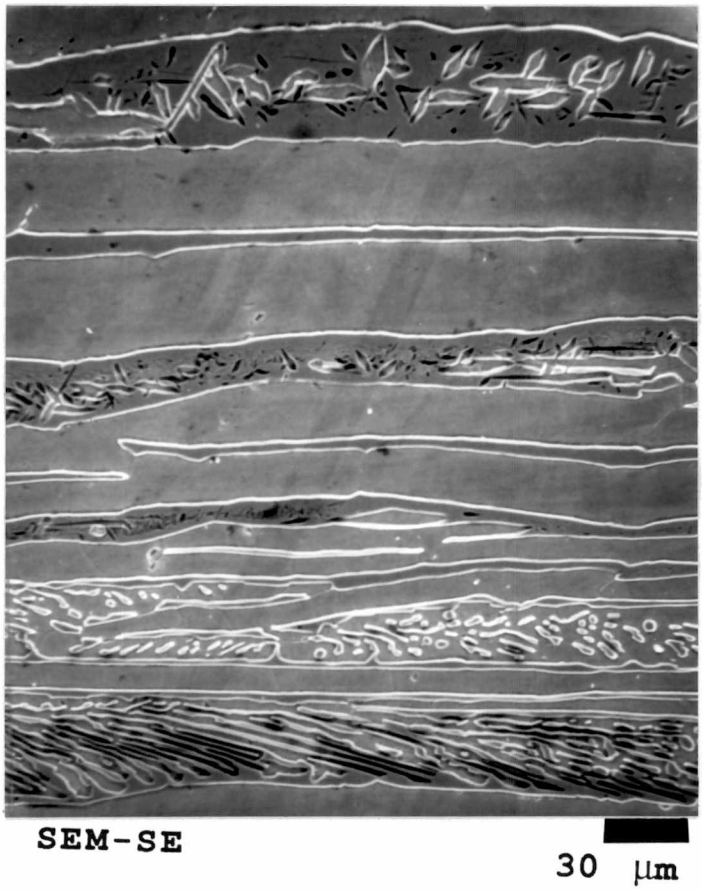

Figure 19. Pearlitic, spheroidal, and acicular plessite regions in a stringer.

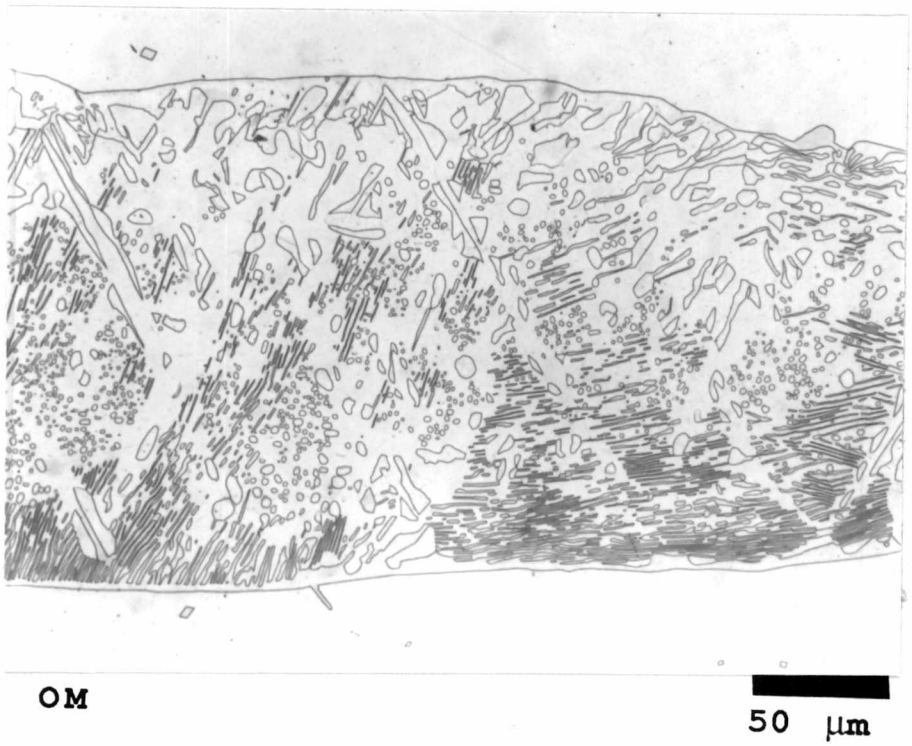

Figure 20. Multiple plessitic morphologies present in one area of a stringer.

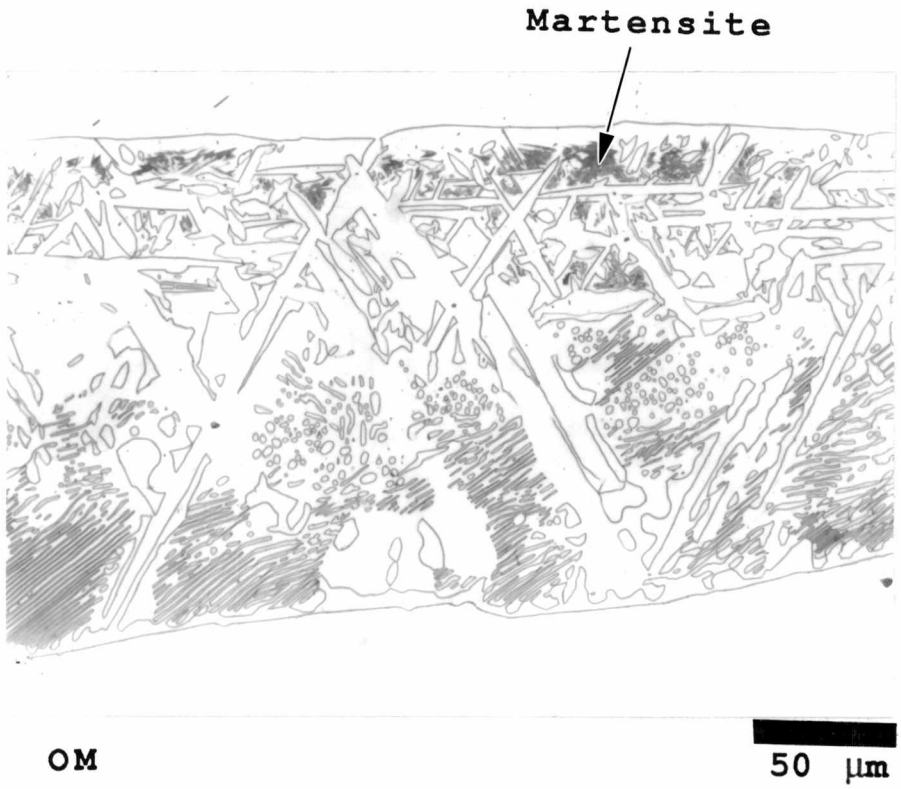

Figure 21. Multiple plessitic morphologies in a stringer with martensite present in the acicular plessite region.

Figure 22. Altered acicular plessite.

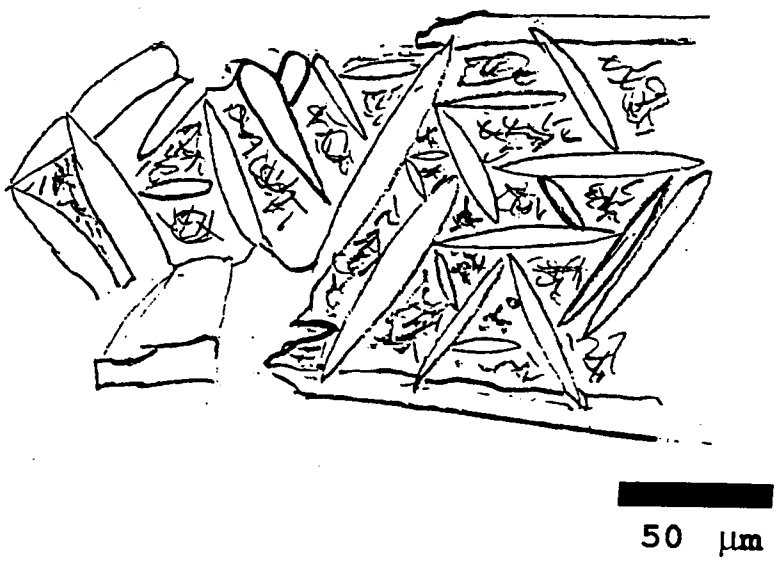

Figure 23. Schematic representation of stringer containing altered region of acicular plessite.

observed to be continuous with the surrounding kamacite, and martensite is present between some of the kamacite plates. Subgrain boundaries can also be seen, and the lower isolated region of taenite contains cracks.

One stringer observed exhibited typical acicular structure in one side of the stringer, with martensite appearing between the plates, but with an unidentified structure present between the plates in the other side of the stringer (Figure 24). This unidentified structure appears to be two-phase, with one of the phases possibly removed during etching (Figure 25). Since kamacite is preferentially attacked by nital, it could be a two-phase structure of kamacite and taenite with the kamacite removed.

2. Non-metallic Inclusions

The presence of non-metallic inclusions greatly affected the resulting microstructure of Arispe, particularly in the retained taenite stringers.

a. Schreibersite and Rhabdite

Both morphologies of this phosphide are common in Arispe. Rhabdite is found throughout the meteorite, with the

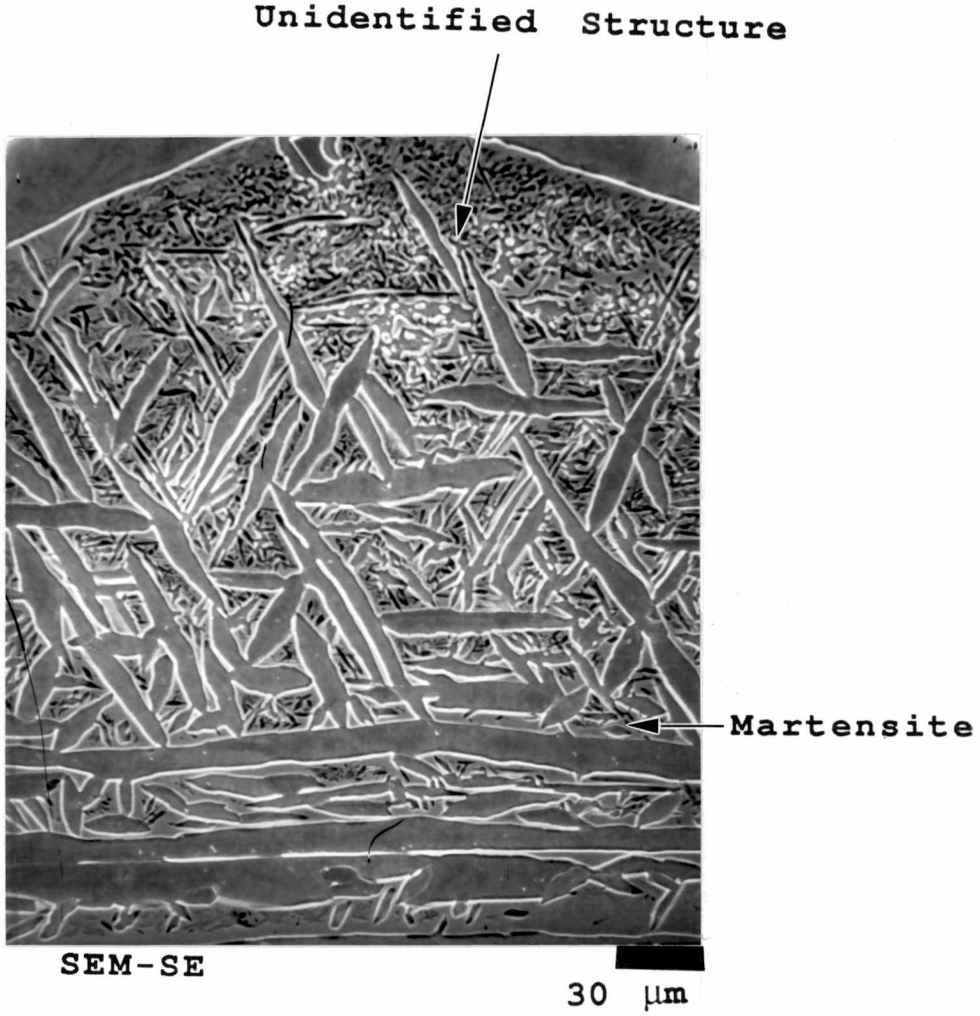

Figure 24. Stringer of acicular plessite exhibiting different structure in the retained taenite regions between the kamacite plates.

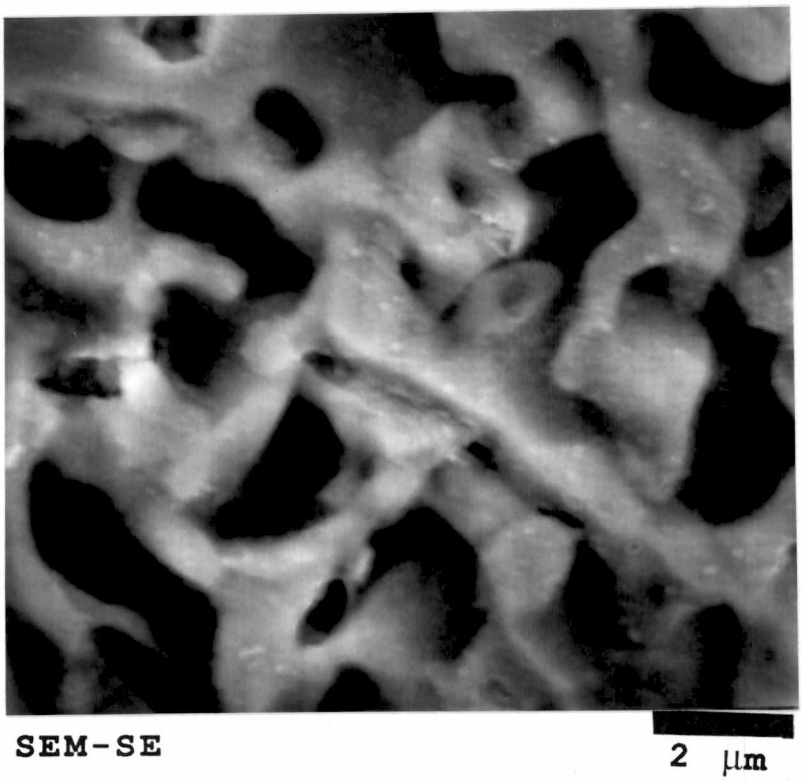

Figure 25. Unidentified structure between kamacite plates.

exception of regions that have been depleted of phosphorous by large schreibersite inclusions.

Schreibersite is found as independent inclusions, as well as being an additional mineral present in the cohenite nests.

b. Cohenite

The cohenite nests were not pure cohenite. They often included other structures such as regions of schreibersite and sometimes taenite (Figure 26, 27).

The nests seem to indirectly affect the plessitic structure present (higher incidence of pearlitic plessite near nests), but they also occasionally have a direct effect.

Occasionally the cohenite was seen to impinge into the pearlitic stringers (Figure 28). Another area shows cohenite impinging into the pearlitic structure in the lower right of the micrograph (Figure 29), as well as two particles, possibly schreibersite, inhibiting the continuation of the stringer in the upper left.

There are also cases where cohenite completely bisects a stringer (Figure 30) with small regions of taenite present with the cohenite inclusion. The stringer continued along the same path after crossing the inclusion. It is believed

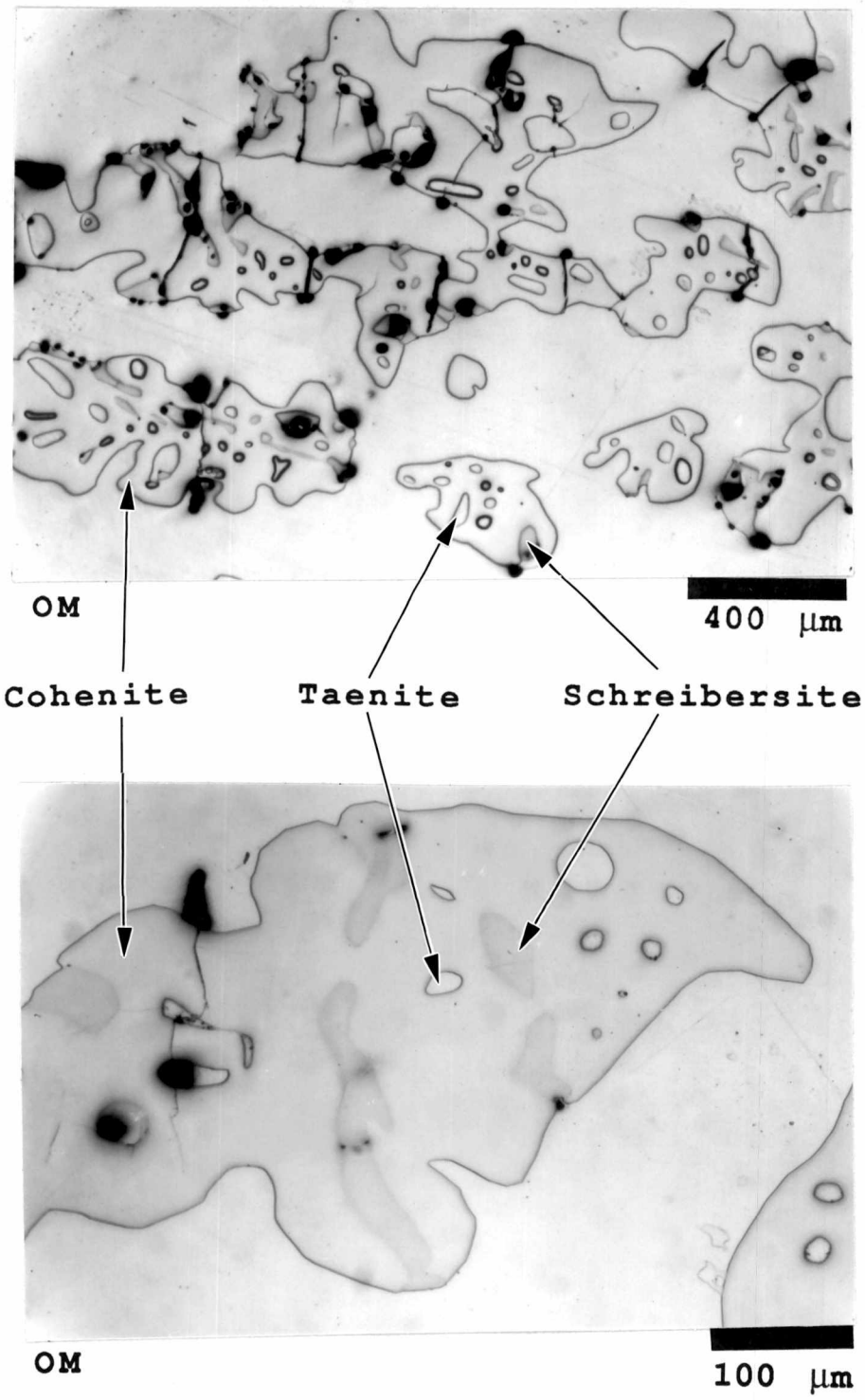

Figure 26. Typical structure of cohenite 'nests', with regions of schreibersite and taenite.

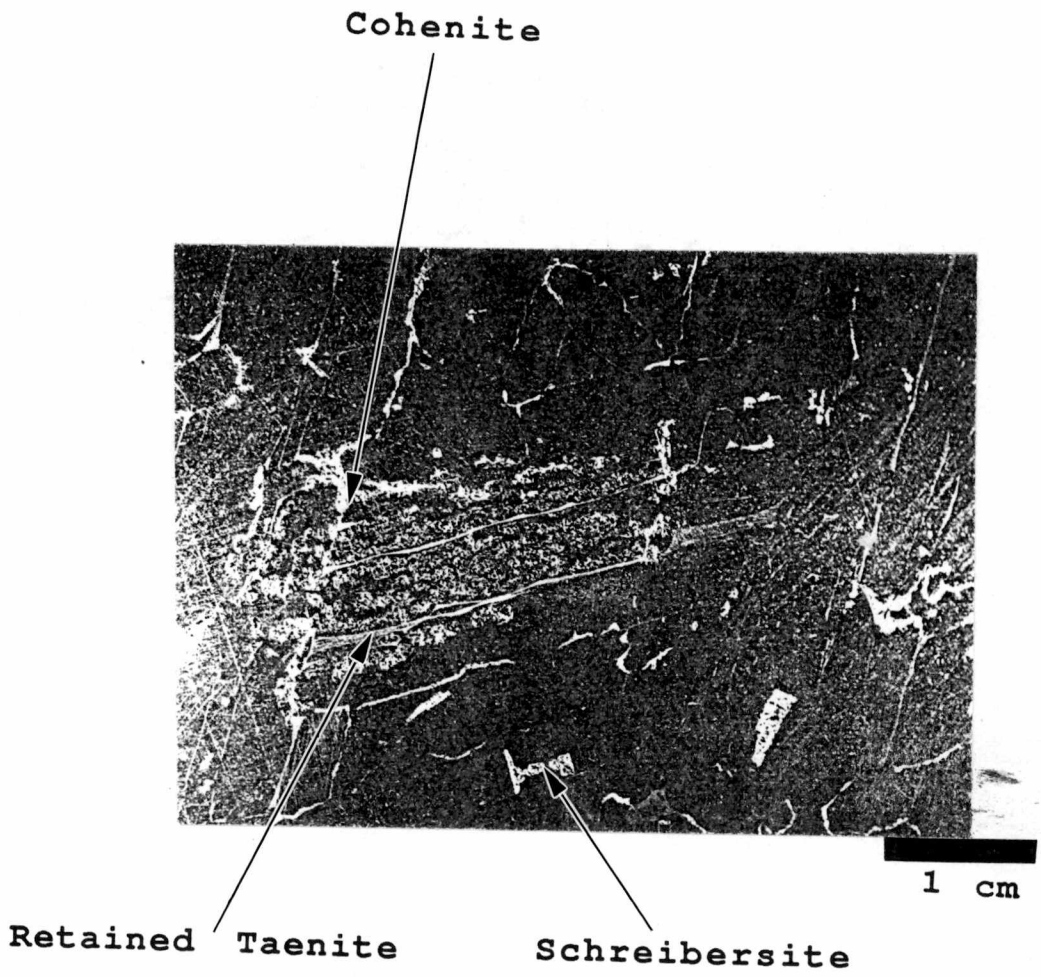

Figure 27. Cohenite 'nest'.

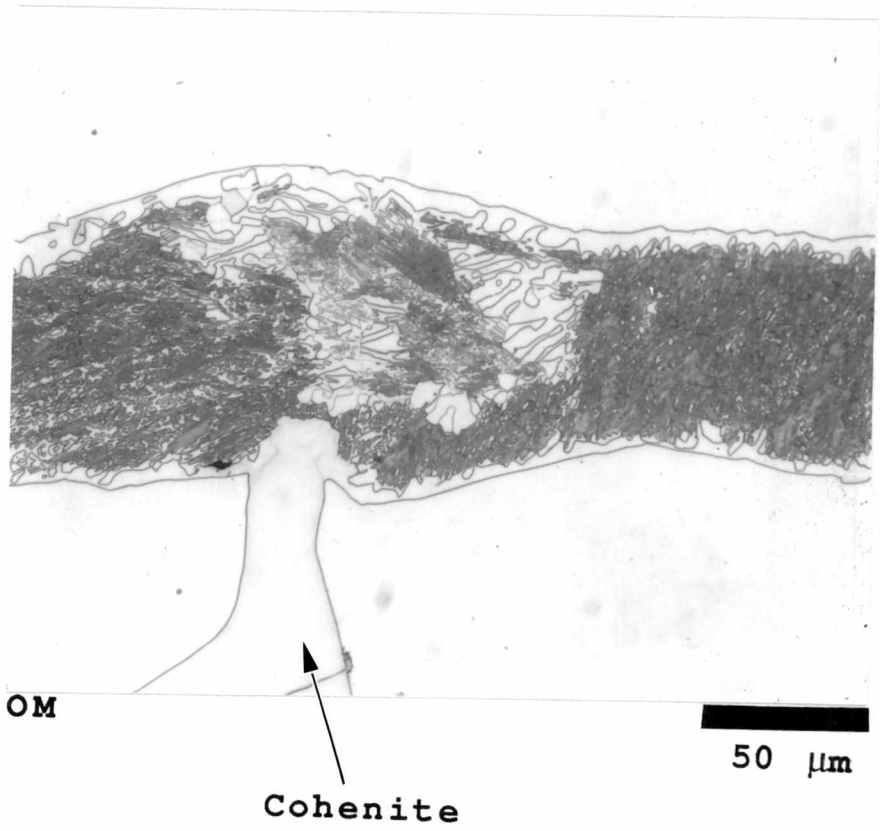

Figure 28. Cohenite impingement on pearlitic stringer.

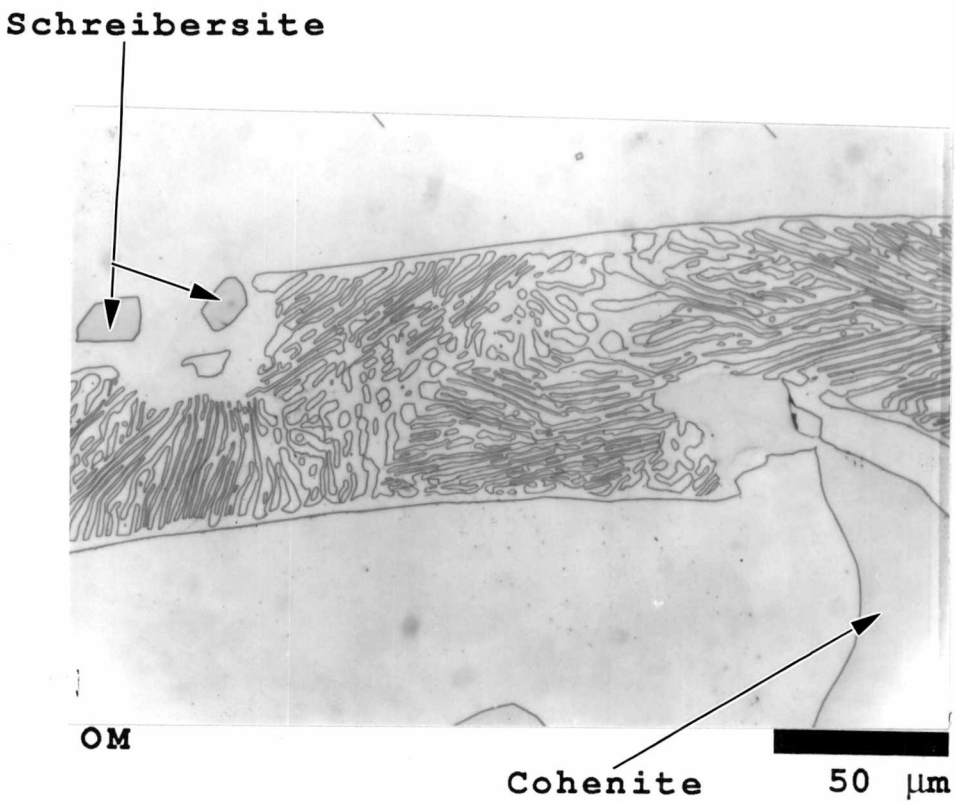

Figure 29. Cohenite impinging on taenite stringer with two schreibersite particles present.

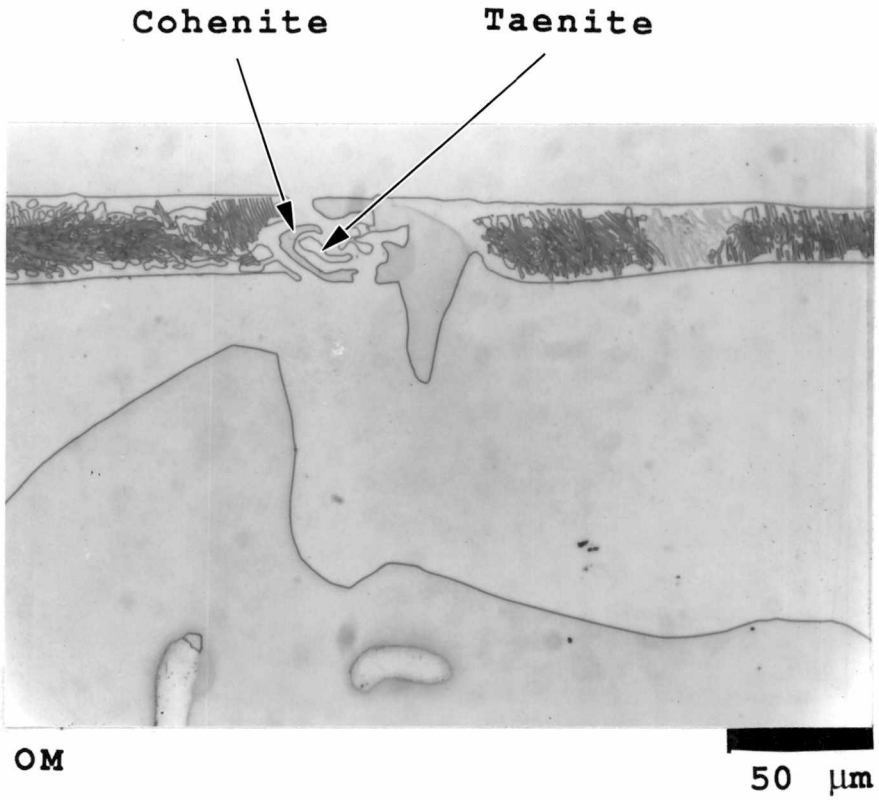

Figure 30. Cohenite and taenite inclusion completely bisecting stringer.

that the cohenite inclusion was originally present, and the stringer grew around the inclusion, since cohenite nucleates at high temperatures, but still in the two-phase $\alpha + \gamma$ region, before the kamacite plates have fully grown. Buchwald states that the carbides are some of the last minerals to form, usually precipitating from solid solution after the major structural components have formed [11].

Stringers were also seen that contained small non-metallic inclusions (Figure 31). Two neighboring stringers, one acicular, the other pearlitic and spheroidal, were observed. The inclusions had a definite effect on the structure, particularly the acicular region where the inclusion disrupted the oriented kamacite bands and appeared to be surrounded with swathing kamacite.

C. Neumann Bands

Neumann bands were plentiful in the kamacite plates of the Widmanstatten pattern (Figure 32), but did not cross into the plessitic structures in the taenite stringers. These mechanical twins are orientation sensitive, so some grains exhibited denser regions of Neumann bands than others.

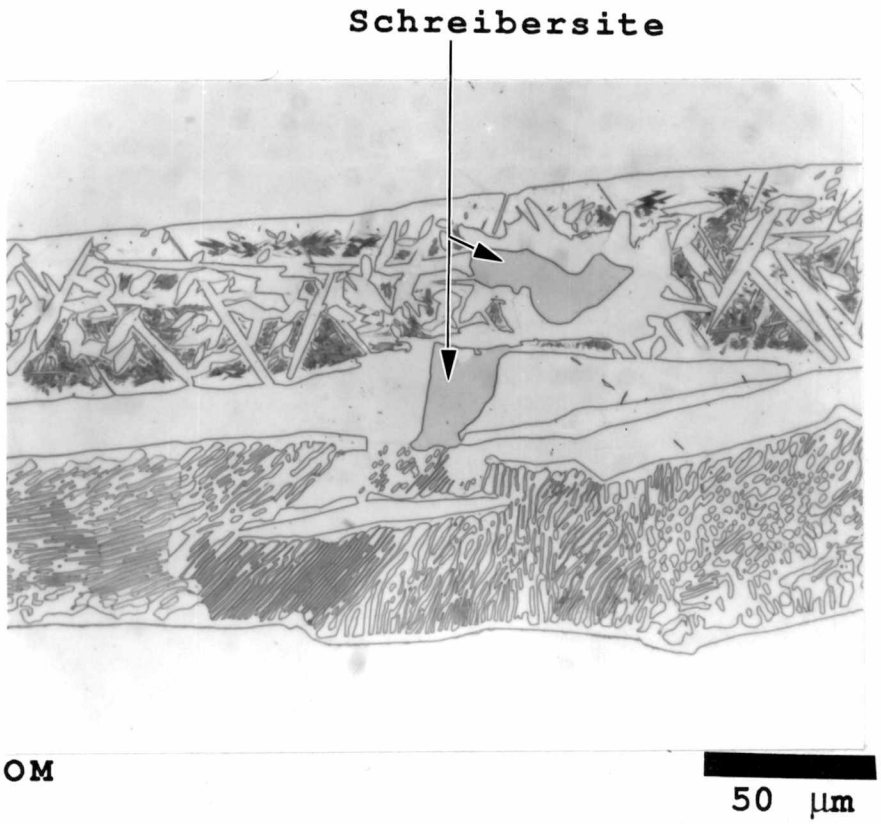

Figure 31. Effect of two schreibersite particles on the plessitic structure.

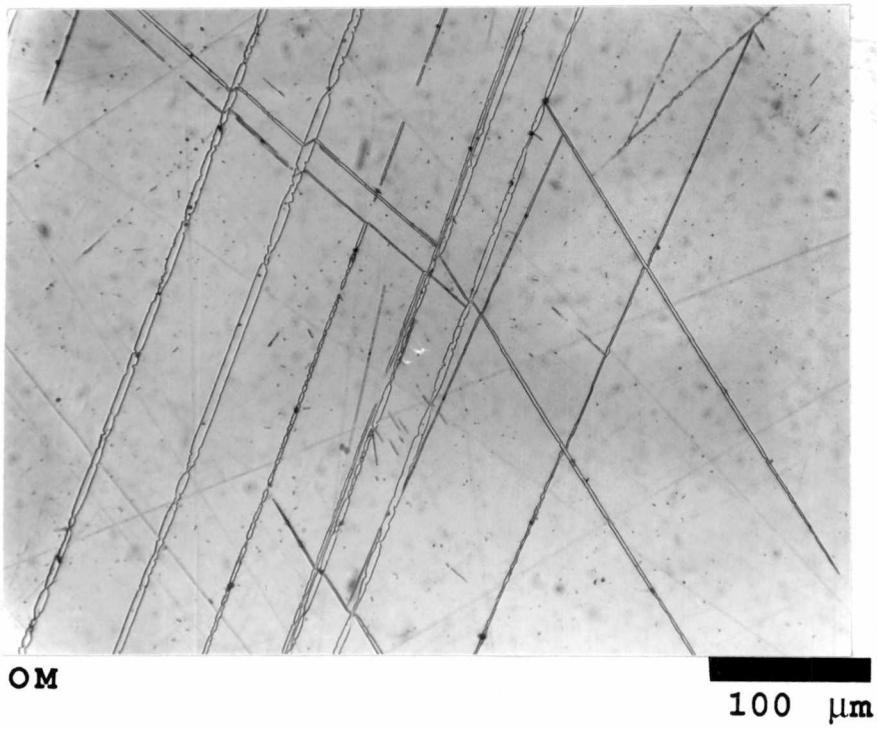

Figure 32. Neumann bands in Arispe. Some appear slightly degraded, others are clear.

II. Inland Forts

A. Macrostructure

The macrostructure of the Inland Forts meteorite consists of small particles in a banded matrix. The banded matrix appears as dark and light bands, running the length of the specimen.

1. Particles

Various particles could be seen in the structure of the Inland Forts meteorite. They appear to be in no regular pattern, with their morphology consisting of large, irregularly shaped particles. Due to their small size, macroscopically it was impossible to determine their structure. It is believed the particles were kamacite, following from the general trend of ataxites with similar composition in the literature [27].

2. Banded Matrix

The matrix of Inland Forts consists of alternating dark and light bands. These bands showed no uniform thickness

through out the sample, and tended to run the full length of the specimen.

Macroscopically, the structure composing the bands could not be resolved.

B. Microstructure

The microstructure of Inland Forts was found to consist of approximately 8% kamacite particles with associated phosphides, in a banded matrix.

1. Kamacite and Schreibersite Particles

The particles in Inland Forts generally consist of kamacite and schreibersite. The particles seem to have no particular orientation (Figure 33). EDS has confirmed the darker gray particles as schreibersite, and the lighter particle as kamacite (Figure 34). These particles are often surrounded by a layer of retained taenite.

These particle groups are irregular in shape and may have a varying number of schreibersite and kamacite regions present (Figure 35). Some of these particles are quite complex, with multiple kamacite and phosphide regions (Figure 36).

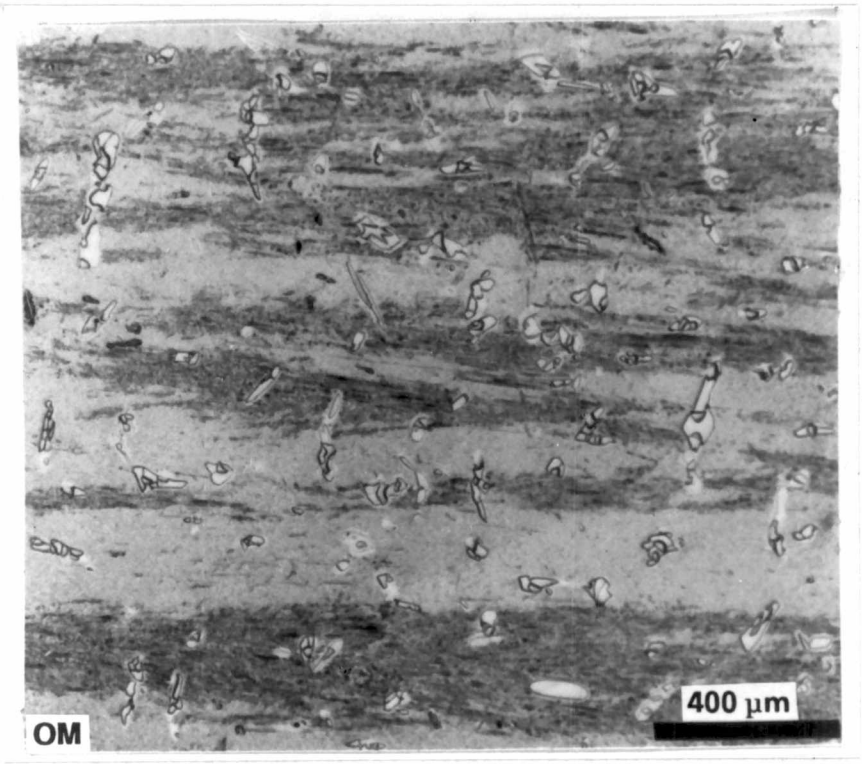

Figure 33. Non-oriented kamacite and schreibersite particles in the banded matrix of Inland Forts.

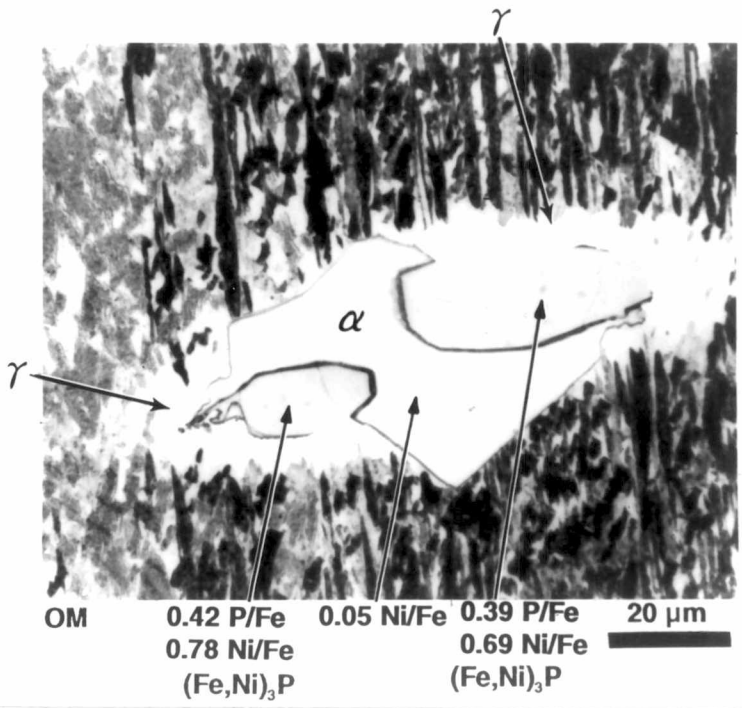

Figure 34. Kamacite and schreibersite particle in Inland Forts. Particles are often surrounded by retained taenite.

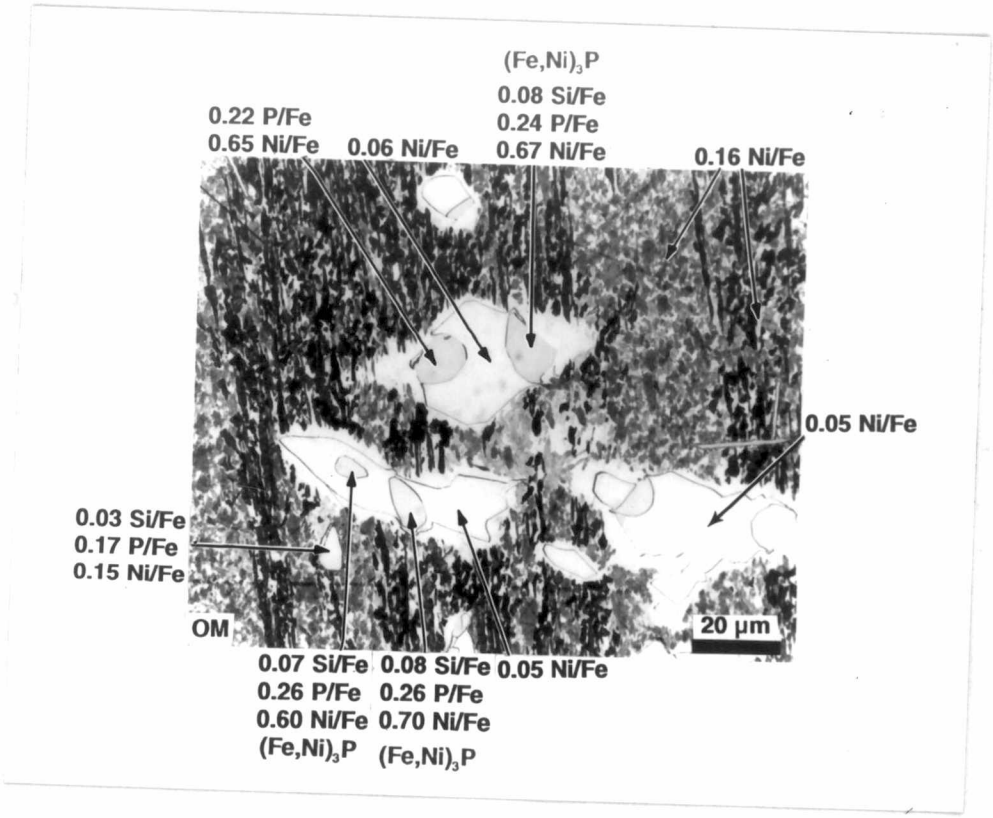

Figure 35. Irregular shaped kamacite and schreibersite particles.

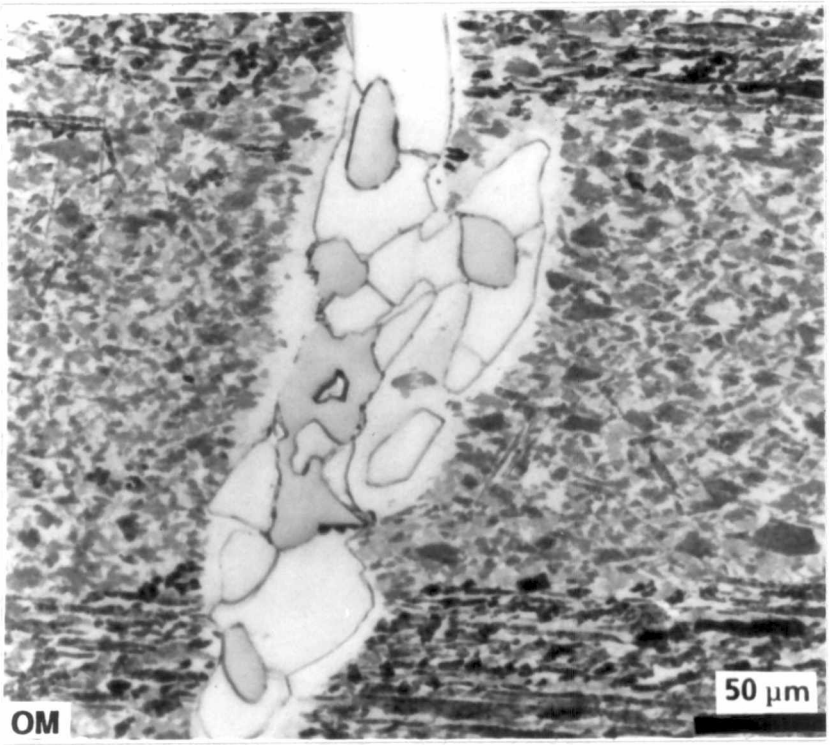

Figure 36. Complex kamacite and schreibersite particle in Inland Forts.

Particles of kamacite and schreibersite are associated with each other. Occasionally kamacite regions are observed in the matrix without the presence of schreibersite (Figure 37). It is important to remember that these particles exist in three dimensions, and we are only observing one plane. Therefore, even though these kamacite regions appear independent of schreibersite, it is believed schreibersite is present in these particles on a different plane.

The retained taenite region around some of these particles varies in thickness. EDS analysis has shown a nickel concentration gradient exists within the retained taenite region. The nickel content is high near the particle boundary, and decreases with distance to the composition of the banded structure as the matrix is approached (Figure 38).

2. Banded Matrix

At higher magnifications (Figure 39), the contrast difference of the banded structure is more clearly seen. The dark region appears to consist of elongated particles, while the lighter region does not exhibit elongated particles. It is possible that in the lighter region the elongated particles are being observed 'head on', resulting in the

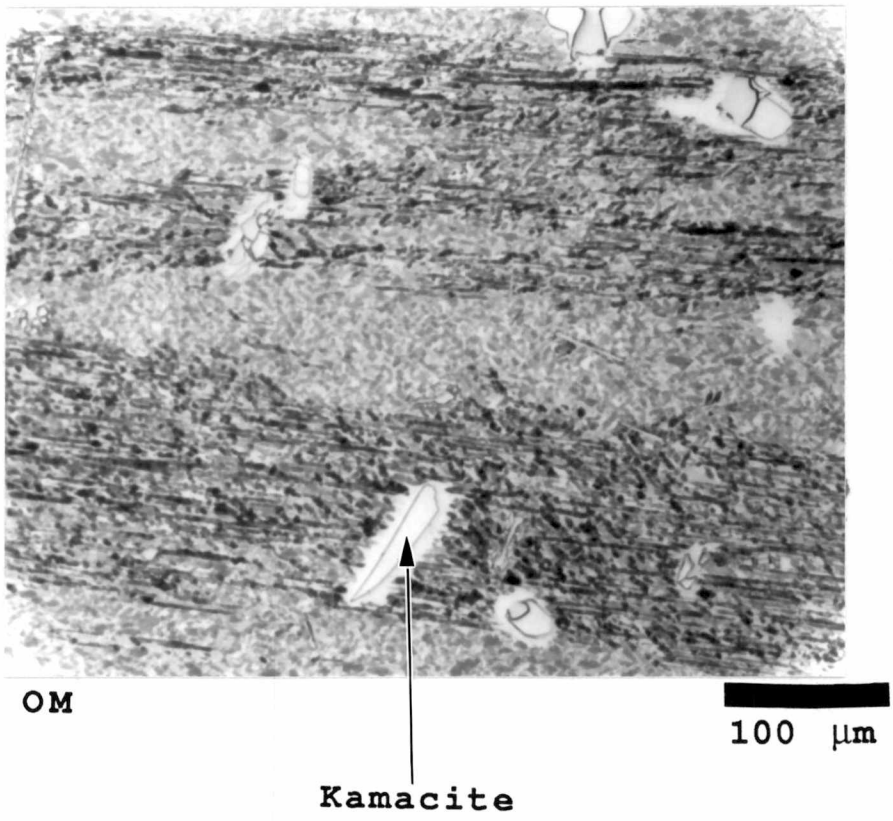

Figure 37. Kamacite regions independent of schreibersite regions. These kamacite regions are believed to be in contact with schreibersite on another plane.

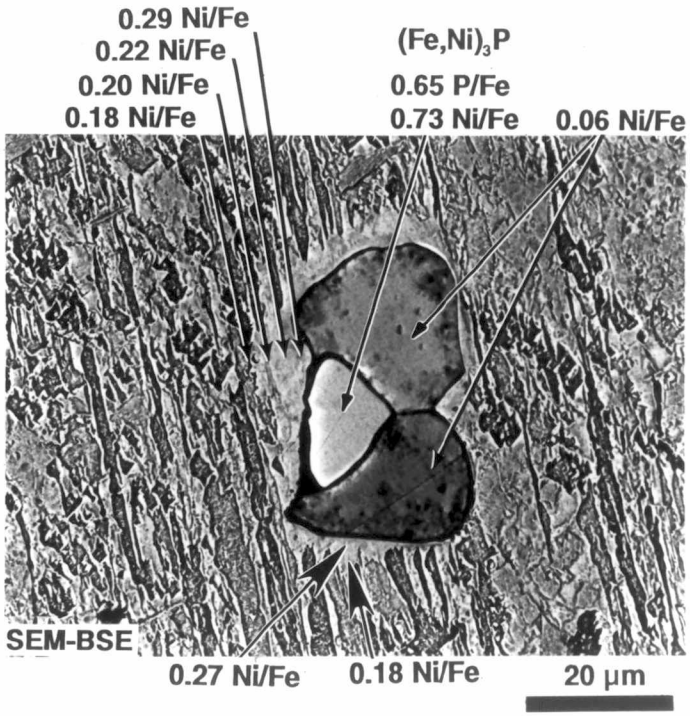

Figure 38. Particle consisting of schreibersite and two kamacite regions. Concentration gradient in retained taenite is shown.

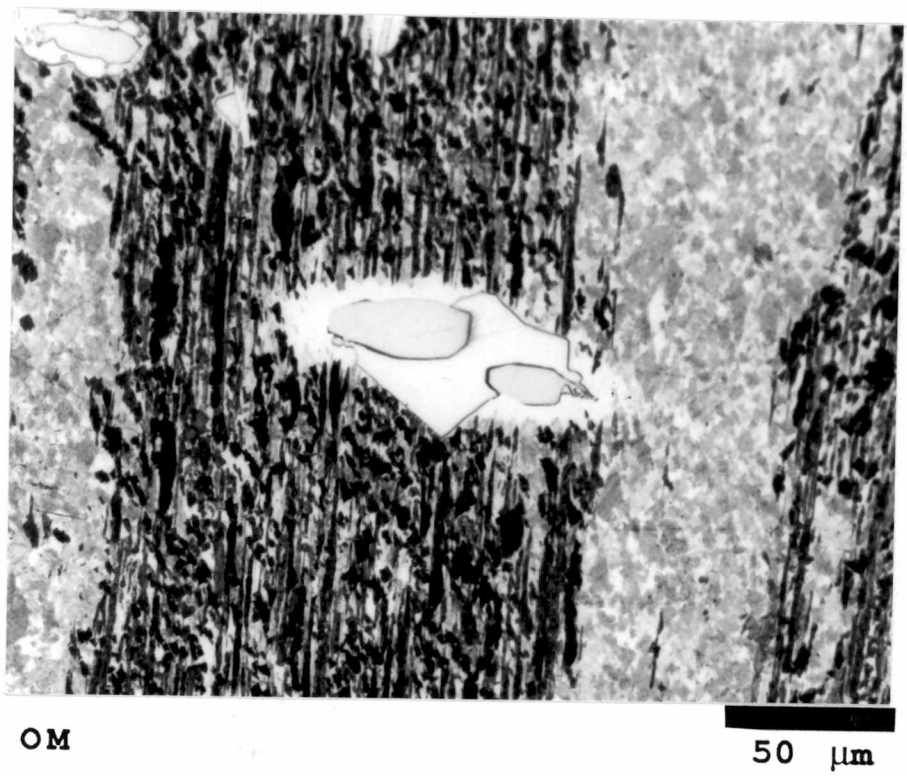

Figure 39. Orientation effect of matrix structure that makes it appear banded.

appearance of only smaller particles being present in this region.

At higher magnification, further analysis could be made of the matrix structure. The structure observed depended on whether a light or heavy etch was used.

A light etch revealed three distinct regions present in the matrix structure (Figure 40). A coarse two-phase region, termed region 1, a fine two-phase region, termed region 2, and a clear, unaffected region, termed region 3, could be identified (Figure 41).

The two-phase structure present in regions 1 and 2 appears to reveal that one of the phases of this region is present as Widmanstatten oriented plates (Figure 42). Both of these two regions exhibited this orientation behavior of one of the phases; the difference in these regions is the plate thickness.

Close examination of these three regions reveals that region 1 (coarse structure) appears to have been severely attacked by the etchant, region 2 (fine structure) exhibits mild effects of the etch, and region 3 (clear structure) shows very little effects of the etch (Figure 43). This varying effect of the etchant between the regions can be illustrated by the the appearance of the sides of adjacent regions visible in region 1. Regions 2 and 3 do not appear

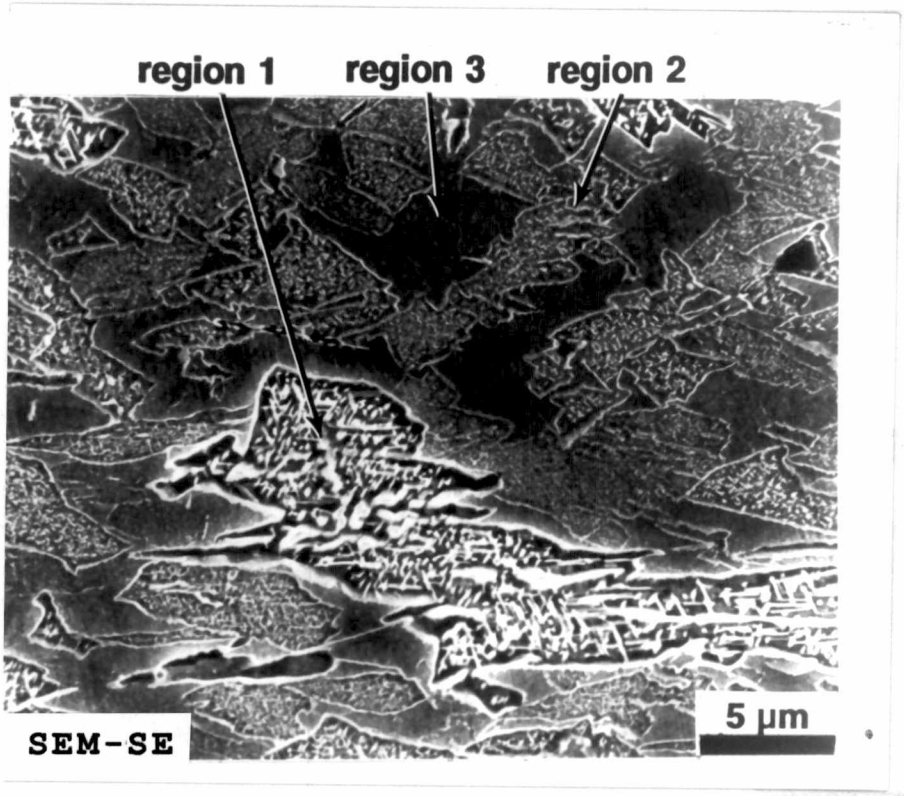

Figure 40. SEM photomicrograph revealing coarse structure (region 1), fine structure (region 2), and clear structure (region 3).

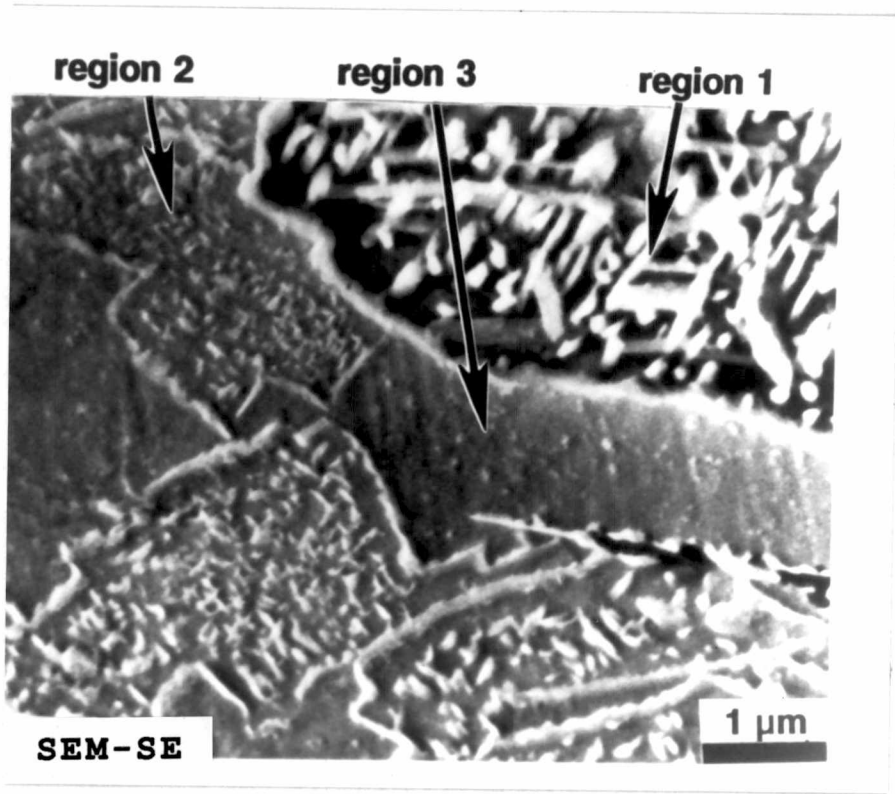

Figure 41. Coarse, fine, and clear regions of the matrix.

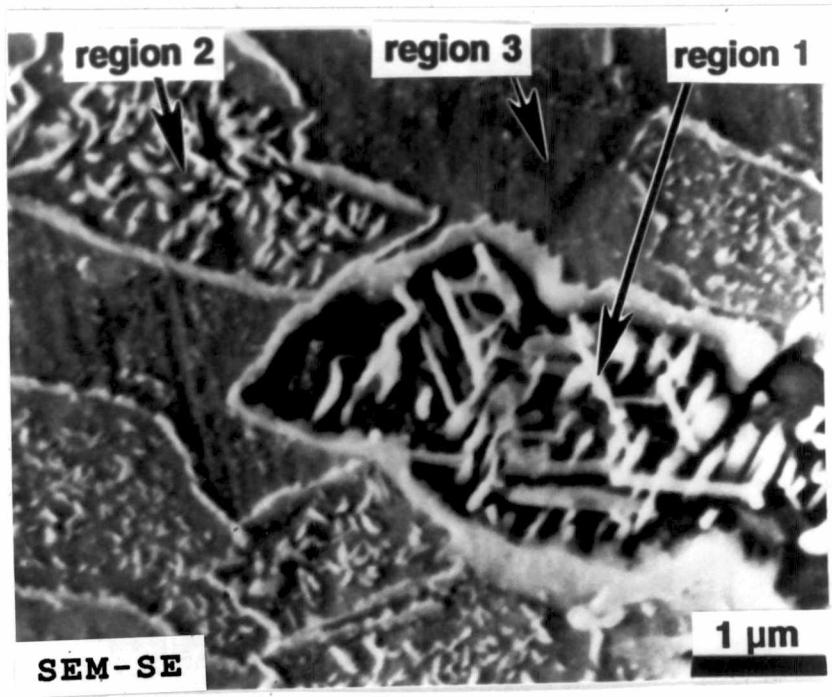

Figure 42. Oriented plates present in regions 1 and 2.

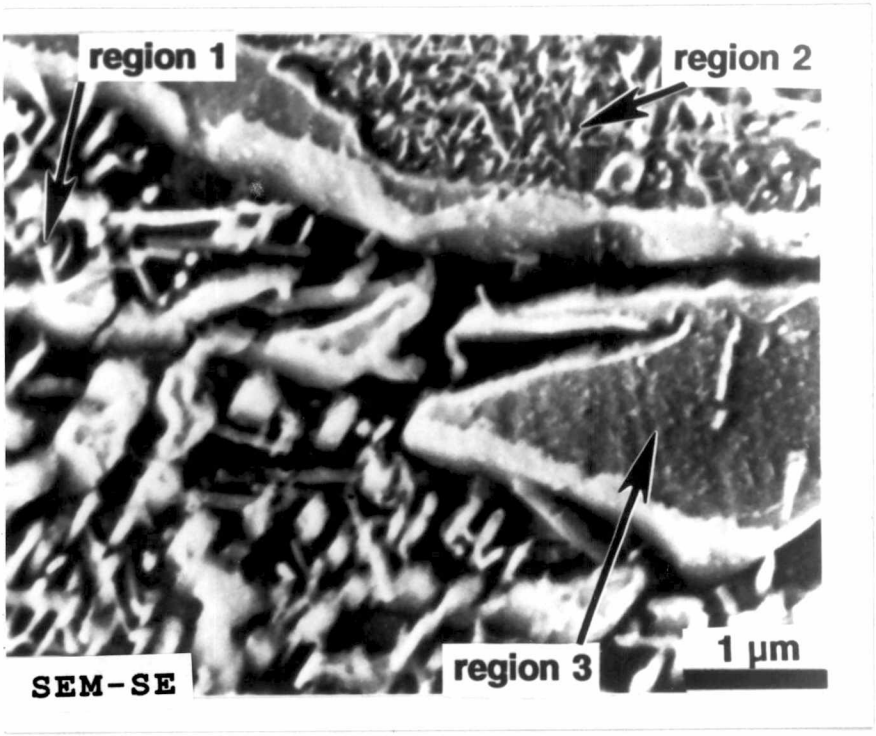

Figure 43. Deep etching effect in region 1.

to be at very different levels, but region 1 appears much heavier etched than the other two regions.

EDS analysis shows that all three regions have the same bulk composition (Figure 44).

When applying a heavy etch, only two distinct regions are discernable (Figure 45). One region appears clear and smooth, while the other region exhibits a coarse Widmanstatten oriented structure (Figure 46).

It is not clear whether a heavier etch was necessary to bring out the true structure (the three region structure was underetched), or whether the lighter etch revealed the true structure and overetching erased the distinction between regions 1 and 2.

III. Ocotillo

A. Macrostructure

The Ocotillo meteorite is classified as a coarse octahedrite, and therefore exhibits the Widmanstatten kamacite and the associated retained taenite stringers. A large non-metallic inclusion was also contained in the sample.

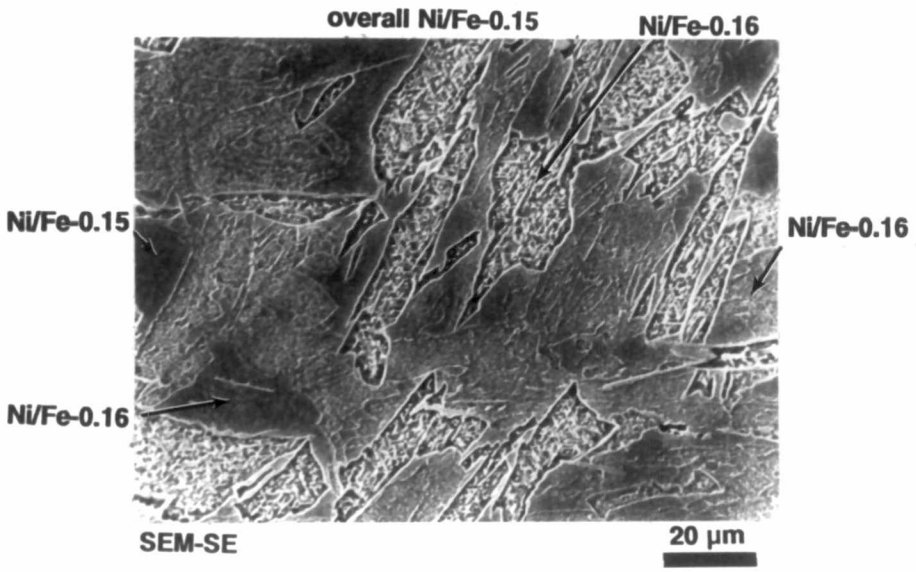

Figure 44. EDS analysis of the three regions in the matrix structure.

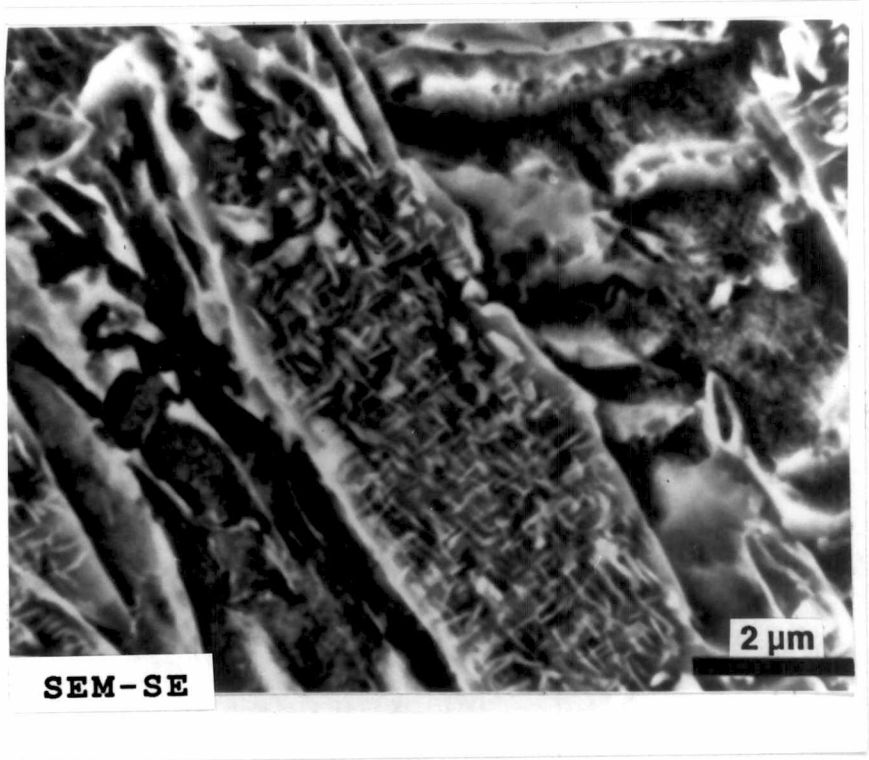

Figure 45. Heavy etching reveals only two distinct regions in the matrix.

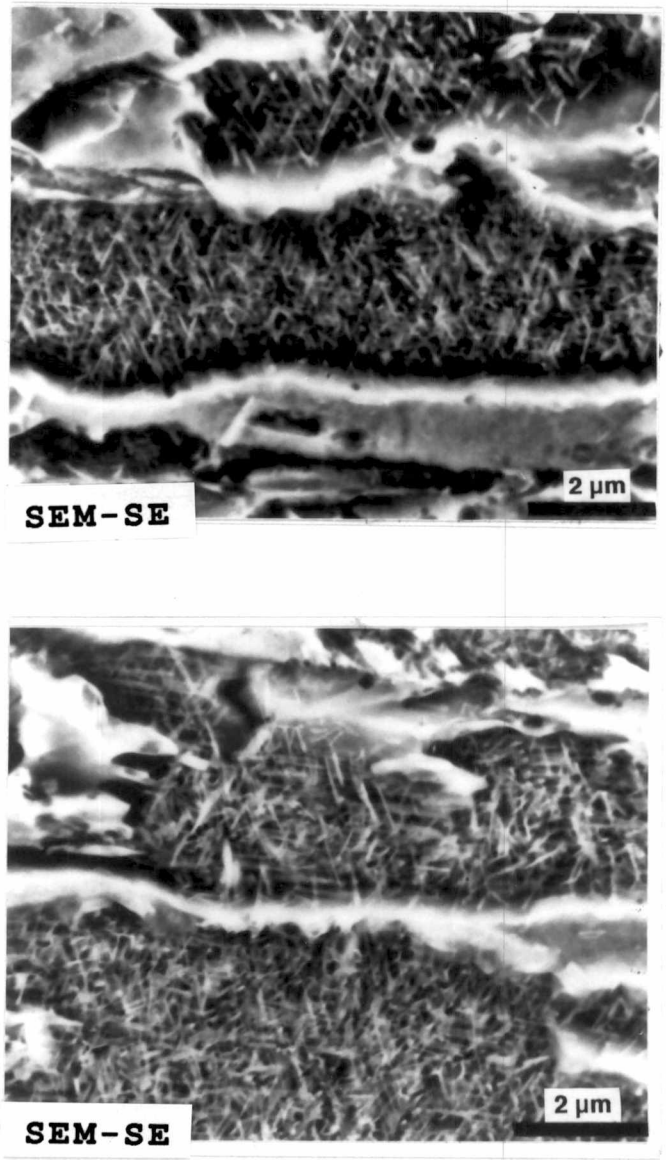

Figure 46. Clear region and coarse oriented structure present with heavy etch.

1. Widmanstatten Kamacite

The oriented kamacite plates in Ocotillo are very coarse, and yield many retained taenite stringers. The kamacite plates do not contain many non-metallic inclusions, with the exception of the two large inclusions to be mentioned in further detail in the following section. Neumann bands are also present in some grains.

2. Non-metallic Inclusions

There are two obvious inclusions in the macrostructure of Ocotillo, one large (1 cm^2) inclusion and an associated smaller inclusion.

The large inclusion does not seem to be a single homogeneous phase. Rather it appears to consist of many minerals, and possibly regions of kamacite and taenite.

The smaller inclusion appears visually similar to the large inclusion. Because of its similarity in appearance and proximity to the large inclusion, it is possible the small inclusion was once a part of the large inclusion. It is also possible that they are still the same inclusion and are continuous on a different plane from the one we are observing.

A few narrow cracks can also be observed, primarily near the oxide crust. Within these cracks, some terrestrial corrosion products can be seen.

B. Microstructure

The primary structures of interest in Ocotillo are the different morphologies of plessite in the numerous taenite stringers, and the large, primarily non-metallic, inclusion.

1. Plessite

Many of the retained stringers in Ocotillo exhibited interesting structures. We will concentrate on the more unusual plessitic structures observed, but it is important to remember many stringers contained standard pearlitic, spheroidal, and acicular plessitic structures.

Ocotillo exhibited an abundance of pearlitic structures coarsening or spheroidizing. A typical stringer undergoing spheroidization from pearlitic to spheroidal plessite is seen in Figure 47. This particular stringer was located near a crack. The interface between the two regions becomes visible at higher magnification (Figure 48), and in the optical micrograph (Figure 48a), some of the taenite spheres show the

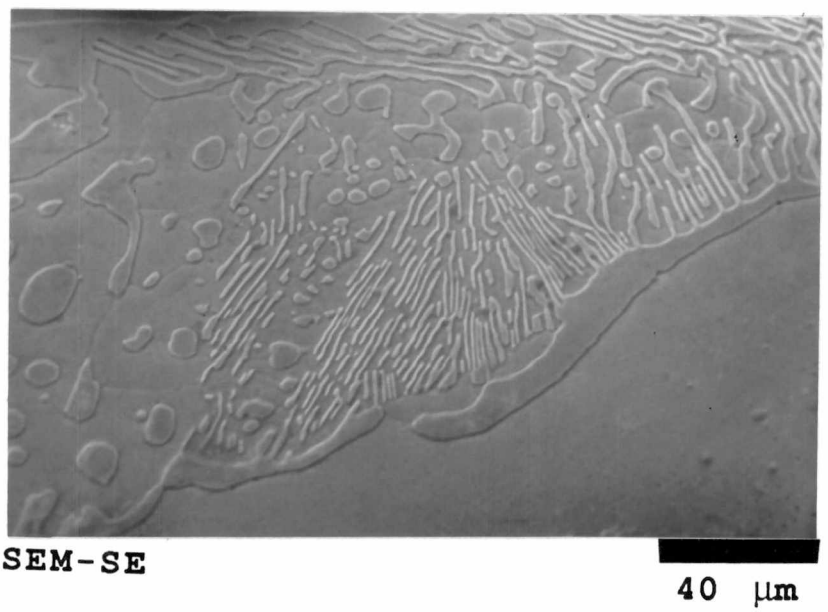

Figure 47. Typical spheroidization interface of pearlitic plessite in Ocotillo.

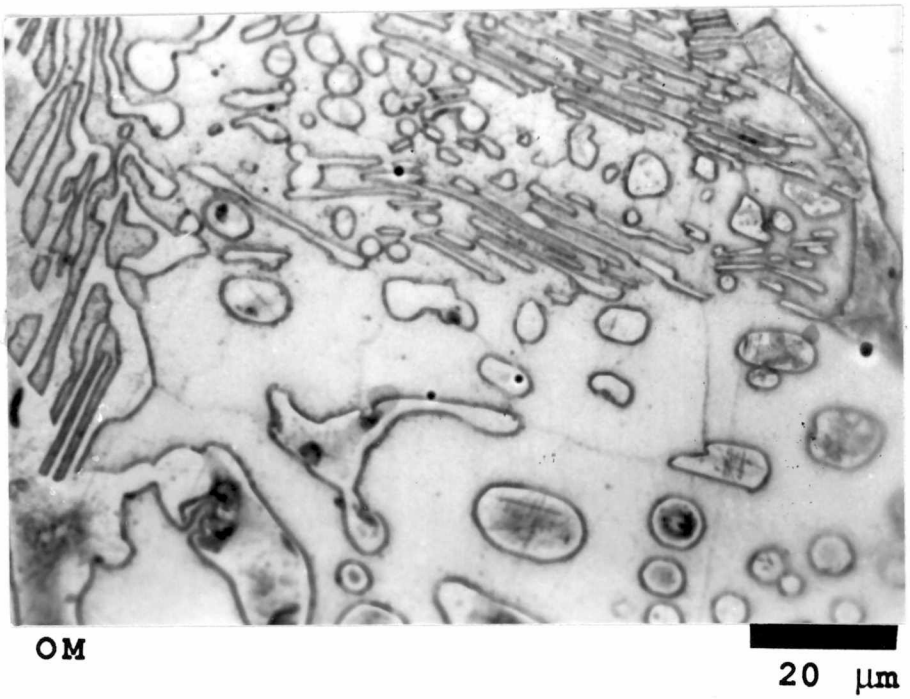

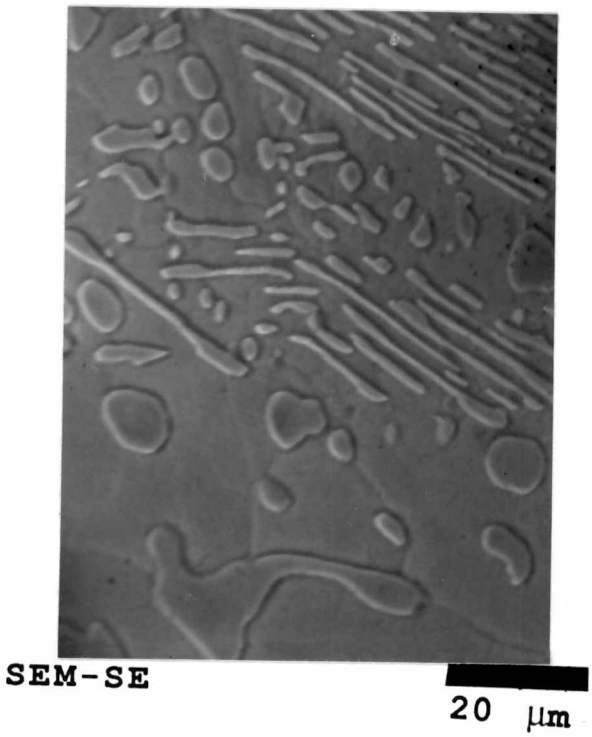

Figure 48. Spheroidization interface of pearlitic plessite. Some spheres exhibit the cloudy zone structure in the OM.

presence of the cloudy zone structure.

These plessitic structures can be considered spheroidal rather than rod-like for three reasons. First, if the structure consisted of rods, any cut at an oblique angle would result in ellipses of taenite. Only seen generally circular structures have been observed. Also, the circles vary in size, which would be expected if spheres were randomly bisected. Finally, these spheres seem to be randomly spaced, not evenly spaced in straight rows, which would be expected from rod-like structures evolving from the evenly spaced pearlite.

Stringers were observed that showed pearlitic plessite coarsening (Figure 49), with the presence of a spheroidized region and large kamacite regions. Higher magnification SEM analysis reveals the definite presence of a coarsening interface, even continuing between the kamacite region of the two different morphologies within the stringer (Figure 50).

Stringers did not always exhibit single coarsening interfaces (Figure 51). Regions of pearlite divided by regions of spheroidite with multiple reaction interfaces within a single stringer were observed. Another coarsening reaction in the same stringer shows the definite presence of an interface (Figure 52). Some of the pearlite appears to have spheroidized, while other pearlite in the same vicinity

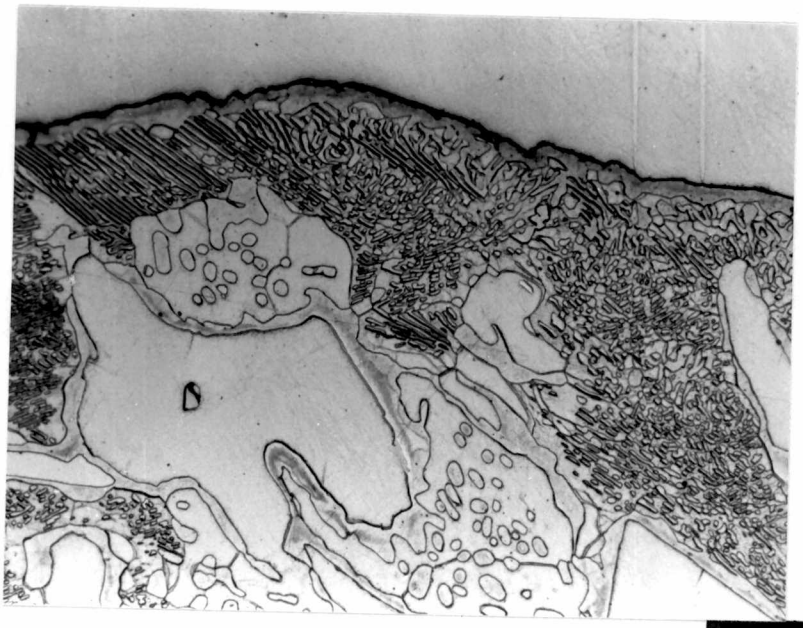

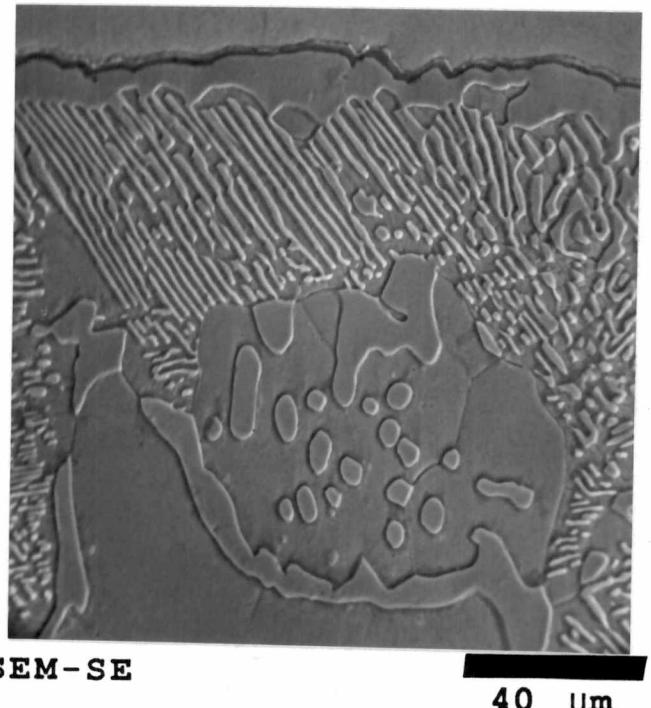

Figure 49. Coarsening of pearlitic plessite in Ocotillo.

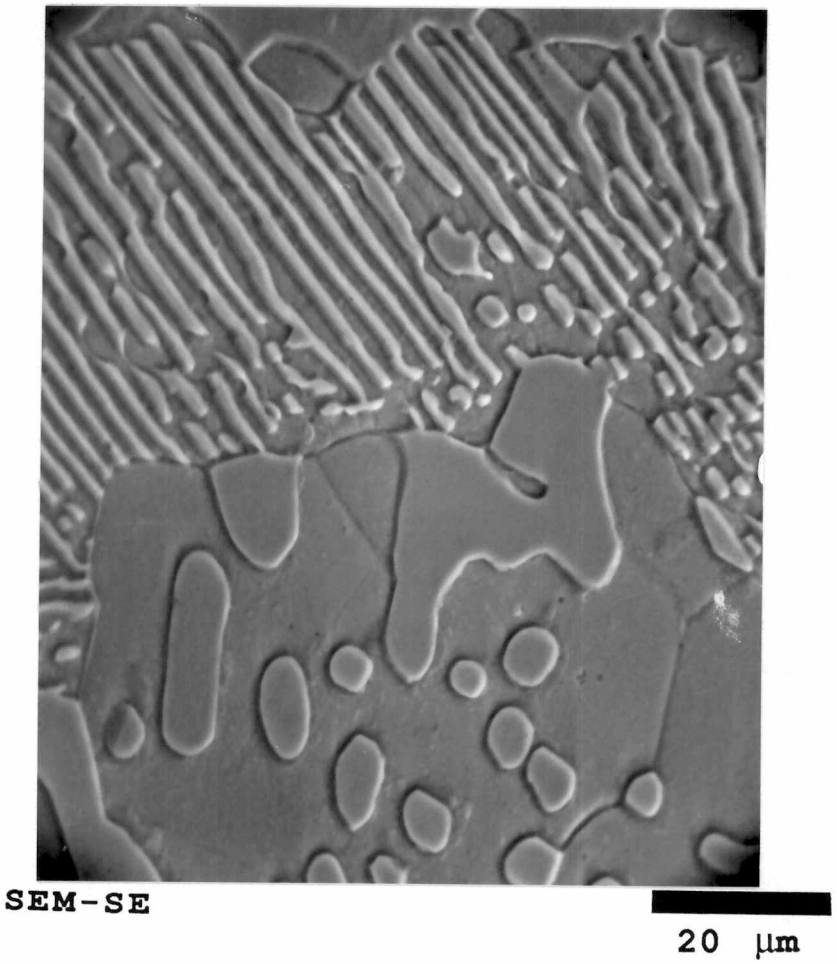

Figure 50. Obvious interface between two plessitic regions.

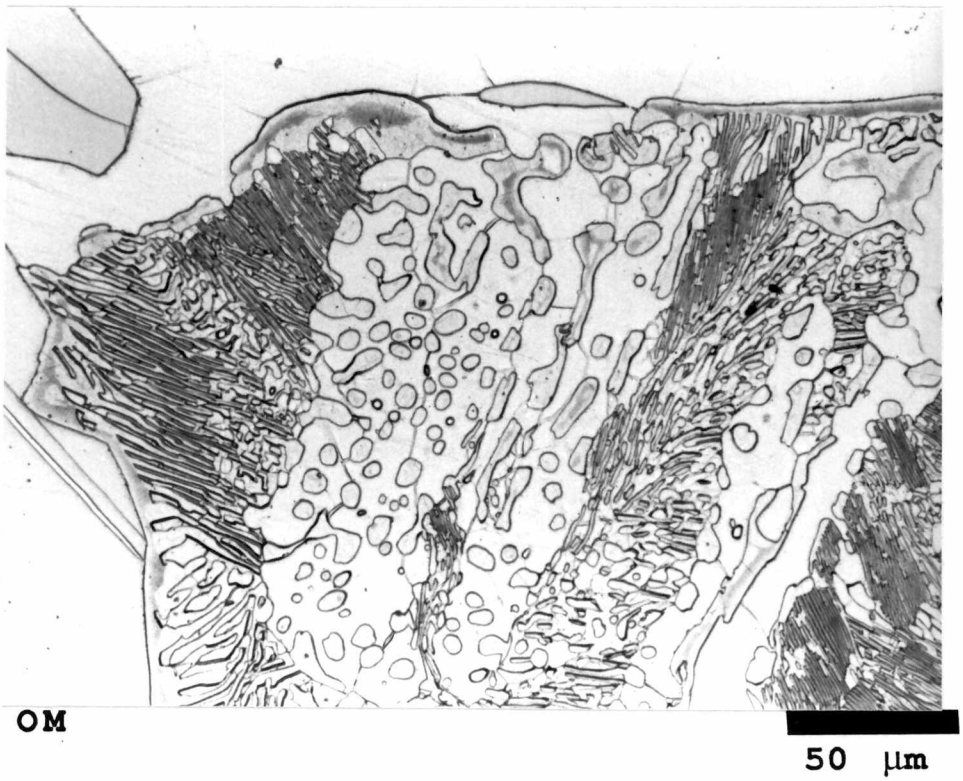

Figure 51. Multiple coarsening reactions present in one stringer.

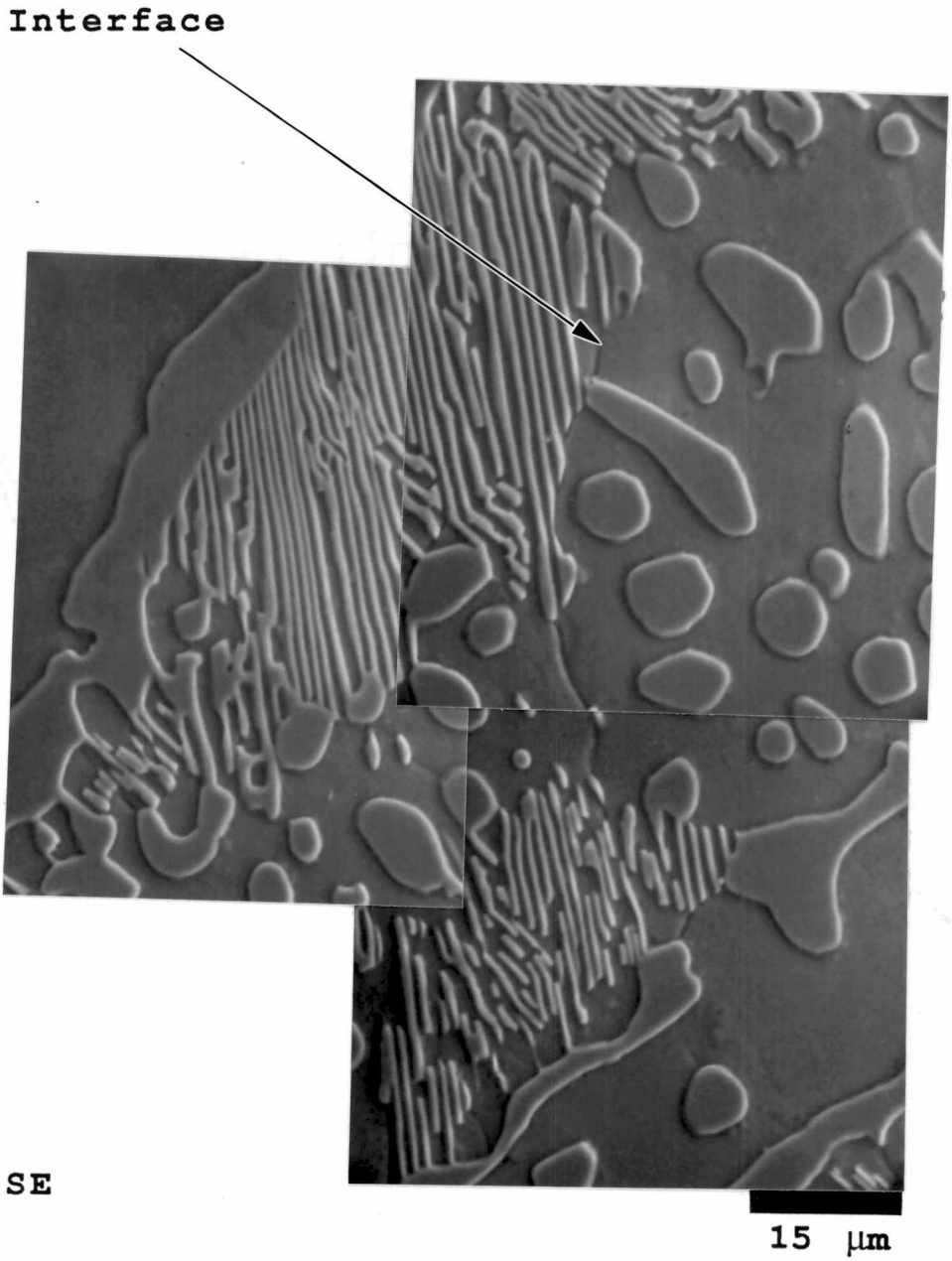

Figure 52. Coarsening interface between pearlitic and spheroidal plessite.

seems to have coarsened into a structure not very spheroidal in nature.

An odd-shaped stringer was observed to exhibit pearlitic plessite undergoing spheroidization (Figure 53). This stringer does not have the long and thin shape of typical retained taenite stringers. The fine pearlite can be seen coarsening into spheres, in which the traces of the cloudy zone structure can be occasionally seen. Higher magnification SEM analysis again reveals the presence of an interface between the two morphologies (Figure 54).

Some stringers exhibited a pearlitic rim with a spheroidal interior (Figure 55). The pearlite can be seen spheroidizing, with perturbations of the rim obvious. Some of the larger taenite spheres in the interior exhibit the cloudy zone structure (Figure 56).

In some stringers, major perturbations of the pearlitic rim with an interior of spheroidal plessite were observed (Figure 57).

An interesting stringer that exhibits two levels of spheroidization was also observed (Figure 58). The pearlitic region is seen to transform to a spheroidal structure (Figure 59, 60), and then the taenite edge of the stringer breaks down and a coarse spheroidal structure is seen (refer to Figure 58). The cloudy zone is present in the larger taenite

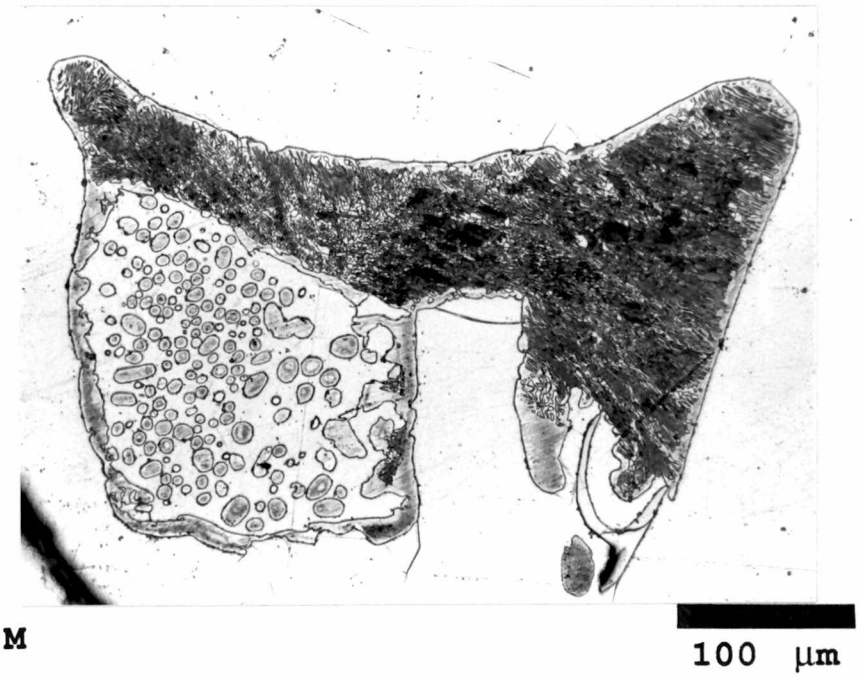

Figure 53. Atypical shaped stringer with a spheroidization reaction occuring.

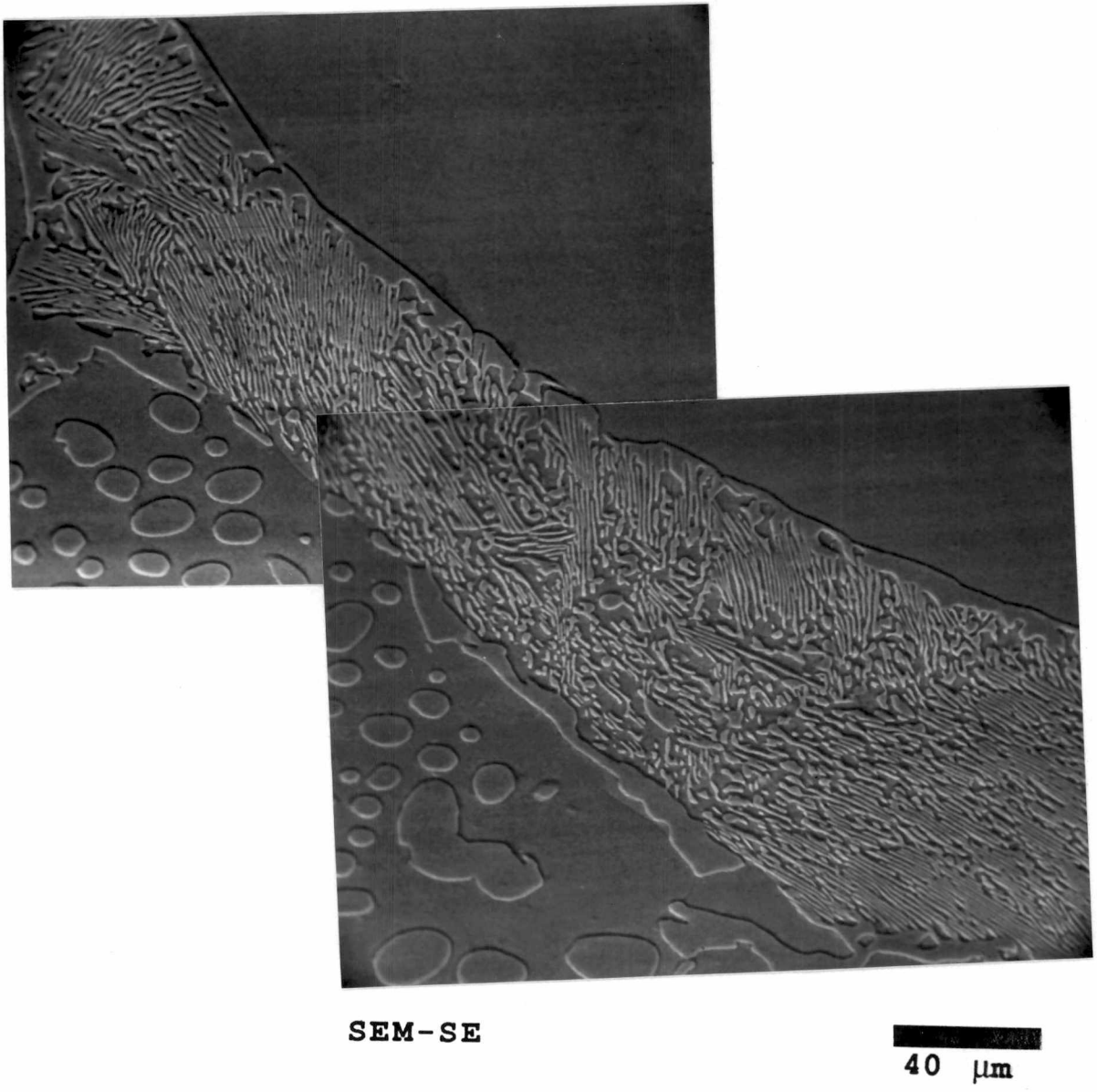

Figure 54. Spheroidization interface in odd-shaped stringer.

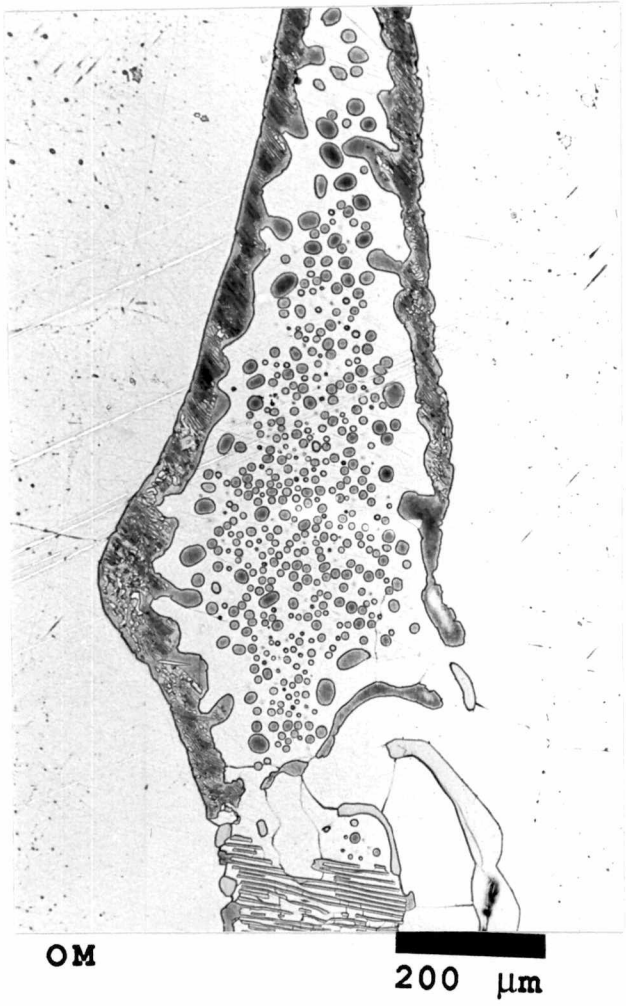

Figure 55. Stringer showing a pearlitic rim with a spheroidized interior.

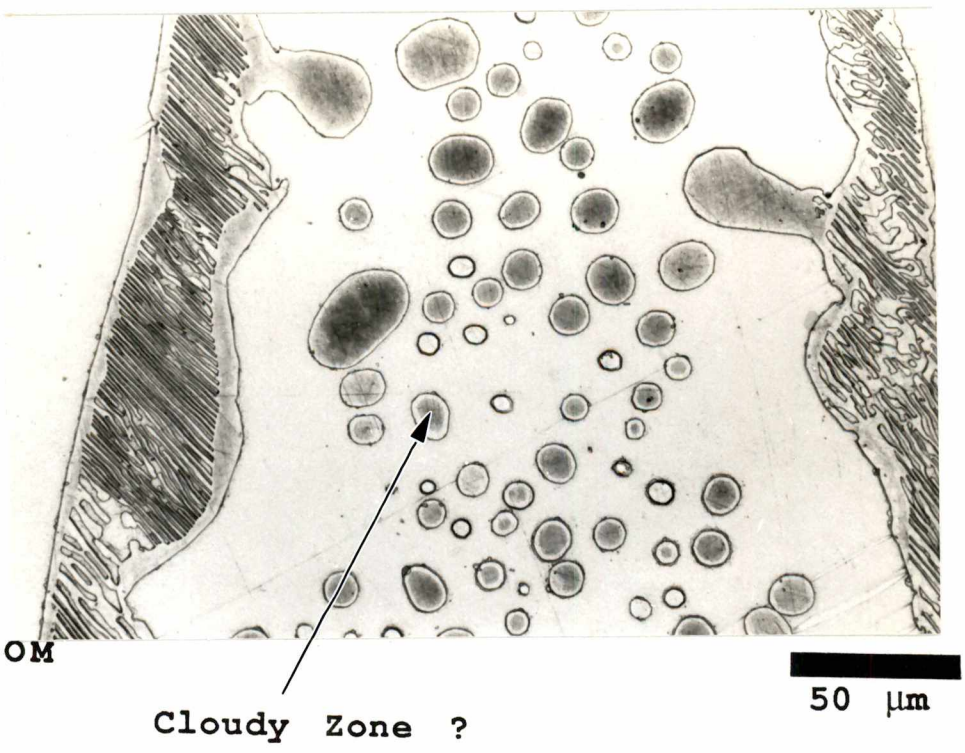

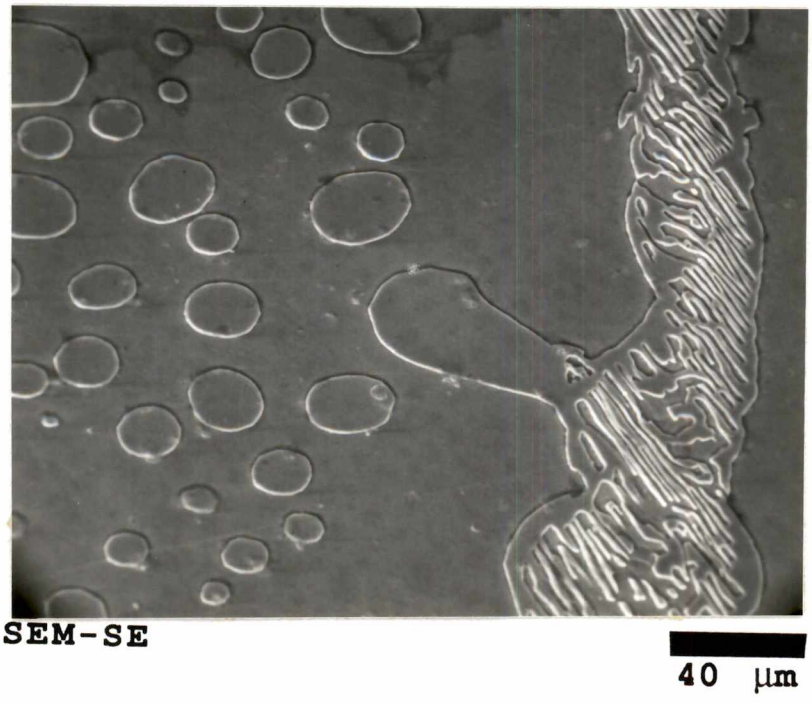

Figure 56. Pearlitic rim transforming to spheroidized structure. Some spheres exhibit the cloudy zone structure.

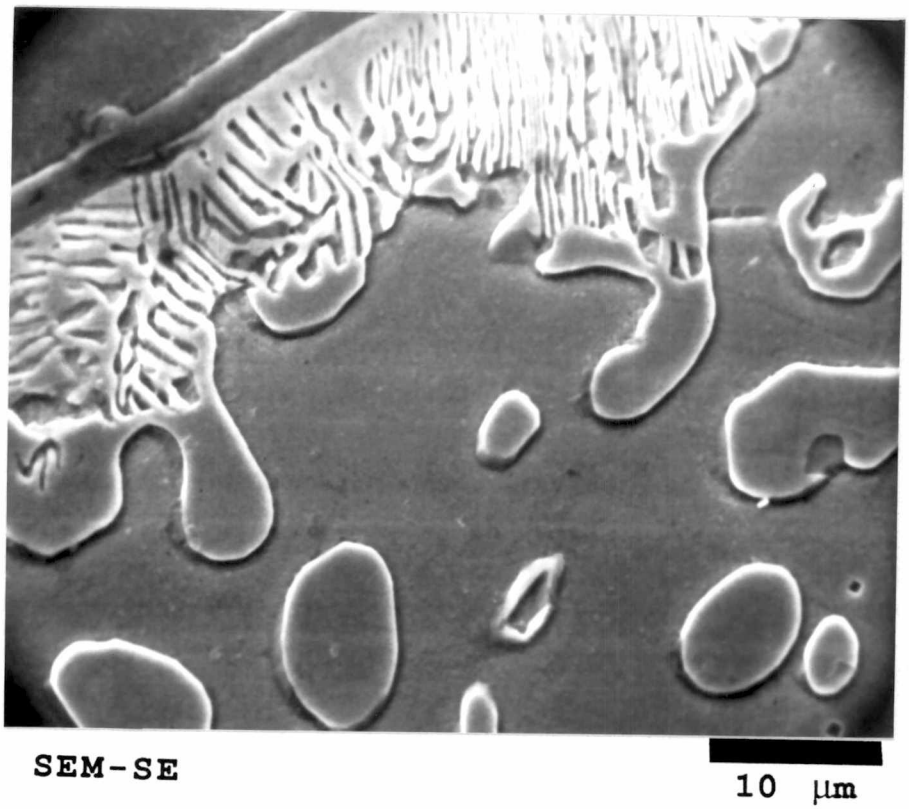

Figure 57. Stringer with major perturbations of the pearlitic rim.

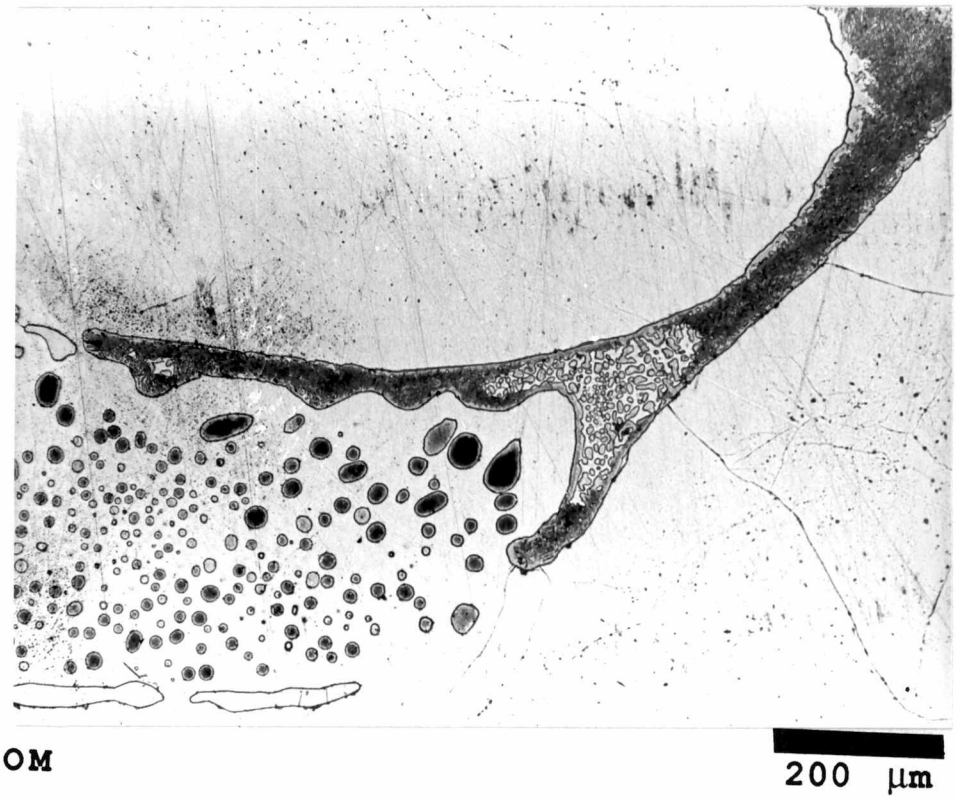

Figure 58. Stringer which exhibits two levels of spheroidization.

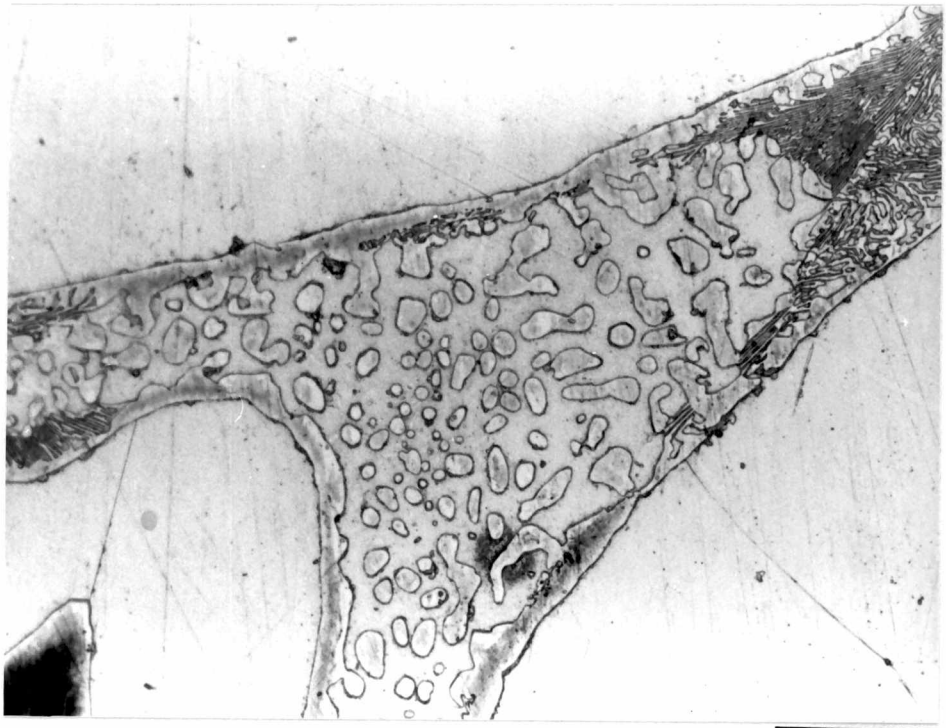

Figure 59. Pearlitic to spheroidal plessite reaction in two-level stringer.

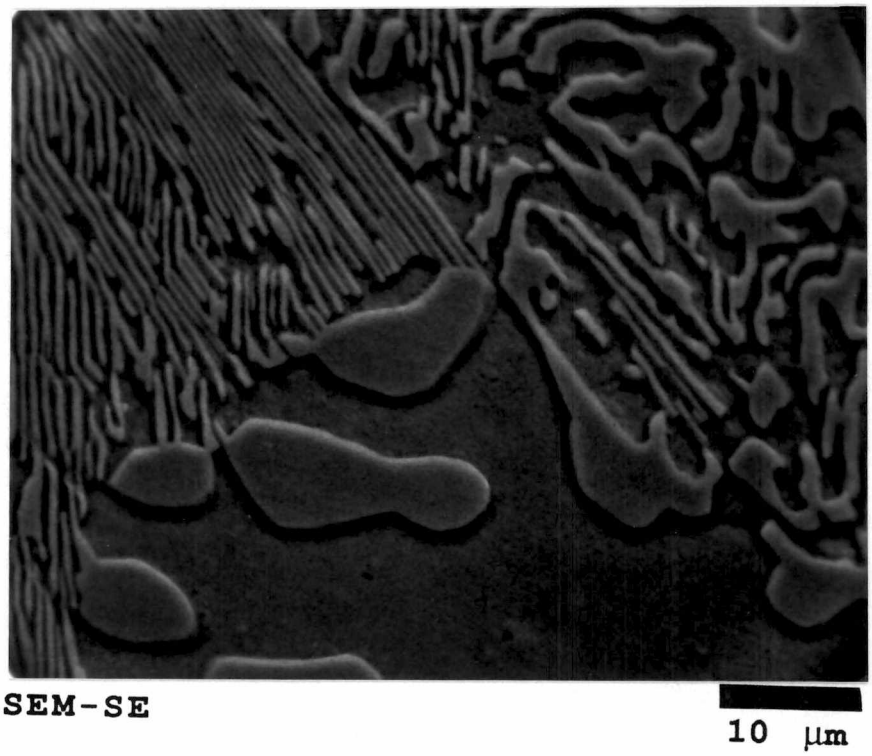

Figure 60. Fine pearlite to spheroidal plessite in 2-level spheroidizing stringer.

spheres. Another interesting point in this stringer is the size of the spheres. When the structure spheroidizes, it would be expected that as the interface moves, the spheres away from the interface would grow at the expense of the smaller spheres. However, we observe the opposite in this case. The spheres that are near the interface are larger than the spheres away from the interface.

A stringer was also observed containing a fine pearlitic structure, with large kamacite inclusions surrounded by taenite (Figure 61). A distinct boundary can be seen between the kamacite inclusion and the kamacite of the pearlitic structure. EDS has confirmed the inclusion as kamacite surrounded by taenite.

Many stringers have separate pearlite colonies growing in different orientations. The particular stringer in Figure 62 shows a region of fine pearlitic plessite next to a region where the pearlitic plates are oriented a few degrees from parallel to the cut surface, resulting in the appearance of very wide bands.

Another stringer shows pearlite colonies that appear to be darker and lighter (Figure 63). SEM observation shows that the kamacite component seems to be less affected by the etch in one region than the other (Figure 64).

Another plessitic structure has also exhibited this

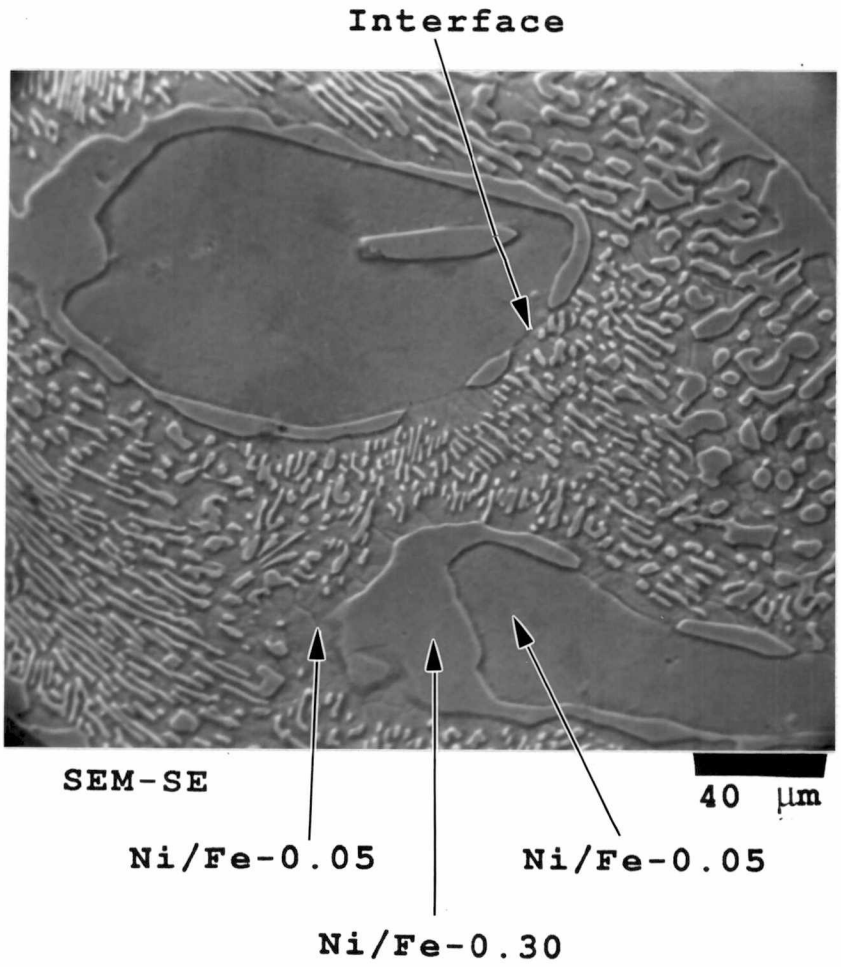

Figure 61. Large kamacite inclusion surrounded by taenite in a pearlitic plessite stringer. Kamacite of pearlite and inclusion are not continuous.

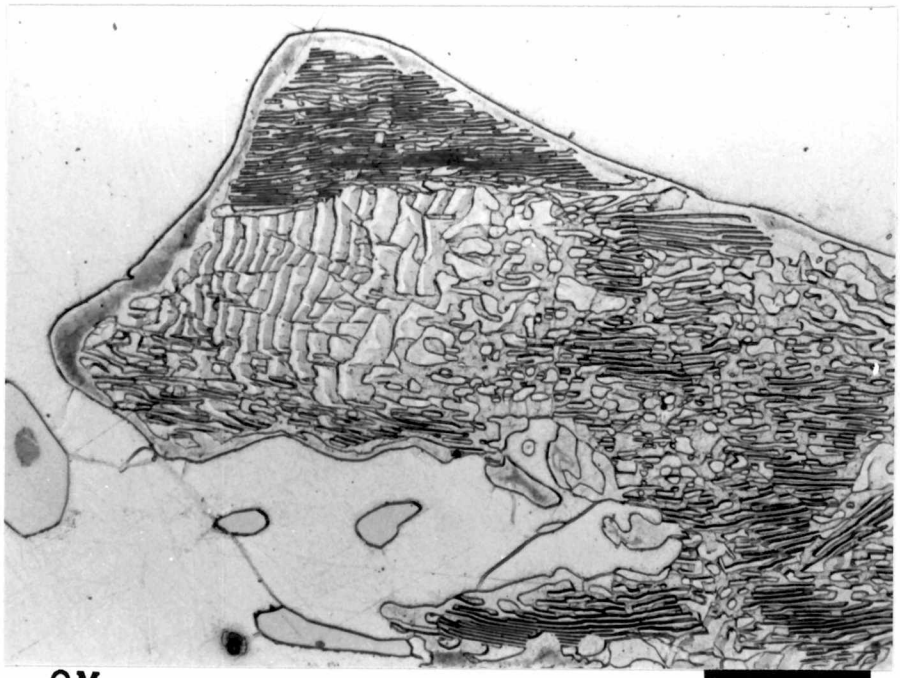

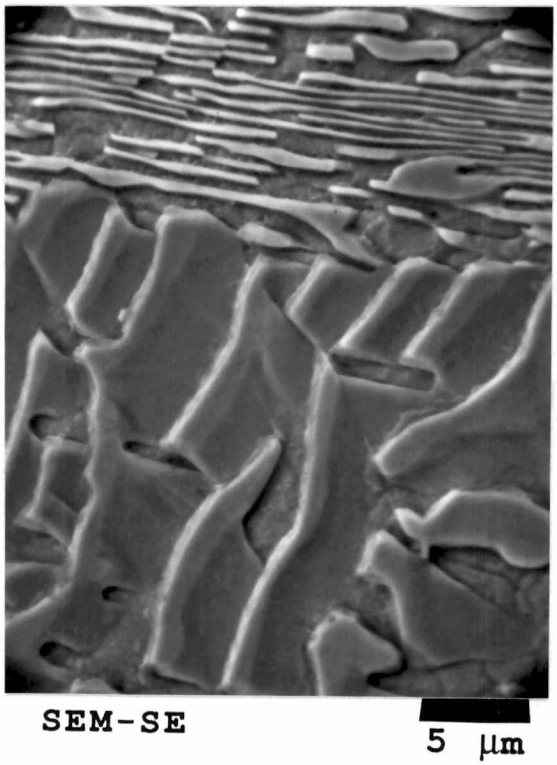

Figure 62. Pearlitic plessite plates with different orientations.

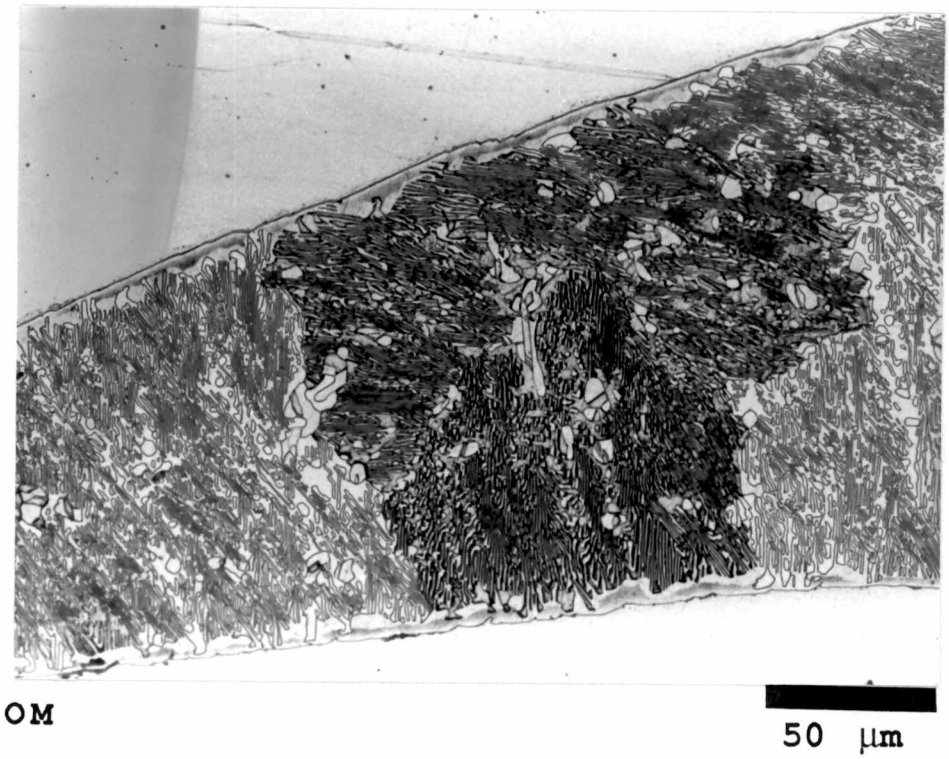

Figure 63. Light and dark regions of pearlite in a stringer.

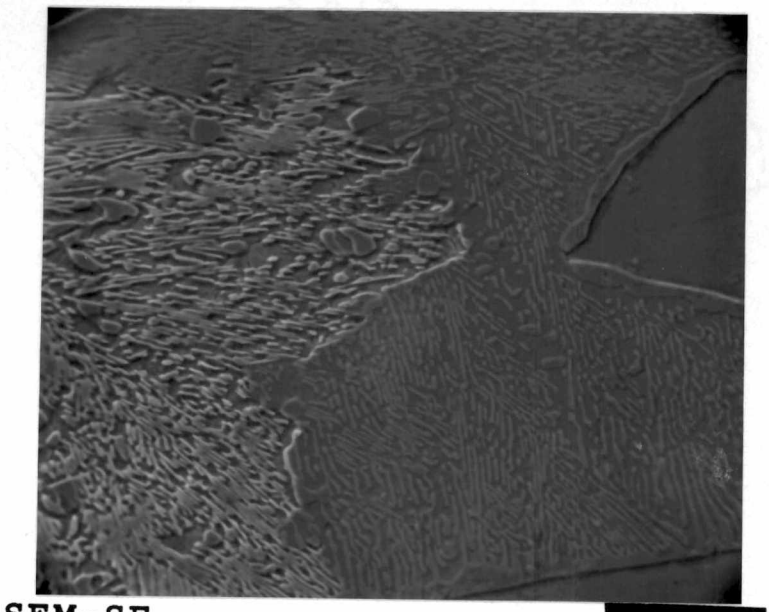

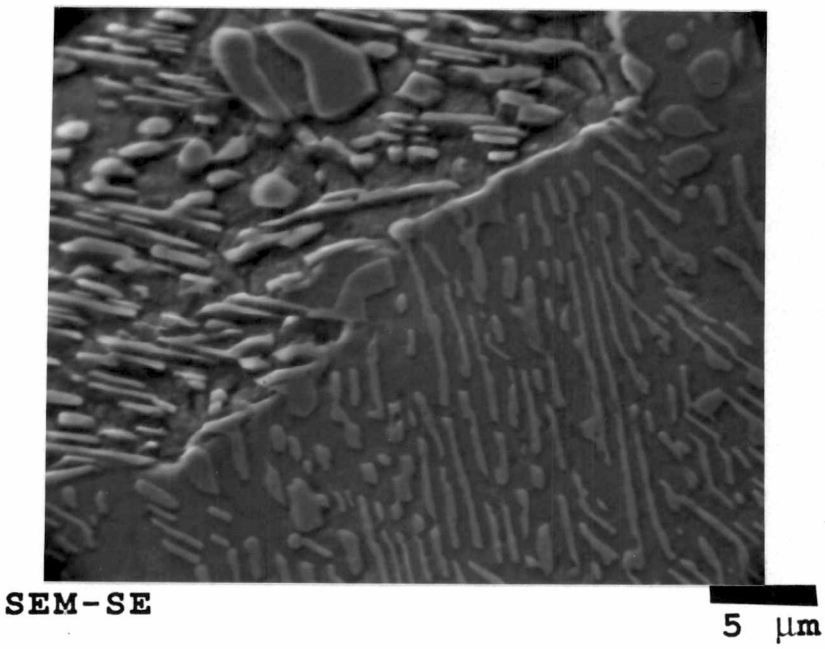

Figure 64. Interface between light and dark pearlite regions. Kamacite in dark region appears to be more affected by the etch.

orientation effect within the stringer. One stringer exhibits a structure that appears to be pearlitic with randomly dispersed spheroids, along with an interface between the two regions (Figure 65). High magnification SEM observation reveals the plessitic structure, as well as the interface between the two orientations (Figure 66).

Another stringer also shows some interesting features (Figure 67). This particular stringer shows the clear taenite 1 region (tetrataenite) near the edge, followed by the cloudy zone. The majority of the plessite in the middle of the stringer appears to be pearlitic, but there is a large region where the pearlite is absent. A few individual colonies of pearlitic plessite are present within this region. It is possible this region was reheated to remove the lamellar structure. However, the presence of the cloudy zone, which is sensitive to reheating, is still present. This would lead to the conclusion that such a reheating event has not occurred.

One stringer exhibited some interesting variations of the standard acicular plessite structure (Figure 68). The CT1 and cloudy zone can be distinguished at the rim, with the center containing acicular plessite. The variation occurs within the structure between the oriented plates. There appears to be two different structures appearing between the

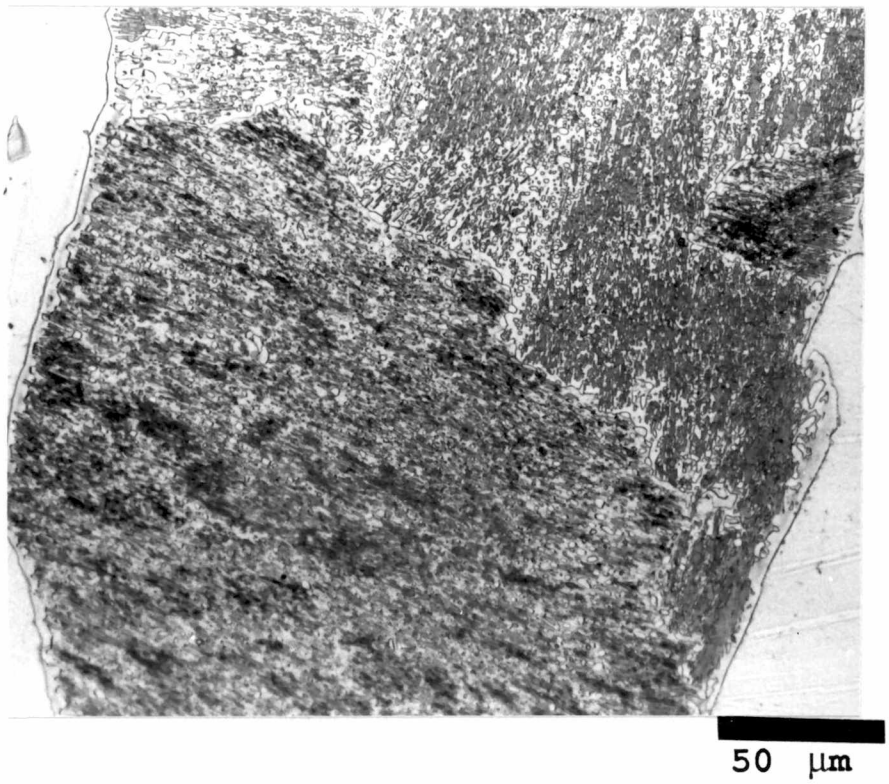

Figure 65. Orientation effect of plessite in a fine pearlitic stringer.

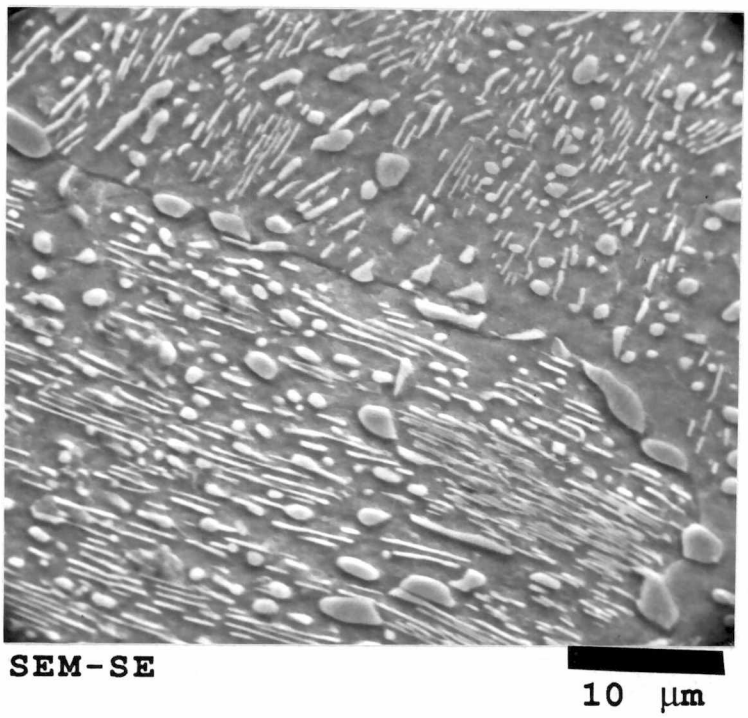

Figure 66. Interface between two plessite regions of different orientation.

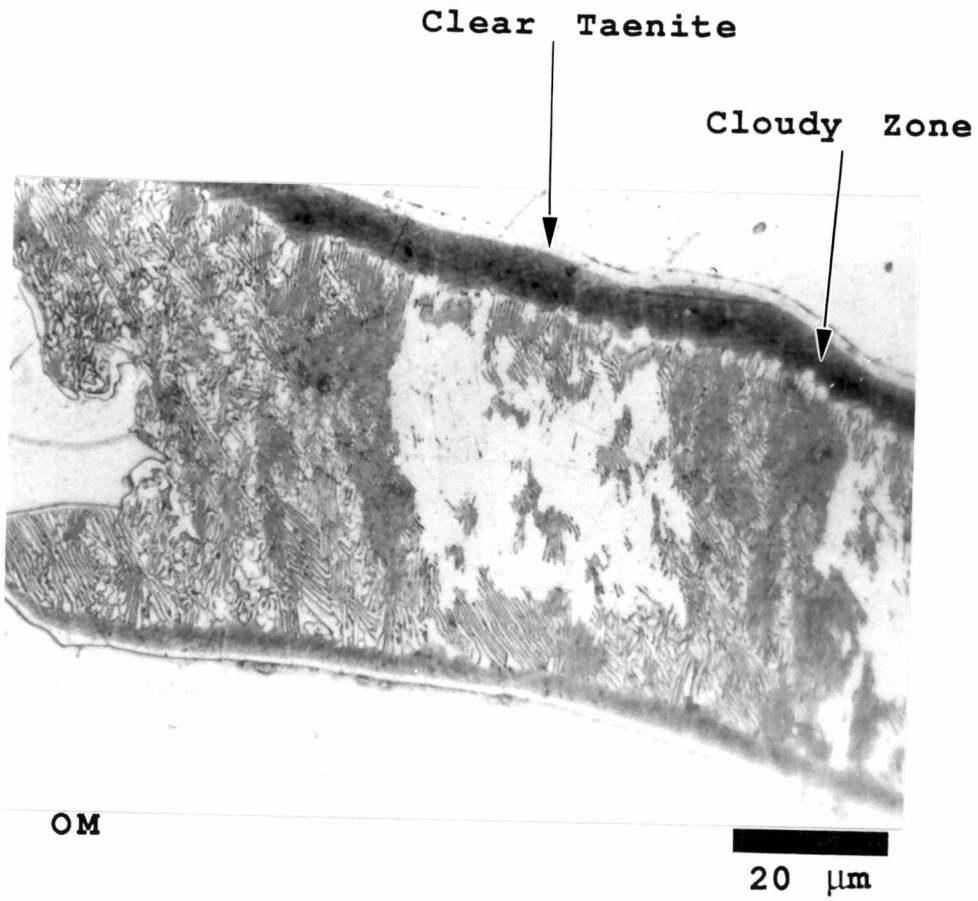

Figure 67. Stringer containing a region where the pearlitic structure is absent.

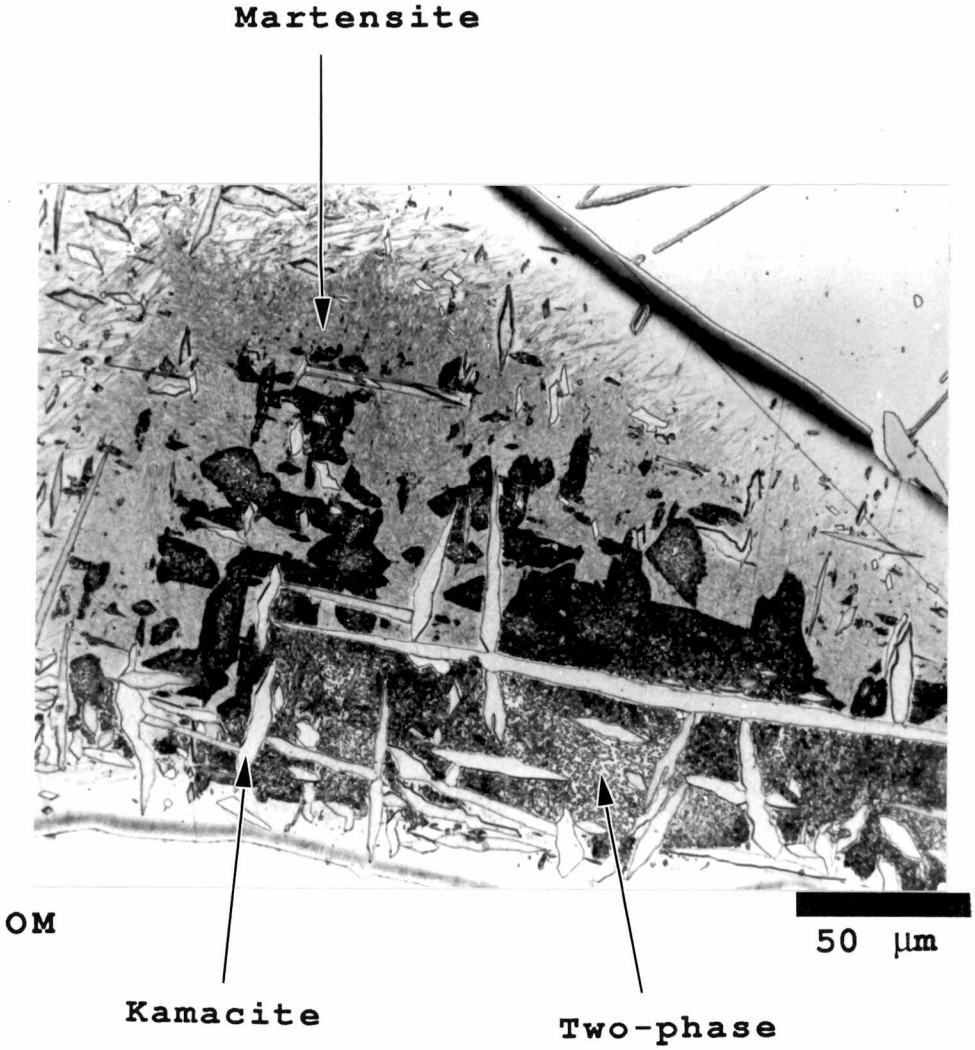

Figure 68. Variation of acicular plessite. Martensitic structure and two-phase structure present in retained taenite between the kamacite plates.

kamacite plates (Figure 69). The lighter structure appears to be martensitic (refer to Figure 68), while the darker region appears to be two-phase structure. Higher magnification (Figure 70) reveals the darker region does appear two-phase, and a heavier etch would probably reveal the martensitic structure.

2. Non-metallic Inclusion

Upon SEM investigation, the inclusion was seen to consist of multiple structures, not a single mineral (Figure 71). At least four distinct regions could be identified (Figure 72), not counting the small taenite and kamacite regions within the inclusion. Optical microscopy revealed the presence of a thick mineral layer surrounding the main inclusion (Figure 73). The presence of this layer of schreibersite is not obvious in Figure 71.

EDS analysis has shown the main mass of the inclusion to be troilite (FeS). Many other structures are associated with this troilite nodule. Other structures present appear to be graphite, schreibersite $(Fe,Ni)_3P$, chromite $(FeCr_2O_4)$, and a silicate. In this case, a magnesium silicate is present. It is common for graphite, chromite, and silicates to be associated with troilite in Group I meteorites [4].

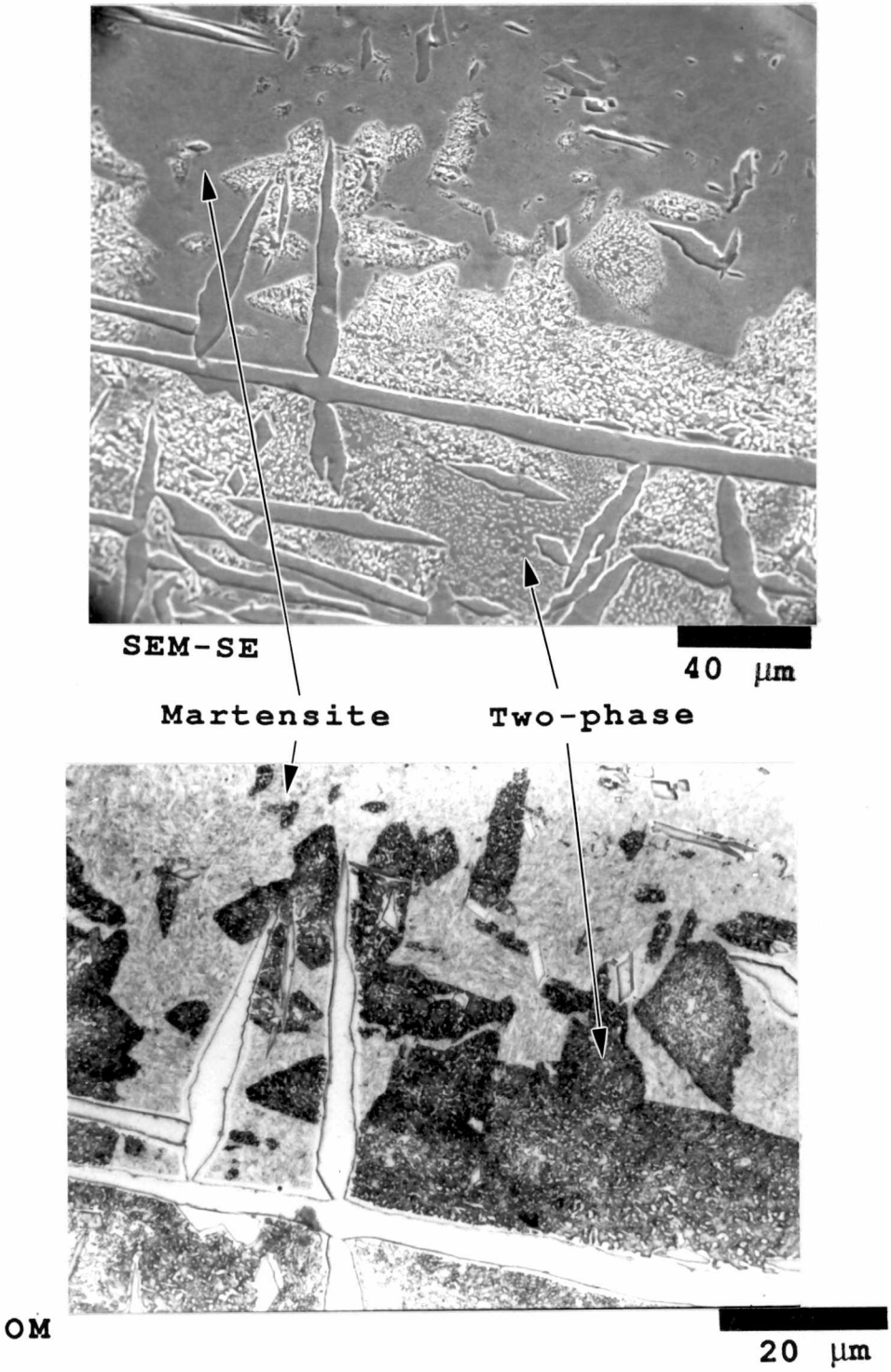

Figure 69. Two different structures present in retained taenite regions.

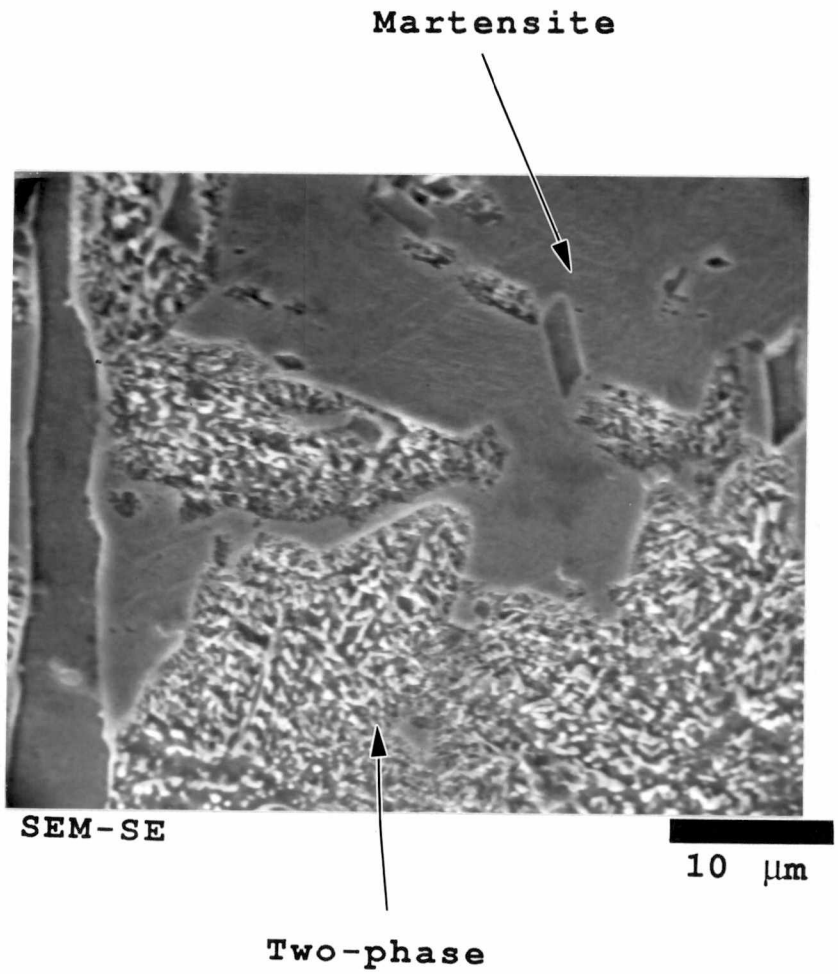

Figure 70. Martensite and two-phase structure of acicular plessite variation.

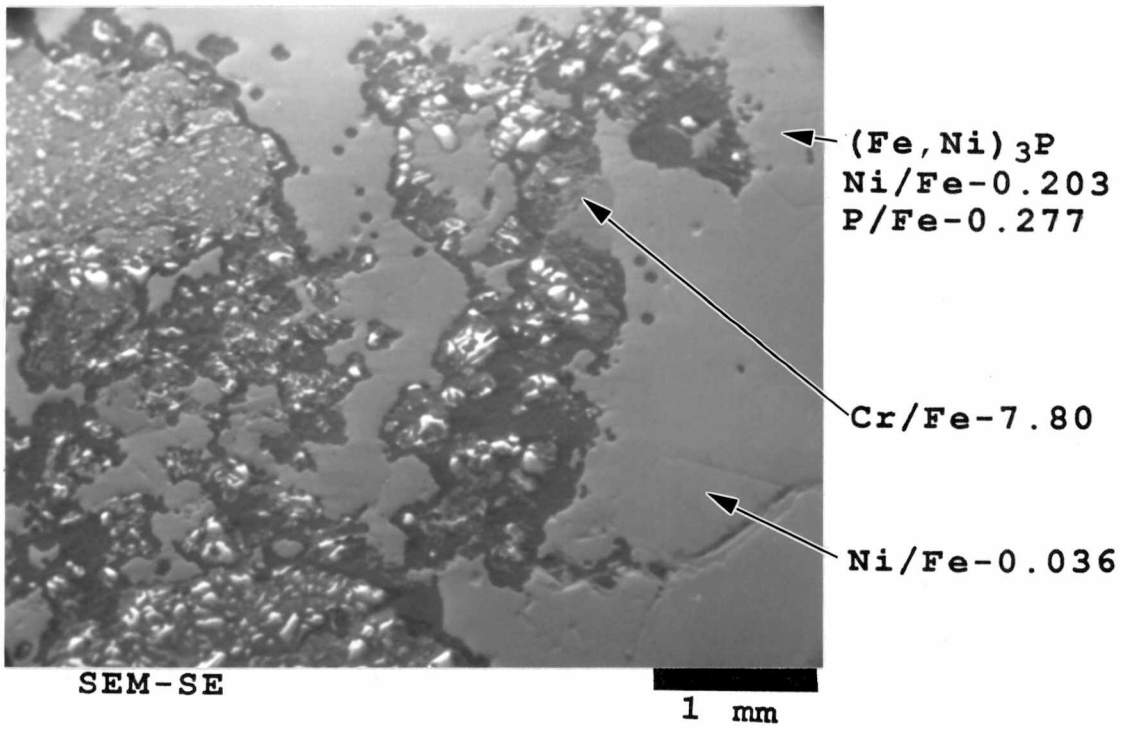

Figure 71. Troilite-graphite inclusion.

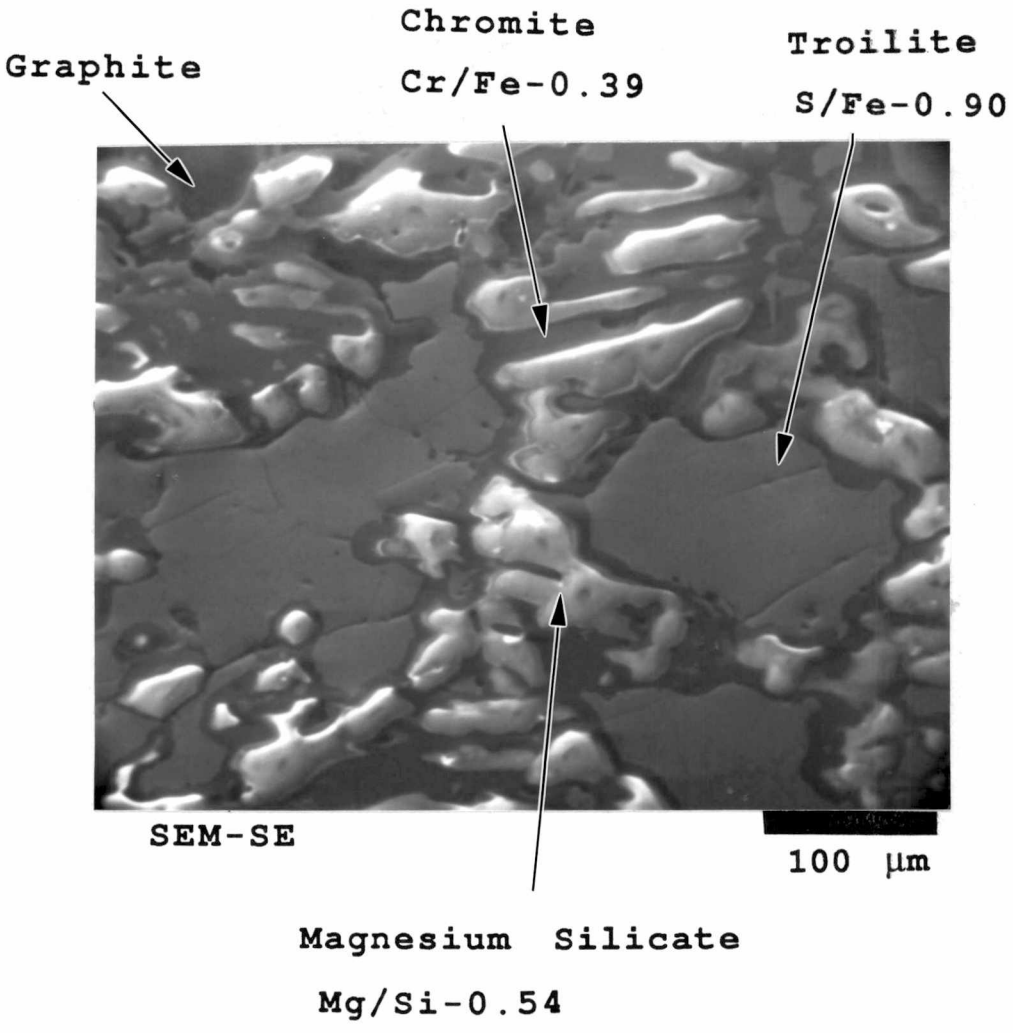

Figure 72. Troilite-graphite inclusion, with regions of chromite and magnesium silicate.

Figure 73. OM of troilite-graphite inclusion showing rim of schreibersite around inclusion.

Troilite, chromite, and taenite are usually the only structures present at austenitic temperatures, so upon cooling these minerals often act as heterogeneous nucleation sites for other structures [26].

Chapter VII

Discussion

The formation of the Widmanstatten pattern has been discussed in a previous section, so our discussion will be limited to the formation of microscopic structures within these three meteorites. Due to their similarity in structure, Arispe and Ocotillo will be discussed together, followed by a discussion of the structure of Inland Forts.

I. The Octahedrites: Arispe and Ocotillo

Both Arispe and Ocotillo are coarse octahedrites, and exhibit similar structural features, so their discussion will be grouped together with the exception of where distinction is necessary. Possible formation mechanisms of the microstructural features present in these two meteorites, primarily plessite, will be discussed.

A. Plessite

1. Formation

As stated previously, plessite has been divided into three types; Type I, Type II, and Type III, depending on the formation mechanism. These formation mechanisms have an effect on the final structure present.

By the time ~500°C is reached, most Widmanstatten growth is complete and the retained taenite stringers are present [6]. In the center of these nickel enriched stringers, the nickel content is lower than at the edges. This is due to the low diffusion rates at these lower temperatures causing the formation of the characteristic M-type concentration profile. The nickel content across retained taenite stringers in Arispe has been measured [36]. The nickel content at the interface of the stringer and kamacite was found to be ~30% nickel, and dropped to ~14% nickel in the center of the stringer. However, there is no direct correlation to the morphology of the $\alpha + \gamma$ structure in this designation.

These unstable stringers of taenite are considered to undergo decomposition by one of two mechanisms: $\gamma \rightarrow \alpha + \gamma$ (Type I Plessite), or $\gamma \rightarrow \alpha_2 \rightarrow \alpha + \gamma$ (Type III Plessite).

Type III plessite forms through a martensitic transformation, which then transforms to $\alpha + \gamma$. Goldstein et. al argue that in this decomposition reaction, γ nucleates at the martensite grain boundaries, depleting the nearby regions of nickel and resulting in α forming in these low nickel regions [37].

During this reaction, γ must first transform to α_2 (martensite). From examination of the iron-nickel phase diagram, this occurs when the temperature drops below M_S (approximately 575°C for a 7% nickel alloy). The M_S temperature depends on factors such as the nickel content and localized carbon content. Increases in nickel content suppress the martensitic transformation, lowering the M_S temperature. The M_S for a 14% nickel alloy is ~380°C, and for a 28% nickel alloy is ~-60°C [36]. M_S decreases approximately 50°C for every additional 0.1% carbon present [6]. A lower M_S temperature due to high carbon content could force the formation of Type I plessite, $\gamma \rightarrow \alpha + \gamma$, rather than Type III plessite.

When regions of pearlitic plessite are formed, the low nickel kamacite bands expel nickel into the retained taenite. This excess nickel helps the taenite lamallae become more stable.

Type I plessite results in a microwidmanstatten

(acicular) plessite structure [14]. One possible mechanism for the formation of acicular plessite is by a mechanism similar to the formation of the macroscopic Widmanstatten pattern, but with slight variations due to the high nickel content in the stringers. As the oriented kamacite plates nucleate and grow, they stop before complete conversion of taenite to kamacite due to the high nickel concentration present within the stringer. This exsolution of nickel from the kamacite plates into the surrounding region raises the nickel content of these regions. At high nickel contents the M_S temperature is low, so the formation of martensite is suppressed.

These taenite regions between the kamacite plates often contain martensite (Figure 9) or martensite decomposition products, but occasionally show other structures (Figure 25). Some of these other structures could be tempered martensitic structures, with a slight heating event altering the morphology of the martensite between these plates.

2. Coarsening and Spheroidization

The typical lamallae size of Group I meteorites is less than 1 μm [38], and coarsening and spheroidization of these pearlitic lamallae are common in Arispe and Ocotillo.

Coarsening occurs due to a thermodynamic mechanism; total interfacial free energy wants to be a minimum, and this drives the coarsening reaction. Given a constant amount of a phase in a matrix, a larger particle configuration has a smaller surface area, so it has lower total interfacial free energy. Therefore, regions with high densities of small particles tend to go to regions with low densities of larger particles.

This coarsening of the plates occurs by a ledge mechanism. This ledge mechanism causes the plates to thicken by lateral movement of the ledges. In order for precipitation to occur at the ledges and for plate thickening to occur, the necessary composition changes must occur by long range diffusion [39].

Spheroidization is a further decrease of the total interfacial free energy of the taenite, driven by the Gibbs-Thomson effect. This attempt by the taenite to minimize the interfacial free energy causes the spheres to grow after spheroidization.

Due to the Gibbs-Thomson effect, solute concentration in the matrix adjacent to particles increases as the radius of curvature of the particle decreases. Therefore, small particles have higher solute concentrations in the matrix adjacent to them than do large particles. This forms a

concentration gradient that causes solute to diffuse away from the small particle toward larger particles where the solute concentration is lower. This supply of solute to the larger particles allows them to continue growing, while the solute depletion adjacent to the smaller particles causes them to shrink. The smaller particles are forced to shrink in order to maintain the solute balance required by the Gibbs-Thomson effect [39].

This spheroidization reaction could possibly occur by segmentation of pearlitic lamallae, but most of the spheroidal structure seen was not spheres in a straight line, rather a randomly oriented structure of spheres (Figure 56).

It is not known why some pearlitic plessite coarsens and other regions spheroidize when spheroidization gives a greater drop in total interfacial energy.

Occasionally a coarsening boundary is observable between the pearlitic and spheroidal regions (Figure 50). This boundary is even present between the kamacite regions, so segmentation does not seem likely. In other cases, there is no coarsening boundary observable.

As taenite spheres grow, optically some appear to exhibit the cloudy zone structure (Figure 56). The cloudy zone is a fine two-phase structure of FeNi and martensite, and it is not known if these spheres undergo a martensite

decomposition to form this structure, or if this cloudy appearing region is an etching effect. Electron diffraction pattern analysis would be required to determine if this structure is ordered FeNi.

3. Diffusion Effects

The effect of the low diffusion rate of nickel in iron at low temperatures on the formation of the plessitic structure is a very important factor to consider. Figure 74 is a plot of temperature against diffusion time. This plot illustrates the amount of time necessary to diffuse a given distance for a specific temperature. A simplistic approach was taken in calculating this curve, using the basic diffusion equation, $x = 0.5\sqrt{Dt}$, and neglecting the affect of other minor elements present.

The diffusion of nickel in iron is effectively stopped at 400°C [40], which can be roughly confirmed in Figure 74. So transformations that occur below this temperature can only rely on short range diffusion mechanisms.

However, it is pointed out that the effect of phosphorous on the diffusion rate cannot be neglected in meteorites with significant phosphorous content. The volume diffusion coefficient of nickel in taenite is raised by a

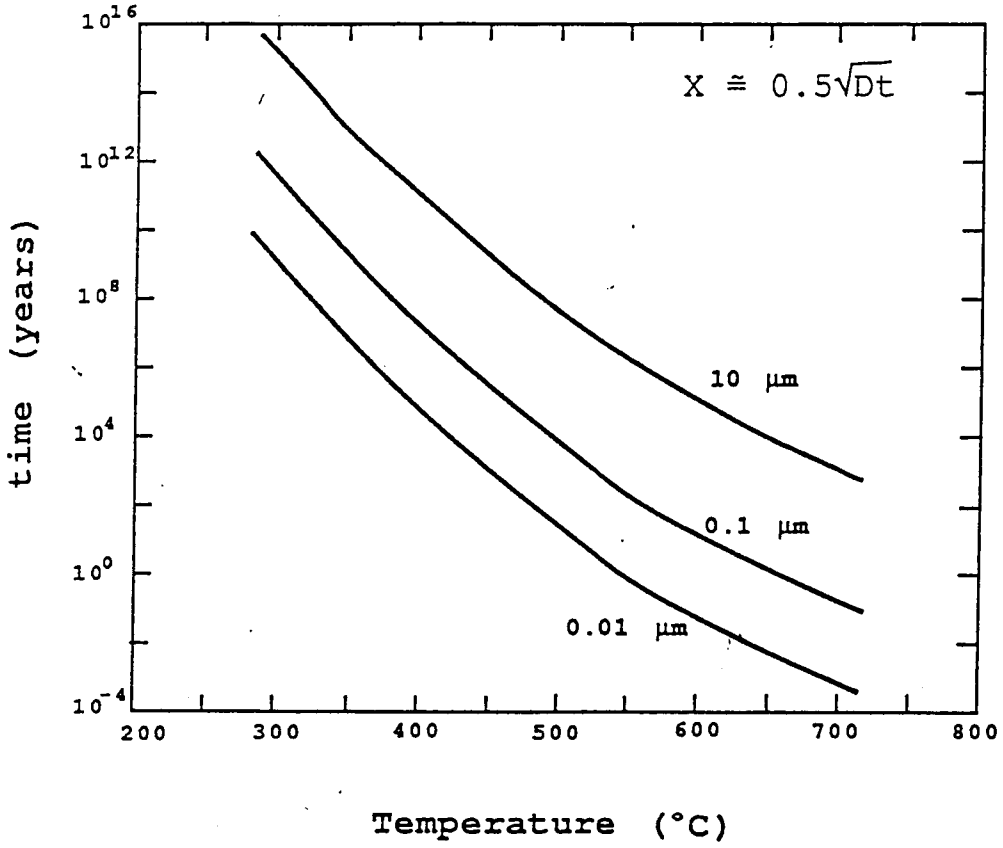

Figure 74. Plot of time vs. temperature for diffusion to occur over a given distance.

factor of 10 at 750°C with the addition of 0.15% phosphorous [25]. Therefore meteorites with high phosphorous content could continue to transform by a diffusion mechanism well below the temperature where diffusion halts in an iron-nickel alloy where phosphorous is not significantly present.

B. Non-metallic Structures

1. Cohenite Nests: Arispe

Cohenite nests definitely effect the structures present in the retained stringers. Near regions of the dense cohenite nests, pearlitic plessite is more common. It is not known whether an excess of carbon exists in this region due to these nests, or if they absorb all the local carbon and leave the neighboring kamacite depleted in carbon.

The detector on our EDS system does not detect carbon, so if a carbon gradient exists, and whether the gradient increases or decreases toward the nests, was not determined.

The rapid transition from pearlitic to acicular plessite (Figure 18) could occur due to these concentration gradients of elements such as carbon. When there is a transformation from pearlitic to acicular plessite, the pearlitic end tends to be toward the area with the cohenite nests.

2. Troilite Inclusion: Ocotillo

In Ocotillo, the large inclusion was found to primarily consist of troilite and graphite. EDS confirmed the troilite regions, and revealed no peaks when a region of what was thought to be graphite was analyzed, due to the inability of the detector to pick up carbon.

Chromite was also found to be present, and is quite common with troilite in Group I meteorites. The presence of silicates also is not unexpected, and in this case EDS detected the presence of a magnesium silicate.

Regions of schreibersite and kamacite were also detected surrounding the inclusion. This variety of structures heterogeneously nucleate on troilite and chromite upon cooling from the taenite region.

II. The Ataxite: Inland Forts

The possible formation mechanisms of the structure of Inland Forts will be discussed separately from that of the octahedrites, due to its drastically different structure. It is important to remember that Inland Forts has a significantly higher nickel content (18.9%) than the octahedrites.

A. Kamacite and Schreibersite Particles

Normally upon cooling from the taenite region, meteorites form the Widmanstatten pattern. Inland Forts exhibits only 8% kamacite present, which do not follow the Widmanstatten orientation (Figure 33).

Due to the high nickel content of Inland Forts (18.9% nickel), the nucleation of α from γ would start at a lower temperature, and therefore formation of the Widmanstatten oriented kamacite plates would be hindered by diffusion kinetics.

Schreibersite nucleates at higher temperatures and serves as heterogeneous nucleation sites for the kamacite, allowing it to nucleate intragranularly.

Since kamacite growth is hindered by starting at a lower temperature due to high nickel content, blocky grains form upon the schreibersite and grow (Figure 35). Occasionally an independent plate of kamacite was seen, but generally the kamacite occurred with schreibersite.

A fast cooling rate restricted the growth of kamacite after its low temperature nucleation. This fast cooling rate also suppressed the eutectoid reaction, $\gamma \rightarrow \alpha$ + FeNi, from occurring.

B. Matrix

One possible mechanism for the formation of the matrix structure is that upon cooling, the 19% nickel alloy crossed into the $\alpha + \gamma$ region, and small amounts of kamacite heterogeneously nucleated onto the schreibersite present. However, the growth rate was limited due to the low temperature and a rapid cooling rate.

The remaining retained taenite, approximately 90% of the structure, was transformed to martensite. For this nickel content, a complete transformation of the retained taenite to martensite occurs [41,42]. The morphology of the martensite depends on nickel content. In iron-nickel alloys, at compositions of below ~25% nickel, taenite transforms to massive martensite, rather than acicular martensite. So at this nickel content the morphology of the martensite formed is massive rather than acicular [42-44].

The structure of the matrix of Inland Forts is believed to be made up of martensite or a martensite decomposition product. The banded effect occurred due to a difference in orientation to the cut surface.

Two-phase structures were observed in the matrix of Inland Forts, but nothing that would normally be considered martensitic. It is believed that after the transformation to

massive martensite occurred, the martensite decomposed to a two-phase structure.

This martensite decomposition could have occurred due to a preterrestrial heating event, or could be similar to the decomposition step in Type III plessite. It is difficult to believe the diffusion kinetics would allow a low temperature equilibrium transformation, but this decomposition has been described in a 25% nickel meteorite at ~100°C [14]. However, the large amounts of phosphorous in Inland Forts (0.29% P) would also increase the diffusion rate of nickel, possibly allowing this decomposition to occur at these low temperatures.

One possible decomposition process would be the eutectoid reaction to kamacite and FeNi (tetrataenite) at 400°C. However, the structure seen in Inland Forts is somewhat similar to iron-nickel samples which were quenched to martensite from the γ region, and then reheated to decompose the martensite to $\alpha + \gamma$ [41,45].

The difference in coarseness of the two-phase regions could be due to a coarsening reaction of the fine structure from region 2 transforming to the coarse structure of region 1.

Chapter VIII

Conclusions

The structures present in these three meteorites are very interesting, and trying to understand their formation mechanisms is quite difficult.

The octahedrites contained a variety of plessitic morphologies in the retained taenite stringers; pearlitic, spheroidal, acicular, martensitic and comb plessite were all observed.

The pearlitic plessite often spheroidized or coarsened, and occasionally an interface was observed between these regions. This leads to the theory that the pearlitic coarsening and the spheroidization possibly occurred by a boundary migration mechanism.

The coarsening of the pearlitic plessite is believed to be an attempt to minimize the total interfacial free energy. Given a constant volume of a phase in a matrix, a configuration of larger plates has less surface area than smaller plates, so the large plates have less interfacial free energy. This is believed to drive regions of high densities of small plates to regions of low densities of large plates.

In Arispe, the pearlitic and spheroidal plessite primarily were observed near the cohenite 'nests', a morphology of cohenite that is unique to Arispe. Acicular

diffusion rate of nickel at low temperatures and the uncertainty of the phase diagram are just a few of the complicating factors that must be considered. Possible mechanisms have been discussed, but these are not definite formation mechanisms for the plessitic structures observed.

and comb plessite were predominantly observed in the bulk of the meteorite away from these nests. This possibly links localized concentrations of carbon, either an excess or a depletion, to the morphology of the plessite.

The Inland Forts meteorite consisted of approximately 8% ferrite with associated schreibersite particles. No Widmanstatten ferrite was observed, as is common in ataxites. Macroscopically the matrix appeared banded, and this banded effect was observed to be due to an orientation difference between the matrix structure. The matrix structure consisted of three regions, a coarse two-phase structure (region 1), and fine two-phase structure (region 2), and a clear, untransformed structure (region 3).

One possible formation mechanism for this structure is that the cooling rate was too rapid to allow equilibrium to continue, and only small amounts of α heterogeneously nucleated on the schreibersite particles. Further cooling transformed the matrix to martensite and retained taenite, which decomposed to form the two-phase regions present in the matrix. It is not clear whether this martensitic decomposition occurred due to a preterrestrial heating event, or if the high amount of phosphorous present (0.29% P) raised the diffusion rate enough to allow a low temperature phase transformation to occur.

For all three meteorites, the formation mechanisms of the plessitic structures are not straight forward. The low

References

References

1. M. K. Miller and K. F. Russell, "An Atom Probe Field-Ion Microscopy Study of Phase Separation in the Twin City and Santa Catharina Meteorites," **Colloque de Physique**, Vol.50, pp.413-418, (1989).

2. M. H. Hey, **Catalogue of Meteorites**, British Museum, London, (1966).

3. J. T. Wasson, **Meteorites-Classification and Properties**, Springer-Verlag, Berlin, (1974).

4. V. F. Buchwald, **Handbook of Iron Meteorites**, Vol. 1, University of California Press, Los Angeles, (1975).

5. S. J. B. Reed, "Electron-Probe Microanalysis of the Metallic Phases in Iron Meteorites," **Geochimica et Cosmochimica Acta**, Vol. 29, pp. 535-549, (1965).

6. L. S. Lin, J. I. Goldstein and D. B. Williams, "Analytical Electron Microscopy Study of the Plessitic Structure in Four IIICD Iron Meteorites," **Geochimica et Cosmochimica Acta**, Vol. 43, pp. 725-737, (1979).

7. A. E. Ringwood, "Cohenite as a Pressure Indicator in Iron Meteorites," **Geochimica et Cosmochimica Acta**, Vol. 20, pp. 155-158, (1960).

8. A. S. Doan and J. I. Goldstein, "The Formation of Phosphides in Iron Meteorites," **Meteorite Research**, P. M. Millman,ed., Dordrecht-Holland, pp. 763-779, (1968).

9. V. F. Buchwald, "The Mineralogy of Iron Meteorites," **Philosophical Transactions of the Royal Society**, London, Vol. 286, pp. 453-491, (1977).

10. Y. Y. Chuang, Y. A. Chang, R. Schmid and J. C. Lin, "Magnetic Contributions tothe Thermodynamic Functions of Alloys and the Phase Equilibria of the Fe-Ni System below 1200K," **Metallurgical Transactions A**, Vol. 17A, pp. 1361-1372, (1986).

11. K. B. Reuter, D. B. Williams and J. I. Goldstein, "Determination of the Fe-Ni Phase Diagram below 400°C," **Metallurgical Transactions A**, Vol. 20A, pp. 719-725, (1989).

12. K. B. Reuter, D. B. Williams and J. I. Goldstein, "Ordering of the Fe-Ni System under Electron Irradiation," **Metallurgical Transactions A**, Vol. 20A, pp. 711-718, (1989).

13. J. F. Albertsen, J. M. Knudsen, N. O. Roy-Poulsen and L. Vistisen, " Meteorites and Thermodynamic Equilibrium in f.c.c. Iron-Nickel Alloys (25-50% Ni)," **Physica Scripta**, Vol. 22, pp. 171-175, (1980).

14. L. S. Lin, J. I. Goldstein and D. B. Williams, "Analytical Electron Microscopy Study of the Plessite Structue in the Carlton Iron Meteorite," **Geochimica et Cosmochimica Acta**, Vol. 41, pp. 1861-1874, (1977).

15. K. B. Reuter, D. B. Williams and J. I. Goldstein, "The Fe-Ni Phase Diagram Below 350°C," **Meteoritics**, Vol. 21, pp. 493-494, (1986).

16. K. B. Reuter, D. B. Williams and J. I. Goldstein, "Low Temperature Phase Transformations in the Metallic Phases of Iron and Stony-Iron Meteorites," **Geochimica et Cosmochimica Acta**, Vol. 52, pp. 617-626, (1988).

17. K. B. Reuter, D. B. Williams and J. I. Goldstein, "Low Temperature Phase Transformations in the Metallic Phases of Meteorites," **Meteoritics**, Vol. 22, pp. 488-489, (1987).

18. J. F. Albertsen, "Tetragonal Lattice of Tetrataenite (Ordered Fe-Ni, 50-50) from 4 Meteorites," **Physica Scripta**, Vol. 23, pp. 301-306, (1981).

19. J. C. Albertsen, G. B. Jensen and J. M. Knudsen, "On Superstructure in Meteoritical Taenite," **Meteoritics**, Vol. 13, pp. 379-383, (1978).

20. T. B. Massalski, T. B. Park and L. F. Vassamillet, "Speculations about Plessite," **Geochimica et Cosmochimica Acta**, Vol 30, pp. 649-662, (1966).

21. C. Narayan and J.I. Goldstein, "A Major Revision of Iron Meteorite Cooling Rates - an Experimental Study of the Growth of the Widmanstatten Pattern," **Geochimica et Cosmochimica Acta**, Vol 49, pp. 397-410, (1985).

22. J.I. Goldstein and R. E. Ogilvie, "The Growth of the Widmanstatten Pattern in Metallic Meteorites," **Geochimica et Coschimica Acta**, Vol. 29, pp. 893-920, (1965).

23. J. A. Wood, "The Cooling Rates and Parent Planets of Several Iron Meteorites," **Icarus**, Vol. 3, pp. 429-459, (1964).

24. J. I. Goldstein and A. S. Doan, "The Effect of Phosphorous on the Formation of the Widmanstatten Pattern in Iron Meteorites," **Geochimica et Cosmochimica Acta**, Vol. 36, pp. 51-69, (1972).

25. C. Narayan and J.I. Goldstein, "A Major Revision of Iron Meteorite Cooling Rates - an Experimental Study of the Growth of the Widmanstatten Pattern, **Meteoritics**, Vol 49, pp. 360-361, (1983).

26. E. R. D. Scott and J. T. Wasson, "Classification and Properties of Iron Meteorites, **Reviews of Geophysics and Space Physics**, Vol. 13, pp. 527-546, (1975).

27. V. F. Buchwald, **Handbook of Iron Meteorites: Their History, Composition and Structures**, Vol. 2, University of California Press, Berkley, (1975).

28. A. DeMint and C. R. Brooks, "Some Preliminary Metallographic Observations of the Arispe Iron Meteorite," In. M. R. Louthan, I. LeMay, and G. F. Vander Voort (eds.), **Microstructural Science**, American Society of Metals, Metals Park, Ohio, pp. 239-258, (1987).

29. C. R. Brooks and A. DeMint, "Some Microstructural Observations of Pearlitic and Spheroiditic Plessite in the Arispe Iron Meteorite," In M. E. Blum, R. M. French, R. M. Middleton, and G. F. VanderVoort (eds.), **Microstructural Science**, American Society for Metals, Metals Park, Ohio, pp. 405-423, (1987).

30. C. R. Brooks and A. DeMint, "Microwidmanstatten Ferrite and Martensite in the Arispe Iron Meteorite," In P. J. Kenny, G. S. Cole, D. O. Northwood, and J. Wylie (eds.), **Microstructural Science**, American Society for Metals, Metals Park, Ohio, pp. 471-490, (1987).

31. V. F. Buchwald and R. S. Clarke, "Corrosion of Fe-Ni Alloys by Cl-Contaning Akageneite (Beta- FeOOH): The Antarctic Meteorite Case," **American Mineralogist**, Vol. 74, pp. 656-667, (1989).

32. R. S. Clarke, "Descriptions of Some Antarctic Meteorites," In U. B. Marvin, and G. J. MacPherson (eds.), **Field and Laboratory Investigations of Meteorites from Victoria Land and the Thiel Mountains Region, Antarctica, 1982-83 and 1983-84**, Smithsonian Institution Press, Washington, D.C., pp. 61-63, (1991).

33. D. New, "David New Geological Specimens", Personal Communication.

34. A. DeMint, "The Microstructure of the Arispe Meteorite," Masters Thesis, (1985).

35. G. Vander Voort, Personal Communication.

36. L. Kaufman and M. Cohen, "The Martensitic Transformation in the Fe-Ni System," **Journal of Metals**, Vol. 8, pp. 1393-1401, (1956).

37. J. I. Goldstein, D. B. Williams and J. Zhang, "The Plessite Structure in Iron Meteorites," **Meteoritics**, Vol. 26, pp. 338-339, (1991).

38. J. A. Kowalik, J.I. Goldstein and D. B. Williams, "Comparison of the Lamellar Plessite Structure in Two Groups of Iron Meteorites - Are The Related?," **Meteoritics**, Vol. 21, p. 425, (1986).

39. D. A. Porter and K. E. Easterling, **Phase Transformations in Metals and Alloys**, Chapman and Hall, London, pp. 314-317, (1981).

40. J. S. Duerr and R. E. Oglivie, "High Voltage Microscopy of Martensite in Plessite," **Meteoritics**, Vol. 5, pp. 194-195 (1970).

41. V. F. Buchwald, "The Iron-Nickel-Phosphorous System and the Structure of Iron Meteorites," **Acta Polytechnica Scandinavica**, No. 51, (1966).

42. J. M. Marder and A. R. Marder, "The Morphology of Iron-Nickel Massive Martensite," **Transactions of ASM**, Vol. 62, p. 1, (1969).

43. W. S. Owen, E. A. Wilson and T. Bell, "The Structure and Properties of Quenched Iron Alloys," in **High-Strength Materials**, V. F. Zackay, editor, Biley, NY., p. 167, (1950).

44. R. H. Goodenow and R. F. Hehemann, "Transformations in Iron and Fe-9 Pct Ni Alloys," **Transactions of the Metallurgical Society of AIME**, Vol. 233, p. 1777, (1965).

45. N. P. Allen and C. E. Early, "The Transformations $\alpha-\gamma$ and $\gamma-\alpha$ in Iron-Rich Binary Iron-Nickel Alloys," **Journal of the Iron and Steel Institute**, Vol. 166, p. 281, (1950).

Vita

The author was born and raised in Plano, Texas, and moved to Johnson City, Tennessee in 1980, where he graduated from Science Hill High School in 1985. He earned a B.S. in Materials Engineering from Virginia Polytechnic Institute and State University in 1990, where he participated in the co-op program with Texas Instruments. He continued his education by entering the Metallurgical Engineering program at the University of Tennessee in the fall of 1990, and received a M.S. in December of 1992.